

The First Cosmic Structures and their Effects

Benedetta Ciardi

Max-Planck-Institut für Astrophysik, Garching, Germany

Andrea Ferrara

SISSA/International School for Advanced Studies, Trieste, Italy

April, 2004

Table of Contents

1	Introduction	2
2	First Structure Formation: Overview	4
	2.1 The Cosmological Model	4
	2.2 Linear Growth of Fluctuations	7
	2.3 Non Linear Evolution: Dark Matter Halos	9
	2.4 Formation of protogalaxies	15
	2.5 Key Observations	20
3	First Stars	26
	3.1 Formation Process	27
	3.2 Emission Spectrum	39
	3.3 Final Fate	41
	3.4 Black Holes and Gamma Ray Bursts from the First Stars	44
	3.5 Key Observations	46
4	Feedback Effects	56
	4.1 Radiative Feedback	58
	4.2 Mechanical Feedback	67
	4.3 Chemical Feedback	71
5	Cosmic Reionization and IGM Metal Enrichment	73
	5.1 Escape Fraction	73
	5.2 Hydrogen Reionization	76
	5.3 Helium Reionization	85
	5.4 IGM Metal Enrichment	87
	5.5 Key Observations	92
6	Conclusions	111



© 2024 Kluwer Academic Publishers. Printed in the Netherlands.

1. Introduction

Our present understanding of the evolution of the universe is based on the Standard Hot Big Bang Model. The expansion of the universe, the synthesis of the light elements and the Cosmic Microwave Background (CMB) radiation are the pillars of this Model. Its definite observational confirmation was the CMB accidental detection in 1965 by Penzias & Wilson, who received the Nobel Prize for this discovery. In the 1990s the COBE¹ (COsmic Background Explorer) satellite improved on the previous observations and measured an almost isotropic blackbody radiation with temperature $T_{\text{CMB}} = 2.726 \pm 0.010$ K (Mather et al. 1994), together with temperature anisotropies on angular scales $\approx 90^\circ$ (Smoot et al. 1992). These discoveries warranted yet another Nobel Prize (in 2006) to the principal investigators of the mission, Smoot and Mather. The isotropy of the microwave background indicates that on large scales (≥ 200 Mpc) the universe is indeed very smooth, as postulated by Einstein in his “cosmological principle”. On small scales, in contrast, it presents inhomogeneities, from planets and stars, to galaxies, clusters and super-clusters of galaxies. These structures are not uniformly distributed, but rather show some spatial correlation, and regions of space almost totally devoid of galaxies are alternated to high density regions. The commonly adopted theory for the formation of these structures is the gravitational instability scenario, in which primordial density perturbations grow through gravitational Jeans instability to form all the structures we observe today. The evidence for the existence of such perturbations is based on combined CMB observations by BOOMERanG² (Balloon Observations Of Millimetric Extragalactic Radiation and Geomagnetism), MAXIMA³ (Millimeter Anisotropy eXperiment IMaging Array), DASI⁴ (Degree Angular Scale Interferometer) and, more recently, WMAP⁵ (Wilkinson Microwave Anisotropy Probe) which provided the power spectrum of temperature anisotropies on a wide range of angular scales (Hu et al. 2001; Sievers et al. 2003; Spergel et al. 2003; Spergel et al. 2007). The anisotropies at scales $< 90^\circ$ are interpreted as the result of perturbations in the energy density at the decoupling epoch and hence are directly related to the primordial density fluctuations from which all present structures originate.

While the observation of the very high-redshift universe, $z \approx 1000$, is possible through the CMB, there is a lack of observational data in the

¹ <http://lambda.gsfc.nasa.gov/product/cobe>

² <http://cmb.phys.cwru.edu/boomerang>

³ <http://cosmology.berkeley.edu/group/cmb>

⁴ <http://astro.uchicago.edu/dasi>

⁵ <http://map.gsfc.nasa.gov>

redshift interval $7 < z < 1000$, with only a few objects with $z \approx 6.5 - 8$ (Hu et al. 2002; Kodaira et al. 2003; Kneib et al. 2004; Bouwens et al. 2004; Malhotra et al. 2005; Mobasher et al. 2005; Iye et al. 2006; Schaerer & Pelló 2005; Ota et al. 2007). A deep, narrow J-band search for Ly α emitting galaxies at $z \approx 9$ by Willis & Courbin (2005) has given no result, but the NICMOS field at $z \approx 10$ has revealed 3 possible galaxies (Bouwens et al. 2005). Another tentative detection of a galaxy at $z \approx 10$ has been reported (Pelló et al. 2004a,b), but this has not been confirmed by an analysis of the same data from a different group (Weatherley, Warren & Babbedge 2004). Other two lensed candidates at $z \approx 10$ have been reported by Stark et al. (2007b).

The state of the art of the telescopes observing in the NIR/optical/UV range is represented by HST⁶ (Hubble Space Telescope), that has allowed to take high resolution images ranging from supernova (SN) explosions, to nebulae with ongoing star formation, to the Hubble Deep Field and Ultra Deep Field. Additional important contributions are brought to the field by the Spitzer⁷ satellite, a space-based infrared telescope launched in 2003 working in the 3-180 μm range. Thanks to its exquisite sensitivity in this band, it has allowed to better understand the evolution of galaxies up to $z \approx 5$ through a variety of mid- and far-infrared imaging surveys and to constrain the nature and amplitude of the Cosmic Infrared Background (CIB). In order to observe radiation from objects at even higher redshift, telescopes with exceptional sensitivity in the IR and radio bands are needed. JWST⁸ (James Webb Space Telescope), for example, with its nJy sensitivity in the 1 – 10 μm infrared regime, is ideally suited for probing optical-UV emission from sources at $z > 10$. Similarly, the planned generation of radio telescopes as SKA⁹ (Square Kilometer Array), LOFAR¹⁰ (LOw Frequency ARray), 21cmA¹¹ (21cm Array; Pen, Wu & Peterson 2004; Peterson, Pen & Wu 2005) and MWA¹² (Murchison Widefield Array) will open a new observational window on the high redshift universe.

Thus, in the near future, we should be able to image the first sources of light that had formed in the universe, and unveil their nature. Nowadays, observational evidence suggests that they are stellar type objects, although the existence of primordial mini-quasars is not completely ruled out.

⁶ <http://www.stsci.edu/hst>

⁷ <http://www.spitzer.caltech.edu/spitzer/index.shtml>

⁸ <http://ngst.gsfc.nasa.gov>

⁹ <http://www.skatelescope.org>

¹⁰ <http://www.lofar.org>

¹¹ <http://astrophysics.phys.cmu.edu/jbp>

¹² <http://web.haystack.mit.edu/arrays/MWA/>

In the standard cosmological hierarchical scenario for structure formation, the objects which form first are predicted to have masses corresponding to virial temperatures $T_{vir} < 10^4$ K. Once the gas has virialized in the potential wells of pre-existing dark matter halos, additional cooling is required to further collapse the gas and form stars. For a gas of primordial composition at such low temperatures the main coolant is molecular hydrogen. The typical primordial H_2 fraction is usually lower than the one required for the formation of such objects, but during the collapse phase the H_2 content can reach suitable values, depending on the mass of the object itself. Once the gas has collapsed and cooled, star formation (SF) is ignited. The study of the star formation process in primordial objects is still in its early stages, and although large improvements have been done in both analytical and numerical approaches, a solid physical scenario requires substantial further investigation.

Once the first sources have formed, their mass deposition, energy injection and emitted radiation can deeply affect the subsequent galaxy formation process and influence the evolution of the Intergalactic Medium (IGM) via a number of so-called “feedback” effects. Although a rigorous classification of the various effects is not feasible, they can be divided into three broad classes: radiative, mechanical and chemical feedback. Into the first class fall all those effects associated, in particular, with ionization/dissociation of hydrogen atoms/molecules; the second class is produced by the mechanical energy injection of massive stars in form of winds or supernova explosions; the chemical feedback is, in contrast, related to the postulated existence of a critical metallicity governing the cosmic transition from very massive stars to “normal” stars.

In this review we will summarize the recent achievements in understanding the first structure formation process.

2. First Structure Formation: Overview

In this Section we will describe the main processes leading from the evolution of primordial density perturbations to the formation of the first structures in the universe.

2.1. THE COSMOLOGICAL MODEL

Throughout this review we will usually refer to the popular Λ CDM model, in which dark matter is composed of cold, weakly interacting, massive particles. The cosmological model is completely defined once the value of the following parameters is specified: the adimensional

density of the universe, $\Omega_0 = \Omega_m + \Omega_\Lambda$ (where Ω_m and Ω_Λ are the contribution from matter and vacuum, respectively), the Hubble constant, $H_0 = 100h \text{ km s}^{-1} \text{ Mpc}^{-1}$, the adimensional baryon density, Ω_b , the rms mass fluctuations on $8h^{-1} \text{ Mpc}$ scale, σ_8 , and the spectral index of the primordial density fluctuation, n . Recent observations have set stringent constraints on the values allowed for these parameters. Studies of the temperature anisotropies in the CMB strongly suggest that the universe is flat, $\Omega_0 \approx 1$ (Balbi et al. 2000, 2001; O’Meara et al. 2001; Pryke et al. 2002), with a matter contribution of $\Omega_m \approx 0.10 - 0.36$. The latter values are derived from the local abundance of galaxy clusters (Pen 1998; Viana & Liddle 1999; Schuecker et al. 2003), their redshift evolution (Bahcall & Fan 1998; Eke et al. 1998; Borgani et al. 2001), mass-to-light ratio of groups of galaxies (Hoekstra et al. 2001), X-ray gas mass fraction of clusters of galaxies (Allen, Schmidt & Fabian 2002), clustering measurements from large galaxy surveys (e.g. Blake et al. 2007) and high- z supernovae (Schmidt et al. 1998; Perlmutter et al. 1999; but see also Rowan-Robinson 2002). The baryon contribution to matter, $\Omega_b h^2 \approx 0.020 - 0.030$, is derived through measurements of CMB anisotropies (Balbi et al. 2000, 2001; Pryke et al. 2002), clustering measurements from large galaxy surveys (e.g. Blake et al. 2007) and D/H abundance in quasars spectra (Tytler et al. 2000; Pettini & Bowen 2001; Levshakov et al. 2002; Crighton et al. 2004). All the estimates of the Hubble constant are based on secondary distance indicators, such as the Tully-Fisher relation, the fundamental plane of elliptical galaxies, Type Ia supernovae and surface brightness fluctuations, and give $h \approx 0.5 - 0.8$ (Theureau et al. 1997; Tonry et al. 1997; Jha et al. 1999; Mould et al. 2000; Freedman et al. 2001; Gibson & Stetson 2001; Liu & Graham 2001; Tutui et al. 2001; Willick & Batra 2001). Local and high- z evolution of galaxy clusters is used to set a limit to $\sigma_8 \approx 0.7 - 1.2$ (Bahcall & Fan 1998; Eke et al. 1998; Pen 1998; Viana & Liddle 1999; Borgani et al. 2001; Hoekstra, Yee & Gladders 2002). Finally, studies of the temperature anisotropies in the CMB give $n \approx 1.01 - 1.08$ (Balbi et al. 2000, 2001; Pryke et al. 2002). These parameters have been confirmed by the CMB data from WMAP (e.g. Spergel et al. 2003, 2006; Dunkley et al. 2008). But, although the excess power at $l \approx 2000 - 6000$ reported by CBI¹³ (Cosmic Background Imager) is roughly consistent with a secondary contribution resulting from the Sunyaev-Zeldovich effect, this requires a normalization for the matter power spectrum higher than measured by other means (Sievers et al. 2003).

¹³ <http://www.astro.caltech.edu/~tjp/CBI>

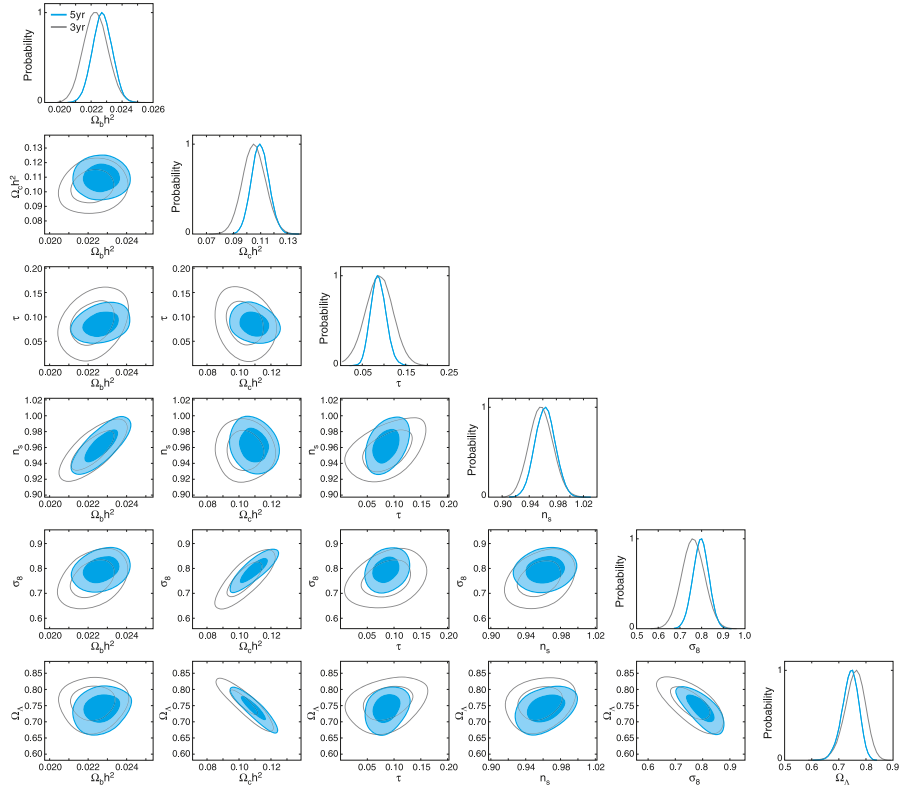


Figure 1. Constraints from the 5-yr WMAP data on Λ CDM parameters (blue), showing marginalized 1-D distributions and 2-D 68% and 95% limits (Dunkley et al. 2008). Parameters are consistent with the 3-yr limits (grey) from Spergel et al. (2007).

The most popular, or concordance, model is a Λ CDM with $\Omega_0 = 1.02 \pm 0.02$, $\Omega_\Lambda = 0.73 \pm 0.04$, $\Omega_m = 0.27 \pm 0.04$, $\Omega_b = 0.044 \pm 0.004$, $h = 0.71_{-0.03}^{+0.04}$, $\sigma_8 = 0.84 \pm 0.04$ and $n = 0.93 \pm 0.03$ (Bennett et al. 2003). The above parameter set, determined from CMB experiments, is in impressively good agreement with that obtained independently by experiments based on high-redshift Type Ia supernovae (Knop et al. 2003) and galaxy cluster evolution data. Throughout the review we will adopt these values. Slight changes to the above values are constantly being made as WMAP is collecting additional data. The results after 5 years of mission have been released very recently (see e.g. Hinshaw et al. 2008). The reader is then referred to the WMAP web page for further updates. In Fig. 1 expected values for the cosmological parameters as measured by WMAP are plotted, while Fig. 2 shows the most recent comparison (i.e. after the 5-th year of WMAP observations) between the CMB temperature fluctuations predicted by such Λ CDM model and those measured by CMB experiments.

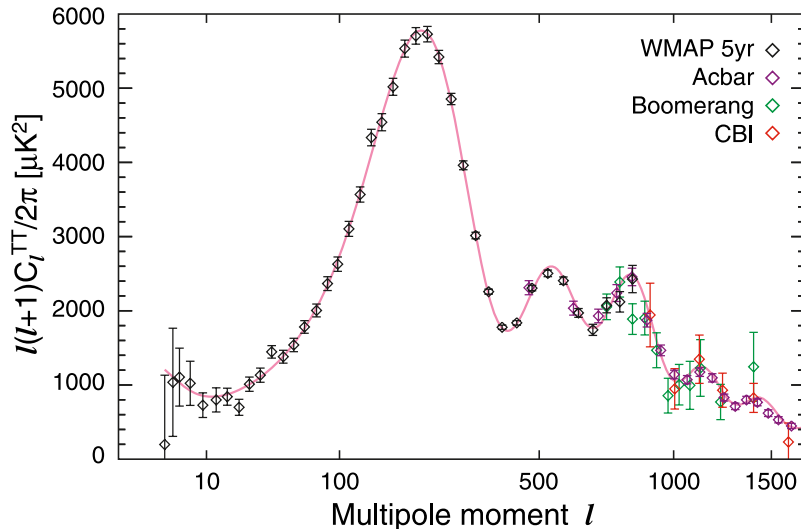


Figure 2. CMB temperature fluctuations as measured by different missions (symbols). The curve is the best-fit Λ CDM model to the WMAP data (see Nolta et al. 2008 for details).

2.2. LINEAR GROWTH OF FLUCTUATIONS

The commonly adopted theory for structure formation is the *gravitational instability scenario*, in which primordial density perturbations grow through gravitational Jeans instability to form all the structures we observe today. The most favored model for the origin of these perturbations is *inflation*. In this scenario, the universe expands exponentially for a brief period of time at early epochs ($t \approx 10^{-35} - 10^{-33}$ s), and, at the end of this inflationary period, it is highly homogeneous on large scales, but is locally perturbed as a consequence of quantistic fluctuations. To derive the evolution of these primordial density fluctuations into bound objects, we can proceed as follows.

Let us describe the universe in terms of a fluid made of collisionless dark matter and baryons, with a mean mass density $\bar{\rho}$. At any time and location, the mass density can be written as $\rho(\mathbf{x}, t) = \bar{\rho}(t)[1 + \delta(\mathbf{x}, t)]$, where \mathbf{x} indicates the comoving spatial coordinates and $\delta(\mathbf{x}, t)$ is the mass density contrast. The time evolution equation for δ during the linear regime ($\delta \ll 1$) reads (Peebles 1993):

$$\ddot{\delta}(\mathbf{x}, t) + 2H(t)\dot{\delta}(\mathbf{x}, t) = 4\pi G\bar{\rho}(t)\delta(\mathbf{x}, t) + \frac{c_s^2}{a(t)^2}\nabla^2\delta(\mathbf{x}, t). \quad (1)$$

Here, c_s is the sound speed, $a \equiv (1+z)^{-1}$ is the scale factor which describes the expansion and $H(t) = H_0[\Omega_m(1+z)^3 + \Omega_\Lambda]^{1/2}$. The second

term on the left hand side of the above equation represents the effect of cosmological expansion. This, together with the pressure support (second term on the right hand side) acts against the growth of the perturbation due to the gravitational collapse (first term on the right hand side). The pressure in the baryonic gas is essentially provided by collisions, while in the collisionless dark matter component the pressure support arises from the readjustment of the particle orbits. The above equation can be used also to follow separately the evolution of the different components of a multi-component medium. In this case, c_s would be the velocity of the perturbed component (which provides the pressure support) and $\bar{\rho}$ would be the density of the component which is most dominant gravitationally (as it drives the collapse of the perturbation). The equation has two independent solutions, one of which grows in time and governs the formation of structures. The total density contrast at any spatial location can be described in the Fourier space as a superposition of modes with different wavelengths:

$$\delta(\mathbf{x}, t) = \int \frac{d^3\mathbf{k}}{(2\pi)^3} \delta_{\mathbf{k}}(t) \exp(i\mathbf{k} \cdot \mathbf{x}), \quad (2)$$

where \mathbf{k} is the comoving wave number of the Fourier series. The evolution of the single Fourier components is then given by:

$$\ddot{\delta}_{\mathbf{k}} + 2H\dot{\delta}_{\mathbf{k}} = \left(4\pi G\bar{\rho} - \frac{k^2 c_s^2}{a^2} \right) \delta_{\mathbf{k}}. \quad (3)$$

This sets a critical wavelength, the Jeans length, at which the competing pressure and gravitational forces cancel (Jeans 1928):

$$\lambda_J = \frac{2\pi a}{k_J} = \left(\frac{\pi c_s^2}{G\bar{\rho}} \right)^{1/2}. \quad (4)$$

For $\lambda \gg \lambda_J$ the pressure term is negligible because the response time for the pressure wave is long compared to the growth time for the density contrast, and the zero pressure solutions apply. On the contrary, at $\lambda < \lambda_J$ the pressure force is able to counteract gravity and the density contrast oscillates as a sound wave. It is conventional to introduce also the Jeans mass as the mass within a sphere of radius $\lambda_J/2$:

$$M_J = \frac{4\pi}{3} \bar{\rho} \left(\frac{\lambda_J}{2} \right)^3. \quad (5)$$

In a perturbation with mass greater than M_J the pressure force is not counteracted by gravity and the structure collapses. This sets a limit on the scales that are able to collapse at each epoch and has a different

value according to the component under consideration, reflecting the differences in the velocity of the perturbed component.

Given the initial power spectrum of the perturbations, $P(k) \equiv |\delta_k|^2$, the evolution of each mode can be followed through eq. 3 and then integrated to recover the global spectrum at any time. The inflationary model predicts that $P(k) \propto k^n$, with $n = 1$. This value corresponds to a scale invariant spectrum, in which neither small nor large scales dominate. Although the initial power spectrum is a pure power-law, perturbation growth results in a modified final power spectrum. In fact, while on large scales the power spectrum follows a simple linear evolution, on small scales it changes shape due to the additional non-linear gravitational growth of perturbations and it results in a bended spectrum, $P(k) \propto k^{n-4}$. The amplitude of the power spectrum, however, is not specified by current models of inflation and must be determined observationally. Note that most of the power of the fluctuation spectrum of the standard CDM model is on small scales; therefore these are the first to become non-linear. In the following Section we will discuss the non-linear evolution of the dark matter halos.

2.3. NON LINEAR EVOLUTION: DARK MATTER HALOS

Because dark matter is made of collisionless particles that interact very weakly with the rest of matter and with the radiation field, density contrast in this component can start to grow at early times. Once a scale has become non-linear, the linear perturbation theory described in the previous Section does not apply anymore. In overdense regions ($\delta > 0$) the self-gravity of the local mass concentration will work against the expansion of the universe. This region will expand at a progressively slower rate compared to the background universe and, eventually, will collapse and form a bound object. The details of this process depend on the initial density profile. A simple and elegant approximation to describe the non-linear stage of gravitational evolution has been developed by Zel'dovich (1970). In this approach, sheetlike structures (“pancakes”) are the first non-linear structures to form from collapse along one of the principal axes, when gravitational instability amplifies density perturbations. Other structures, like filaments and knots, would result from simultaneous contractions along two and three axes, respectively. As the probability distribution for simultaneous contraction along more axes is small, in this scenario pancakes are the dominant features arising from the first stages of non-linear evolution. Numerical simulations have been employed to test the Zeldovich approximation, finding that it works remarkably well at the beginning of the non-linear evolution. At later times, however, its predictions are not as accurate.

Hence, although the perturbations in Gaussian density fields are inherently triaxial (e.g. Bardeen et al. 1986) and an ellipsoidal collapse would be more suitable to follow their evolution (e.g. Eisenstein & Loeb 1995; Sheth, Mo & Tormen 2001; Sheth & Tormen 2002), the simplest model is the one of a spherically symmetric, constant density region, for which the collapse can be followed analytically. At a certain point the region reaches the maximum radius of expansion, then it turns around and starts to contract. In the absence of any symmetry violation, the mass would collapse into a point. However, long before this happens, the dark matter experiences a violent relaxation process and quickly reaches virial equilibrium. If we indicate with z the redshift at which such a condition is reached, the halo can be described in terms of its virial radius, r_{vir} , circular velocity, $v_c = \sqrt{GM/r_{vir}}$, and virial temperature, $T_{vir} = \mu m_p v_c^2 / 2k_B$, whose expressions are (Barkana & Loeb 2001):

$$r_{vir} = 0.784 \left(\frac{M}{10^8 h^{-1} M_\odot} \right)^{1/3} \left[\frac{\Omega_m \Delta_c}{\Omega_m^z 18\pi^2} \right]^{-1/3} \left(\frac{1+z}{10} \right)^{-1} h^{-1} \text{kpc}, \quad (6)$$

$$v_c = 23.4 \left(\frac{M}{10^8 h^{-1} M_\odot} \right)^{1/3} \left[\frac{\Omega_m \Delta_c}{\Omega_m^z 18\pi^2} \right]^{1/6} \left(\frac{1+z}{10} \right)^{1/2} \text{ km s}^{-1}, \quad (7)$$

$$T_{vir} = 2 \times 10^4 \left(\frac{\mu}{0.6} \right) \left(\frac{M}{10^8 h^{-1} M_\odot} \right)^{2/3} \left[\frac{\Omega_m \Delta_c}{\Omega_m^z 18\pi^2} \right]^{1/3} \left(\frac{1+z}{10} \right) \text{ K}. \quad (8)$$

Here, μ is the mean molecular weight, m_p is the proton mass, and (Bryan & Norman 1998):

$$\Delta_c = 18\pi^2 + 82(\Omega_m^z - 1) - 39(\Omega_m^z - 1)^2, \quad (9)$$

$$\Omega_m^z = \frac{\Omega_m(1+z)^3}{\Omega_m(1+z)^3 + \Omega_\Lambda}. \quad (10)$$

Although spherical collapse captures some of the physics governing the formation of halos, their inner structure should be investigated through numerical simulations. Navarro, Frenk & White (1996, 1997 NFW) have simulated the formation of dark matter halos of masses ranging from dwarfs to rich clusters, finding that their density profile has a universal shape, independent of the halo mass, the initial density fluctuation spectrum and the cosmological parameters:

$$\rho(r) = \frac{\rho_s}{(r/r_s)(1+r/r_s)^2}, \quad (11)$$

where ρ_s and r_s are a characteristic density and radius. Usually, the quantity $c \equiv r_{vir}/r_s$, the concentration parameter, is introduced. As

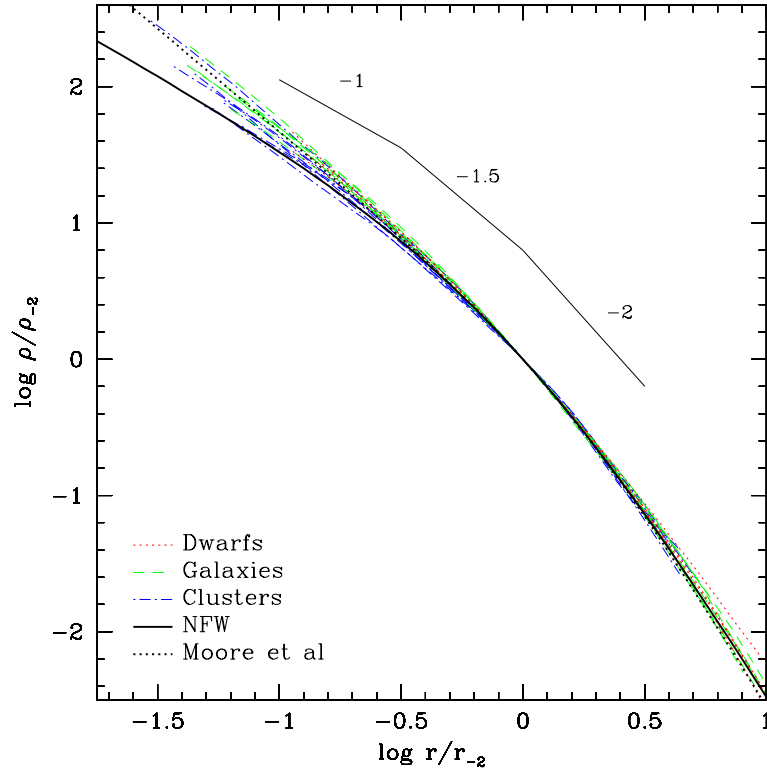


Figure 3. Density profiles of halos in a simulation by Navarro et al. (2004), scaled to the radius, r_{-2} , where the local logarithmic slope of the density profile takes the isothermal value of 2. Densities are scaled to $\rho_{-2} = \rho(r_{-2})$.

ρ_s can be written in terms of c , the above equation is a one-parameter form. An improved fitting formula (which reproduces the more gradual shallowing of the density profile towards the centre, the apparent lack of evidence for convergence to a well-defined central power law and the scatter in profile for different halos) has been developed by Navarro et al. (2004; eqs. 4-5). Fig. 3 shows that, with proper scaling, there is little difference in the shape of density profile of halos of different mass. The halo profiles are approximately isothermal over a large range of radii, but they are shallower ($\rho \propto r^{-1}$) near the center and steeper ($\rho \propto r^{-3}$) near the virial radius. The halo mass and the characteristic density are strongly correlated: low-mass halos are denser than more massive systems, and this reflects the higher collapse redshift of small halos. The existence of a universal shape is explained as the result of the violent relaxation process producing an equilibrium largely independent

of initial conditions. On the other hand, simulations which accurately follow the mass accretion histories of dark matter halos (Wechsler et al. 2002; Zhao et al. 2003), find an early phase of fast accretion, during which the inner structure of halos is mainly built, followed by a late phase of gentle accretion due to the secondary infall, which gives rise to an outer profile matching the universal form. Violent relaxation would be an active process only during the first phase.

A universal shape of the density profile with an internal cusp, has been confirmed by other authors (Moore et al. 1999; Del Popolo et al. 2000; Ghigna et al. 2000; Jing 2000; Jing & Suto 2000; Power et al. 2003; Fukushige, Kawai & Makino 2004), although it has been noted that the halos simulated by NFW are intentionally selected to be in an equilibrium state, and thus the shape would not be, strictly speaking, universal. Moreover, compared with the original NFW simulations, some of these studies find a steeper central profile ($\rho \propto r^{-\beta}$, $1.2 < \beta < 1.5$). This result could be related to an increased resolution of the numerical simulations (Ghigna et al. 2000), which nowadays can resolve down to less than 1% of the virial radius. The simulations by Reed et al. (2005a), which resolve 0.5% of the virial radius, confirm the existence of an internal cusp with $1 < \beta < 1.5$, depending on the mass of the halo (smaller halos have steeper cusps).

Not all the studies converge towards a universal shape of the halo density profile. Rather, some authors (e.g. Kravtsov et al. 1998; Subramanian, Cen & Ostriker 2000; Ricotti 2003; Cen et al. 2004) find that the scatter in the halo profile is large, depending on a different number of items. For example, the outer slope of the density profile strongly depends on the environment (Avila-Reese et al. 1999); the slope at 1% of the virial radius increases with decreasing halo mass (Jing & Suto 2000); the slope depends on the initial fluctuation field and cosmology (Nusser & Sheth 1999); the concentration parameter is not constant but decreases with increasing redshift and mass and halos in dense environment are more concentrated than isolated ones (Bullock et al. 2001; Macciò et al. 2007); clusters (dwarf galaxies) have steeper (shallower) cusps than Milky Way type galaxies with a concentration parameter that is a universal constant at the virialization redshift (Ricotti 2003). Some of the apparent tensions with works that find a universal shape of the density profile might be due to the different method used to analyse the simulations (Ricotti, Pontzen & Viel 2007).

Also on the presence of a central cusp there is no general agreement (e.g. Stoehr 2006). For example, if the effect of gas is included in the calculation a flat core is more plausible than a central cusp. In fact, if the gas is not initially smoothly distributed, but is concentrated in clumps, dynamical friction acting on these clumps dissipates their orbital energy

and deposits it in the dark matter, resulting in a heating of the halo and the formation of a finite, non-divergent core (El-Zant, Shlosman & Hoffman 2001; Mashchenko, Couchman & Wadsley 2006). A core would be also expected if the standard description of the post-collapse object were replaced by a more realistic truncated, non-singular, isothermal sphere (TIS) in virial and hydrostatic equilibrium (Shapiro, Iliev & Raga 1999). An alternative mechanism that could prevent a cusp forming is the following. The build up of dark matter halos by merging satellites inevitably leads to an inner cusp with $\beta > 1$. A flatter core with $\beta < 1$ exerts on each satellite tidal compression which prevents deposit of stripped satellite material in this region. An inner cusp is expected as long as enough satellite material is captured by the inner halo. If, instead, satellites are disrupted in the outer halo, a flatter core is maintained (Dekel, Devor & Hetzroni 2003). A flat core could be also explained with the existence of a dark spheroid of baryons of mass comparable with that of the cold dark matter component (Burkert & Silk 1997).

The density of the dark matter halos and their spatial distribution are better known. Two main methods have emerged to evaluate them: numerical computations that solve the equations of gravitational collapse, and analytical techniques that approximate these results with simple one-dimensional functions. While only numerical simulations give the spatial distribution of halos, analytical techniques are extremely useful as they are much faster and allow the analysis of a wide range of parameters. The most commonly applied method of this type was first developed by Press & Schechter (1974). In their approach, the abundance of halos at a redshift z is determined from the linear density field by applying a model of spherical collapse to associate peaks in the field with virialized objects in a full non-linear treatment. This simple model, later refined by Bond et al. (1991) and Lacey & Cole (1994), has had great success in describing the formation of structures and reproducing the numerical results. The method provides the comoving number density of halos, dn , with mass between M and $M + dM$ as (Peebles 1993):

$$M \frac{dn}{dM} = \left(\frac{2}{\pi}\right)^{1/2} \frac{-d(\ln\sigma)}{d(\ln M)} \frac{\rho_0}{M} \nu_c e^{-\nu_c^2/2}, \quad (12)$$

where ρ_0 is the present mean mass density, σ is the standard deviation of the density contrast smoothed through a certain window and ν_c is the minimum number of standard deviations of a collapsed fluctuation; Fig. 4 shows an application of the above equation.

While the model accurately reproduces the number density of the dark matter halos, it does not predict their spatial distribution, which

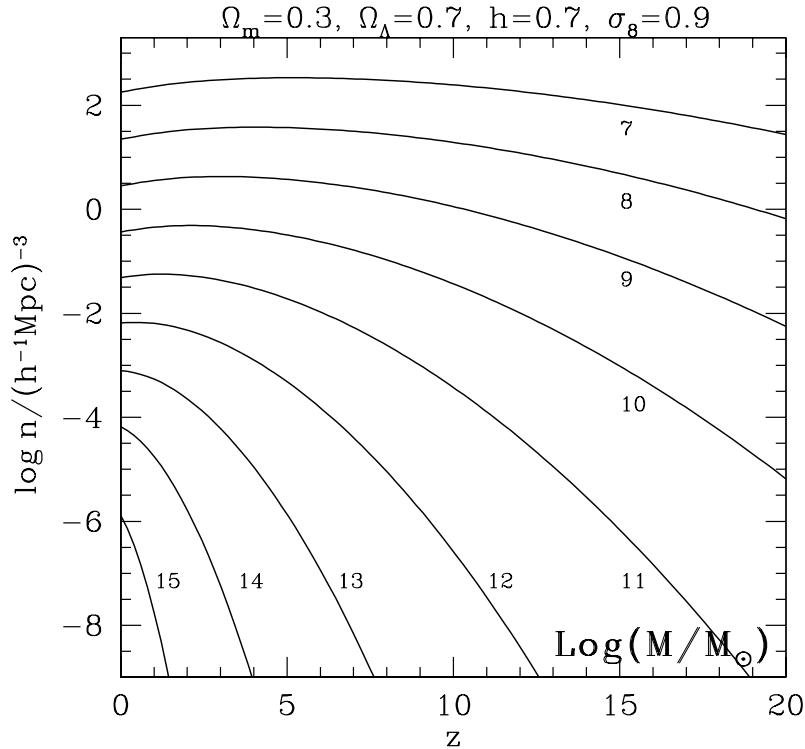


Figure 4. Each curve indicates the variation with redshift of the comoving number density of dark matter halos with masses exceeding a specific value M in the standard Λ CDM model. The label on each curve indicates the corresponding value of $\log(M/M_\odot)$ (see Mo & White 2002 for details).

is important to study structure formation. For this reason, Porciani et al. (1998) and Scannapieco & Barkana (2002) have developed analytical techniques to derive halo correlation functions and non-linear biasing, by studying the joint statistics of dark matter halos forming at two points. An alternative approach to the analytical determination of the abundance and spatial distribution of dark matter halos has been developed by Sheth & Tormen (2002). This is known as the excursion set approach and can be applied in the case of both a spherical (to reproduce the standard Press-Schechter results) and an elliptical collapse, which seems to be in better agreement with numerical simulations.

2.4. FORMATION OF PROTOGALAXIES

In contrast to dark matter, as long as the gas is fully ionized, the radiation drag on free electrons prevents the formation of gravitationally bound systems. When recombination (defined as the time at which the electron fraction has dropped to 0.1) occurs at $z_{rec} \approx 1250$ the primeval plasma combines into neutral atomic hydrogen. The residual ionization of the cosmic gas keeps its temperature locked to the CMB temperature through Compton scattering, down to a redshift $1 + z_t \approx 1000(\Omega_b h^2)^{2/5}$ (Peebles 1993). Following recombination, the nearly neutral matter decouples from the radiation and perturbations in this component are finally able to grow in the pre-existing dark matter halo potential wells and eventually form the first bound objects. The process leading to the virialization of the gaseous component of matter is similar to the dark matter one. In this case, during the contraction following the turnaround, the gas develops shocks and gets reheated to a temperature at which pressure support can prevent further collapse.

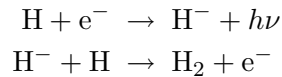
The mass of these first bound objects can be derived from eqs. 4-5, where c_s is the velocity of the baryonic gas. In particular, at $z > z_t$ the Jeans mass is time-independent, while at $z < z_t$, when the gas temperature declines adiabatically, M_J decreases with decreasing redshift:

$$M_J = 3.08 \times 10^3 \left(\frac{\Omega_m h^2}{0.13} \right)^{-1/2} \left(\frac{\Omega_b h^2}{0.022} \right)^{-3/5} \left(\frac{1+z}{10} \right)^{3/2} M_\odot. \quad (13)$$

As the determination of the Jeans mass is based on a perturbative approach, it can only describe the initial phase of the collapse. M_J is simply a limit given by the linear theory to the minimum mass that is able to collapse. It is worth noticing that the Jeans mass represents only a necessary but not sufficient condition for collapse: in addition, one has to require that the atomic/molecular cooling time is shorter than the Hubble time. The dynamical and chemical evolution of collapse must then be derived in detail to assess if the object can actually become a protogalaxy. In the following we will discuss the minimum mass of protogalaxies.

In the standard cosmological hierarchical scenario for structure formation, the objects which collapse first are predicted to have masses corresponding to virial temperatures $T_{vir} < 10^4$ K. Once the gas has virialized in the potential wells of dark matter halos, additional cooling is required to further collapse the gas and form stars. For a gas of primordial composition at such low temperatures the main coolant is molecular hydrogen. We define *Pop III objects* those for which H_2 cooling is required for collapse (note that in the literature Pop III objects

are sometimes also referred to as *minihalos*). After an H_2 molecule gets rotationally or vibrationally excited through a collision with an H atom or another H_2 molecule, a radiative de-excitation leads to cooling of the gas. This mechanism has been investigated in great detail by several authors (Lepp & Shull 1984; Hollenbach & McKee 1989; Martin, Schwarz & Mandy 1996; Galli & Palla 1998) and has been applied to the study of the formation of primordial small mass objects (e.g. Haiman, Thoul & Loeb 1996; Haiman, Rees & Loeb 1996; Abel et al. 1997; Tegmark et al. 1997; Abel et al. 1998; Omukai & Nishi 1999; Abel, Bryan & Norman 2000; Yoshida et al. 2003; Maio et al. 2007). Primordial H_2 forms with a fractional abundance of $\approx 10^{-7}$ at redshifts $\gtrsim 400$ via the H_2^+ formation channel. At redshifts $\lesssim 110$, when the CMB radiation intensity becomes weak enough to allow for significant formation of H^- ions, even more H_2 molecules can be formed:



Due to the lack of molecular data, it has unfortunately not been possible to follow the details of the H_2^+ chemistry as its level distribution decouples from the CMB. Assuming the rotational and vibrational states of H_2^+ to be in equilibrium with the CMB, the H_2^+ photo-dissociation rate is much larger than the one obtained by considering only photo-dissociations out of the ground state. Conservatively, one concludes that these two limits constrain the H_2 fraction to be in the range $10^{-6} - 10^{-4}$. In fact, both limits have been used in the literature (e.g. Lepp & Shull 1984; Palla, Galli & Silk 1995; Haiman, Thoul & Loeb 1996; Tegmark et al. 1997). If we assume that the H^- channel for H_2 formation is the dominant mechanism, i.e. that the H_2^+ photo-dissociation rate at high redshift is close to its equilibrium value, this leads to a typical primordial H_2 fraction of $f_{\text{H}_2} \approx 2 \times 10^{-6}$ (Anninos & Norman 1996) which is found for model universes that satisfy the constraint $\Omega_b h^2 = 0.019$. Hirata & Padmanabhan (2006) have recently revised the formation of primordial H_2 including (i) the effect of spectral distortions due to radiation emitted during hydrogen and helium recombination (which destroys H^- at $z > 70$) and (ii) a detailed treatment of the H_2^+ level population (which suppresses the efficiency of the H_2^+ formation channel). As a result, they find the slightly lower primordial value of 6×10^{-7} . It should be noted that the above effects do not influence the H_2 formation and cooling at lower redshift and in overdense conditions. In any case, this primordial fraction is usually lower than the one required for the formation of Pop III objects, but during the collapse the molecular hydrogen content can reach high enough values to trigger

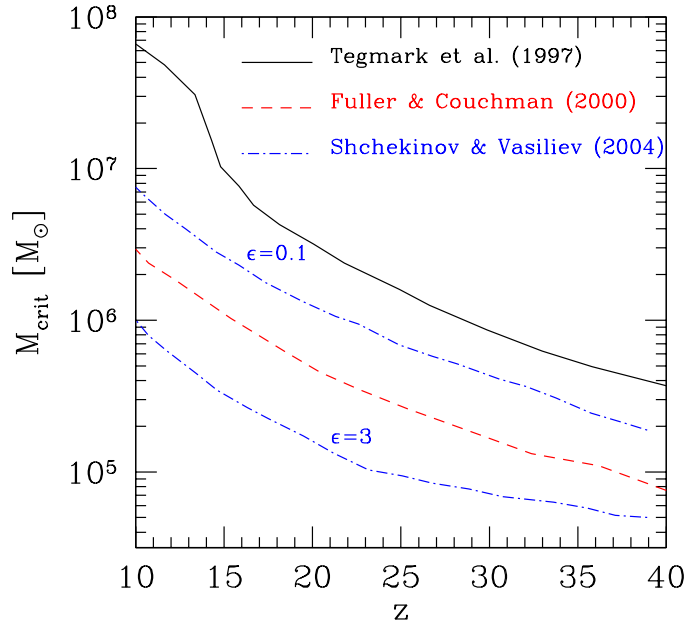


Figure 5. Minimum mass able to cool and collapse as a function of redshift in the formulation of Tegmark et al. (1997) (solid line), Fuller & Couchman (2000) (dashed) and Shchekinov & Vasiliev (2004) (dashed-dotted). The latter curves are derived for two different values of the rate of ionizing photon production by UHECR, $\epsilon = (0.1, 3)/(1+z)$ for the upper and lower line, respectively. See original papers for details.

star formation. Thus, the fate of a virialized lump depends crucially on its ability to rapidly increase its H_2 content during the collapse phase.

Haiman, Thoul & Loeb (1996), have followed the growth of spherical perturbations into the non-linear regime, using a one-dimensional spherical Lagrangian hydrodynamics code to follow the dynamical, thermal and non-equilibrium chemical evolution of the gas. They note that H_2 cooling becomes important only after virialization. Interestingly, though, they find that shell crossing by dark matter allows baryonic objects with masses well below the Jeans mass to form. A similar result is obtained by Haiman & Loeb (1997). Tegmark et al. (1997) have addressed the same question by calculating the evolution of the H_2 abundance for different halo masses and initial conditions for a

standard CDM cosmology. They use an analytical approach to the problem and find that the minimum baryonic mass M_b is strongly redshift dependent, dropping from $10^6 M_\odot$ at $z \approx 15$ to $5 \times 10^3 M_\odot$ at $z \approx 100$, as molecular hydrogen cooling becomes effective (see Fig. 5). They conclude that if the prevailing conditions are such that a molecular hydrogen fraction $\approx 5 \times 10^{-4}$ is produced, then the lump will cool, fragment and eventually form stars. This criterion is met only by larger halos, implying that for each virialization redshift there is a critical mass, M_{crit} , such that protogalaxies with total mass $M > M_{crit}$ will be able to collapse and form stars and those with $M < M_{crit}$ will fail. In a subsequent paper Nishi & Susa (1999) claim that the primordial number fraction of H_2 as calculated by Tegmark et al. (1997) is overestimated by about two orders of magnitude, because the destruction rate of H_2^+ by CMB radiation at high redshift is underestimated (Galli & Palla 1998). Thus, since their primordial value $\approx 10^{-4}$ is comparable to the one necessary to cool, their cooling criterion is not generally reliable. Fuller & Couchman (2000) have included the chemical rate network responsible for the formation of H_2 in an N-body hydrodynamical code, finding a value for M_{crit} considerably lower than the one derived by Tegmark et al. (1997) (see Fig. 5), since they have used a different molecular hydrogen cooling function and have included different chemical reactions, but they nevertheless find the same *critical molecular hydrogen fraction for the collapse of* $f_{\text{H}_2} \approx 5 \times 10^{-4}$. Most studies (e.g. Abel, Bryan & Norman 2000; Machacek, Bryan & Abel 2001; Reed et al. 2005b; O’Shea & Norman 2007) agree that *the minimum mass allowed to collapse is as low as* $10^5 M_\odot$.

The results of recent quantum mechanical calculations of cross-sections for rotational transitions within the vibrational ground state of HD enabled the contribution of HD to the primordial cooling function to be reliably calculated for the first time. In spite of its low abundance (10^{-3}) relative to H_2 , HD can be as important in the thermal balance of the primordial gas. In particular, the permanent dipole moment and lower rotational constant of HD favor cooling by HD at high densities and low kinetic temperatures (Flower 2000; Flower et al. 2000; Galli & Palla 2002), possibly allowing even smaller objects to collapse. If also vibrational transitions are taken into account, the cooling rate is increased (Lipovka, Núñez-Lopez & Avila-Reese 2005). In Fig. 6 a comparison between the H_2 and HD cooling rates is shown.

A considerably smaller characteristic mass (a factor ≈ 10 below the one predicted by Tegmark et al. 1997) of first luminous objects could also result from the presence of ultra-high energy cosmic rays (UHECRs), if they formed in the so-called top-to-bottom scenario from decaying superheavy dark matter particles with masses $\gtrsim 10^{12}$ GeV.

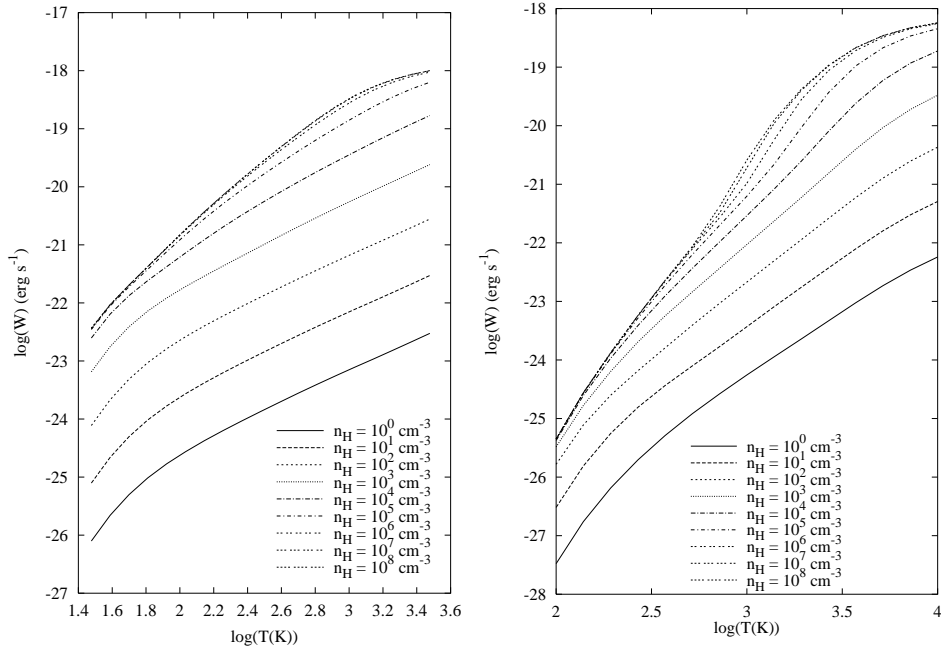


Figure 6. *Left panel:* cooling rate per HD molecule calculated for an ortho/para H_2 density ratio of 1 and an H/H_2 abundance ratio of 1. *Right panel:* cooling rate per H_2 molecule. The parameters are the same as in the left panel. For details refer to Flower et al. (2000) and Le Bourlot, Pineau des Forêts & Flower (1999).

In fact, the small additional electron fraction produced by UHECR photons results in more efficient H_2 and HD molecule formation and cooling (Shchekinov & Vasiliev 2004, 2006; see Fig. 5). Also the presence of an early population of cosmic rays (that would produce free electrons; Jasche, Ciardi & Enßlin 2007; Stacy & Bromm 2007) or of sterile neutrinos with masses of several keV (that would decay in X-rays and produce free electrons; Biermann & Kusenko 2006) could boost the formation of the above molecules. On the other hand, Ripamonti, Mapelli & Ferrara (2007b) find that moderately massive dark matter particle (as sterile neutrinos and light dark matter) decays and annihilations favors the formation of H_2 and HD, but at the same time induce heating of the gas. The net effect in this case is a slight increase of M_{crit} .

It should be noted though that all the above estimates do not take into account the large uncertainties on the reaction rates that govern the H_2 formation and that can have a non negligible impact on the prediction for early structure formation (e.g. Glover, Savin & Jappsen 2006).

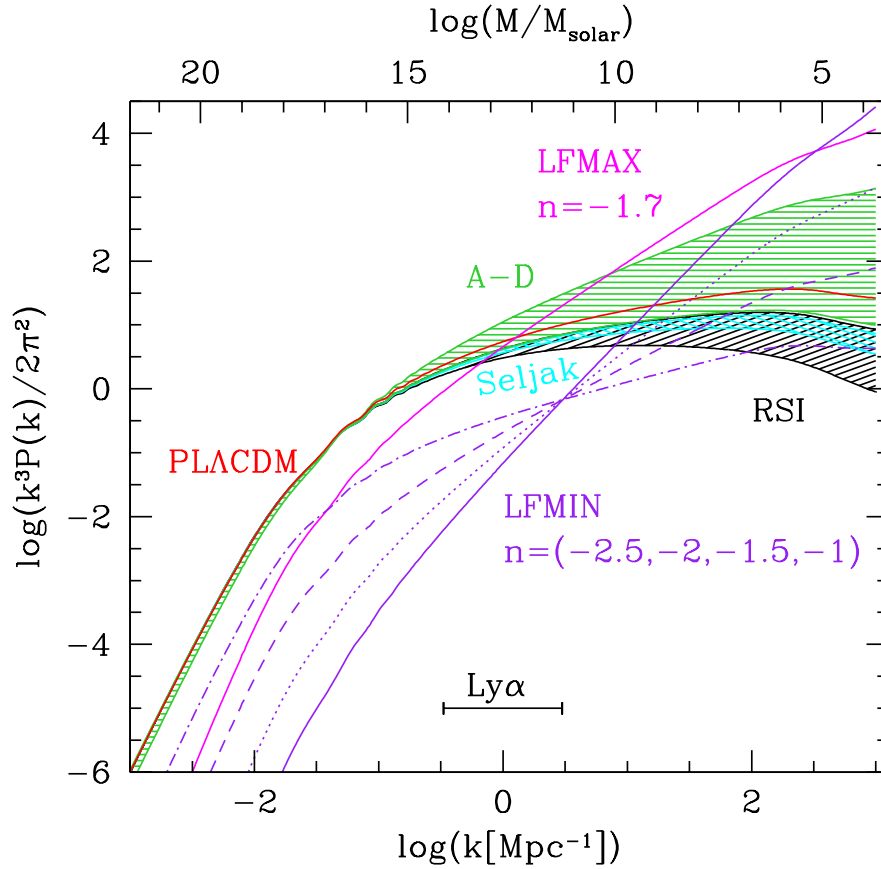


Figure 7. Matter power spectra (from Sugiyama, Zaroubi & Silk 2003). The WMAP best fitted power law result is indicated by PLACDM, and it is compared with the WMAP Running Spectral Index model (RSI) with errors combined with different additional data (hatched regions); the curves are isocurvature spectra with different prescriptions. See original paper for details.

2.5. KEY OBSERVATIONS

2.5.1. Cosmological Model

The main observational evidence in support of the inflationary scenario comes from observations of the CMB, showing temperature anisotropies on large angular scales (e.g. Hu et al. 2001), which are interpreted as the results of the primordial density fluctuations at the decoupling epoch. The same measurements confirm that the fluctuations are adiabatic and the value of the spectral index is the one predicted by the infla-

tionary model (Balbi et al. 2000, 2001; Pryke et al. 2002; Sievers et al. 2003), although there is an indication for a possible running spectral index (e.g. Spergel et al. 2003, 2007), with $n > 1$ on large scales and $n < 1$ on small scales (see Fig. 7 for possible power spectra). This is not confirmed though when the constraints from the recent Ly α forest and galaxy bias analysis of the SDSS¹⁴ (Sloan Digital Sky Survey) are combined with previous constraints from SDSS galaxy clustering, the latest supernovae and the WMAP results (Seljak et al. 2005; Seljak, Slosar & McDonald 2006). In fact, while CMB anisotropies, galaxy clustering from 2dF¹⁵ and SDSS, supernovae and weak lensing trace large scale structures (scales larger than 10 Mpc), tracers on smaller scale are needed to get correct information on the running spectral index. For the same reason, a tension is present also in the σ_8 value measured with or without the Ly α forest data, giving a higher value in the latter case (Seljak, Slosar & McDonald 2006; Viel, Haehnelt & Lewis 2006). More specifically, if only the 3-rd year WMAP data are used, $\sigma_8 = 0.76 \pm 0.05$, but the value increases with additional constraints (Spergel et al. 2007), in particular those from the Ly α forest (see Fig. 8; Seljak, Slosar & McDonald 2006; Viel, Haehnelt & Lewis 2006). In addition, analyses of the WMAP observations have reported evidence for a positive detection of non-Gaussian features (e.g. Chiang et al. 2003; R ath, Schuecker & Banday 2007; Eriksen et al. 2007; McEwen et al. 2008).

As discussed in the previous Sections, the amplitude of the power spectrum is not predicted by the model and has to be set observationally. Historically, this has been derived by comparing the observed CMB quadrupole anisotropies with theoretical ones (e.g. Wright et al. 1992; Efstathiou, Bond & White 1992) or from the abundance of galaxy clusters (see Sec. 2.1). More recently, this method has been complemented by measuring the amplitude of the power spectrum from available large galaxy redshift surveys (e.g. Lahav et al. 2002). The main problem related to the latter method is the attempt to estimate the distribution of matter using galaxies as tracers. In fact, as the galaxies form preferentially in high density regions of the mass distribution, they are more strongly correlated than the underlying distribution and an additional factor, the bias, should be specified. It has been found from the 2dF Galaxy Redshift Survey that, at least on large scales ($5 - 30h^{-1}$ Mpc), optically selected galaxies do indeed trace the underlying mass distribution (Verde et al. 2002).

An alternative method to measure $P(k)$ is based on observations of the high-redshift Ly α forest. The method is motivated by the physical

¹⁴ <http://www.sdss.org/>

¹⁵ <http://magnum.anu.edu.au/TDFgg/>

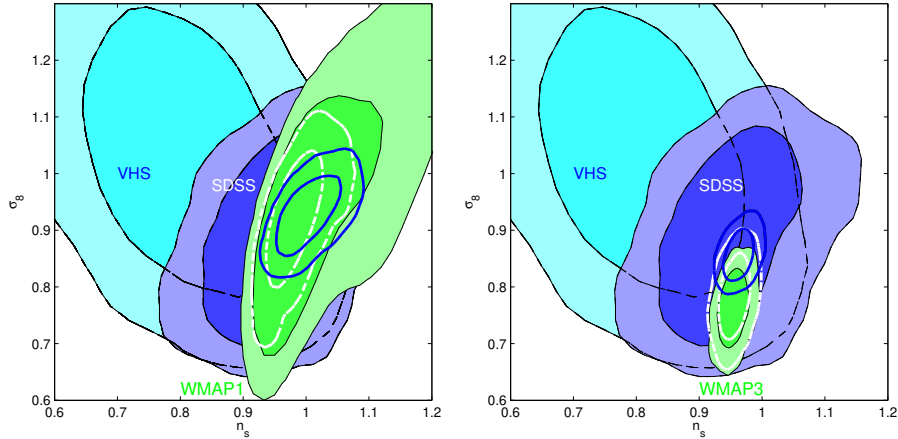


Figure 8. 1σ and 2σ likelihoods for σ_8 and the spectral index (in this figure indicated with n_s), marginalized over all other parameters. *Left panel:* constraints for 1-yr WMAP only (green), the LUQAS (Kim et al. 2004) + Croft et al. (2002) data set as analyzed by Viel, Haehnelt & Springel (2004, VHS) (cyan) and the SDSS Ly α forest data of McDonald et al. (2005) (blue). The thick dashed white empty contours refer to 1-yr WMAP + VHS, while the solid blue contours are for 1-yr WMAP + SDSS. *Right panel:* as in the left panel but for the 3-yr WMAP.

picture that has emerged from hydrodynamical cosmological simulations and related semi-analytical models, in which typical Ly α forest lines arise in a diffuse IGM. The thermal state of this low-density gas is governed by simple physical processes, which lead to a tight correlation between the Ly α optical depth, τ , and the underlying matter density (e.g. Bi & Davidsen 1997; Hui, Gnedin & Zhang 1997). Thus, as the transmitted flux in a QSO spectrum is $F = e^{-\tau}$, one can extract information about the underlying mass density field from the observed flux distribution (Croft et al. 1998, 1999, 2002; Viel, Haehnelt & Springel 2004; McDonald et al. 2005). These works confirm a basic prediction of the inflationary CDM scenario, an approximately scale invariant spectrum of primeval fluctuations modulated by a transfer function that bends it toward k^{n-4} on small scales. A possible caveat on these applications is that radiative transfer effects (Abel & Haehnelt 1999; Bolton, Meiksin & White 2004) are not included in current numerical simulations of the Ly α forest. Such effects might (i) blur the polytropic temperature-density relation derived from the simulations and usually adopted, hence introducing a non-negligible error on the predicted cosmological spectrum, and (ii) produce an inversion of the temperature-density relation in regions of low density (voids), as pointed out by Bolton et al. (2008).

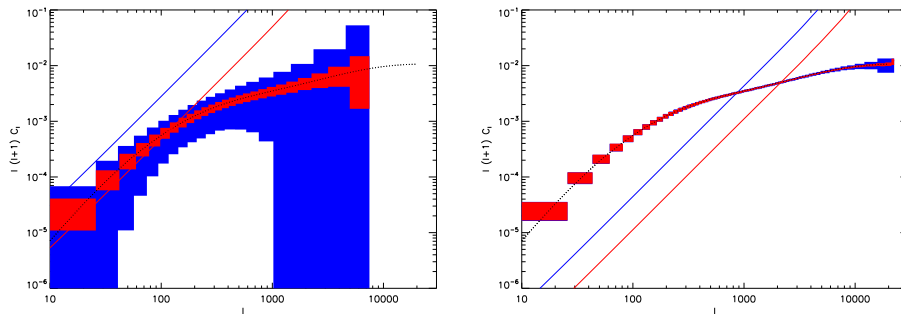


Figure 9. *Left panel:* Forecasts of the 1σ uncertainties in estimates of the convergence power spectrum for a LOFAR-1yr (blue) and LOFAR-3yr (red) type experiment of 21 cm weak lensing. The solid straight lines give the noise per mode, while the dotted curve is the underlying model power spectrum. *Right panel:* As the left panel but for a SKA type experiment. For details see Metcalf & White (2008).

It has been proposed (Loeb & Zaldarriaga 2004; Ali, Bharadwaj & Panday 2005; Barkana & Loeb 2005a; Bharadwaj & Ali 2005; Pillepich, Porciani & Matarrese 2007; Lewis & Challinor 2007; Cooray, Li & Melchiorri 2008; Mao et al. 2008) that a wealth of information about the initial density fluctuations (e.g. the presence of a running spectral index or deviations from gaussianity) could come from the 21 cm line in absorption against the CMB, from $z \approx 200$ down to lower redshift (as long as the effects of reionization are not dominant; Bowman, Morales & Hewitt 2007) or from the application of the Alcock-Paczyński test to the 21 cm line (Nusser 2005b). In these cases, measurements from upcoming radio telescopes in combination with CMB data, would produce constraints on cosmological parameters tighter than those obtained by CMB data alone (McQuinn et al. 2006). To make precision cosmology though, particular care should be used in the modeling of the spin temperature (Hirata & Sigurdson 2007).

Another 21 cm related experiment that could be used to reconstruct matter density fluctuations and to obtain constraints on cosmological parameter is weak lensing, using 21 cm emission as background source (see Fig. 9). Zahn & Zaldarriaga (2006) show that the lensing effect is lower compared to the case in which CMB fluctuations are used, but it has the advantage of retrieving information from a range of redshifts. In any case, 21 cm lensing experiments could provide constraints on cosmological parameters better than those obtained from comparably sized surveys of galaxy lensing (Metcalf & White 2007; Hilbert, Metcalf & White 2007; Lu & Pen 2008; Metcalf & White 2008).

2.5.2. *Dark Matter Halo Density Profile*

To prove or disprove the existence of a universal density profile for dark matter halos, accurate and extensive observations are needed. A method largely applied in the past to the study of the density profiles relies on HI rotation curves, although the spatial resolution of these observations is rarely good enough to set meaningful constraints. This is true both for the rotation curves of Low Surface Brightness Galaxies (LSBGs) and late-type dwarf galaxies (e.g. van den Bosch et al. 2000; Borriello & Salucci 2001; de Blok et al. 2001; van den Bosch & Swaters 2001; de Blok, Bosma & McGaugh 2003; Kleyna et al. 2003), which are sometimes consistent with both a constant density core and an inner cusp, indicating that HI rotation curves do not have enough resolution to discriminate between the two models. Only in a few cases it has been possible to derive a meaningful value of β (β is the power-index of the density profile in the central regions), giving $0.55 < \beta < 1.26$ at a 99.73% confidence level for an LSBG, which would be consistent with the NFW slope, and a $\beta < 0.5$ for two dwarf galaxies at the same confidence level (van den Bosch et al. 2000), more consistent with a flat core, as the nearby Ursa Minor dwarf spheroidal measured by Kleyna et al. (2003) or the sample of LBGs analysed by de Blok, Bosma & McGaugh (2003), who find an average $\beta = 0.2$. H_α rotation curves have a higher spatial resolution and rise more steeply in the inner parts than the HI rotation curves (Swaters, Madore & Trewhella 2000). Also optical rotation curves have been used, indicating that the NFW profile provides a good fit to 66% of the 400 galaxies in the sample analyzed by Jimenez, Verde & Oh (2003), while 68% of the galaxies are well fitted by an isothermal profile with a core. Based on optical and radio rotation curves, Persic, Salucci & Stel (1996) have confirmed that spiral galaxies have a universal rotation curve, characterized by one single free parameter, the (I-band) luminosity: low-luminosity spiral galaxies show rising rotation curves out to the optical radius, while high-luminosity ones are flat or even decreasing. These findings are reiterated in Salucci et al. (2007). On the other hand, recent HST observations have revealed that elliptical galaxies have cusps which continue toward the center until the resolution limit. Bright elliptical galaxies have a shallow cuspy core with $0.5 < \beta < 1$, while faint ones have $\beta \approx 2$ (Merritt & Fridman 1996).

Alternatively, the density profile of dark matter halos can be investigated through gravitational lensing experiments. It has been argued that radially distorted, gravitationally lensed images of background sources in galaxy clusters, the so-called radial arcs, require a flat core in the cluster density profile. This would be consistent with the high resolution map of a cluster in which a very smooth, symmetric and

non-singular core is observed (Tyson, Kochanski & Dell’Antonio 1998). Nevertheless, Bartelmann (1996) shows that the NFW profile can produce radial arcs despite its central singularity, as indicated by more recent observational data (Oguri, Taruya & Suto 2001). Observations of radial arcs though are so scarce that larger samples are needed for a more significant study.

Finally, as integral measures of weak gravitational lensing by dark matter halos, like the aperture mass, are sensitive to the density profile, these can be used to discriminate between an isothermal and a NFW profile. In particular, as the halo mass range probed by the aperture mass is much wider for a NFW profile, counts of halos with significant weak lensing signal are powerful discriminators (Bartelmann, King & Schneider 2001).

In summary, *available observations are not sufficient to significantly constrain the profile of dark matter halos.*

2.5.3. Formation of Protogalaxies

As primordial gas condenses within dark matter potential wells, forming luminous galaxies, it emits copious radiation. The energy radiated in this process is comparable to the gravitational binding energy of the baryons. Most of this cooling radiation is emitted by gas with $T < 20,000$ K. As a consequence, roughly 50% of it emerges in the Ly α line. As such emission is predominantly emitted from the outskirts of the collapsing system, it is less likely to be extinguished by dust (if present) than the more deeply embedded stellar light. This radiation has been advocated (Haiman, Spaans & Quataert 1999; Fardal et al. 2001) to explain the large (≈ 100 kpc), luminous ($L \approx 10^{44}$ erg s $^{-1}$) “blobs” of Ly α emission found in narrow-band surveys of $z \approx 3$ proto-clusters (Steidel et al. 2000) and similar arguments could be applied to higher redshift objects.

In addition to Ly α radiation, molecules could also produce a detectable signal. Flower & Pineau des Forêts (2001) calculated the spectrum of H $_2$ that is produced by collisional excitation in the shock waves generated when the speed of collapse becomes locally supersonic, finding that the rotational transitions within the vibrational ground state might be observable as inhomogeneities in the CMB. The H $_2$ cooling emission of forming galaxies has been studied by Omukai & Kitayama (2003), who discuss its observability (in particular the rotational lines 0-0S(3) at 9.7 μm and 0-0S(1) at 17 μm) through SAFIR¹⁶ (Single Aperture Far-Infrared observatory) and by Mizusawa, Omukai & Nishi (2005), who find that both rovibrational and pure rotational H $_2$ lines

¹⁶ <http://safir.jpl.nasa.gov/index.asp>

can be detected by SPICA¹⁷ (SPace Infrared telescope for Cosmology and Astrophysics), if emitted by metal-free clouds at $z < 10$.

3. First Stars

As described in the previous Section, hierarchical models of structure formation predict that the first collapsed objects have small masses and are of primordial composition and thus the formation and cooling of these objects is mainly governed by the molecular hydrogen chemistry. As the collapse proceeds, the gas density increases and the first stars are likely to form. However, the primordial star formation process and its final products are presently quite unknown. This largely depends on our persisting ignorance of the fragmentation process and on its relationship with the thermodynamical conditions of the gas. Despite these uncertainties, it is presently accepted that *the first stars, being formed out of a gas of primordial composition, are metal-free (Pop III stars)*. In addition to this theoretical justification, the existence of Pop III stars have been historically invoked for many different reasons. Among other issues (see e.g. Larson 1998 and Chiosi 2000 for more complete reviews), Pop III stars could help explaining:

- the gap between the Big Bang nucleosynthesis (BBN) metal abundances ($Z \approx 10^{-10} - 10^{-12}$) and those observed in the lowest metallicity Pop II stars ($Z \approx 10^{-4} - 10^{-3}$);
- the G-dwarf problem, i.e. the paucity of metal-poor stars in the solar neighborhood relative to predictions from simple models of chemical evolution (van den Bergh 1962; Norris, Peterson & Beers 1993; Primas, Molaro & Castelli 1994; Sneden et al. 1994);
- the oxygen anomaly or enhancement of α -elements in galactic metal-poor stars (Sneden, Lambert & Whitaker 1979) and the existence of extremely metal-poor stars showing s-process elements in their envelopes (Truran 1980);
- the missing mass in clusters of galaxies and galactic halos (White & Rees 1978) formed by their dark remnants;
- the reionization of the universe and the starting engine for the formation of the first galaxies;
- the constant lithium abundance of metal-poor halo stars (the Spite Plateau) which is lower than the predictions from the BBN (Piau et al. 2006; Asplund et al. 2006);

¹⁷ <http://www.ir.isas.ac.jp/SPICA/>

- the contaminants of the intergalactic medium as inferred from metallic absorption lines in the Ly α forest seen in quasar light;
- the cosmological helium abundance (Talbot & Arnett 1971; Marigo et al. 2003; Salvaterra & Ferrara 2003b);
- the formation of massive black holes.

In the following Section we will discuss the physical processes governing the formation and evolution of the first stars.

3.1. FORMATION PROCESS

To study the formation of the first stars it is crucial to understand the physics of the cooling in the early universe, primarily the number of channels available for the gas to cool, their efficiency (Rees & Ostriker 1977) and the physical processes that set the scales of fragment masses and hence the stellar mass spectrum. For a recent review see McKee & Tan (2008).

In general (e.g. Schneider et al. 2002), cooling is efficient when $t_{\text{cool}} \ll t_{\text{ff}}$, where $t_{\text{cool}} = 3nkT/2\Lambda(n, T)$ is the cooling time, $t_{\text{ff}} = (3\pi/32G\rho)^{1/2}$ is the free-fall time, n (ρ) is the gas number (mass) density and $\Lambda(n, T)$ is the net radiative cooling rate (in units of $\text{erg cm}^{-3}\text{s}^{-1}$). This efficiency criterium implies that the energy deposited by gravitational contraction cannot balance the radiative losses; as a consequence, temperature decreases with increasing density. When the above condition is satisfied, the cloud cools and possibly fragments. At any given time, fragments form on a scale, R_F , that is small enough to ensure pressure equilibrium at the corresponding temperature, i.e. $R_F \approx \lambda_J \propto c_s t_{\text{ff}} \propto n^{\gamma/2-1}$ where the sound speed $c_s = (\mathcal{R}T/\mu)^{1/2}$, $T \propto n^{\gamma-1}$, \mathcal{R} is the universal gas constant and γ is the polytropic index. Since c_s varies on the cooling timescale, the corresponding R_F becomes smaller as T decreases. Similarly, the corresponding fragment mass is the Jeans mass,

$$M_F \propto nR_F^\eta \propto n^{\eta\gamma/2+(1-\eta)}, \quad (14)$$

with $\eta = 2$ for filaments and $\eta = 3$ for spherical fragments (Spitzer 1978). This hierarchical fragmentation process comes to an end when cooling becomes inefficient because (i) the critical density for Local Thermodynamical Equilibrium (LTE) is reached or (ii) the gas becomes optically thick to cooling radiation. In both cases, t_{cool} becomes larger than t_{ff} . At this stage, the temperature cannot decrease any further and it either remains constant (if energy deposition by gravitational contraction is exactly balanced by radiative losses) or increases. The

necessary condition to stop fragmentation and start gravitational contraction within each fragment is that the Jeans mass does not decrease any further, thus favoring fragmentation into sub-clumps. From eq. 14, this implies the condition $\gamma \gtrsim 2(\eta - 1)/\eta$, which translates into $\gamma \gtrsim 4/3$ for a spherical fragment and $\gamma \gtrsim 1$ for a filament. Thus, a filament is marginally stable and contracts quasi-statically when $t_{\text{cool}} \approx t_{\text{ff}}$, and the gas becomes isothermal. Finally, when $t_{\text{cool}} \gg t_{\text{ff}}$ or the fragments become optically thick to cooling radiation, the temperature increases as the contraction proceeds adiabatically.

The very first generation of stars must have formed out of probably unmagnetized, pure H/He gas, since heavy elements can only be produced in the interior of stars. These characteristics render the primordial star formation problem very different from the present-day case, and lead to a significant simplification of the relevant physics. Nevertheless, the complexity and interactions of the hydrodynamical, chemical and radiative processes, have forced many early studies to use the steady state shock assumption, a spherical or highly idealized collapse model. Only recently have more realistic models been proposed. The first self-consistent three-dimensional cosmological hydrodynamical simulations were presented by Abel et al. (1998). Because of the limited spatial resolution, it was not possible to study the collapse to stellar densities and address the nature of the first objects. A higher resolution simulation has been performed by Bromm, Coppi & Larson (1999). They investigate, by means of a Smooth Particle Hydrodynamics (SPH) simulation, the evolution of an isolated $3\text{-}\sigma$ peak of mass $2 \times 10^6 M_{\odot}$ collapsing at $z \approx 30$. They find that the gas dissipatively settles into a rotationally supported disk, which eventually fragments in high density clumps ($n \approx 10^8 \text{ cm}^{-3}$) of mass $M_{\text{clump}} \approx 10^2 - 10^3 M_{\odot}$. Mass accretion and merging could subsequently raise the clump masses up to $\approx 10^4 M_{\odot}$. Changing initial conditions does not affect the disk formation and fragmentation, although the accretion and merging history can change (Bromm, Coppi & Larson 2002). Bromm & Loeb (2004) extended the results of the simulations by Bromm and collaborators down to a scale of ≈ 100 AU, following the collapse of the cloud to a fully-molecular protostellar core and the subsequent accretion phase. Although improving on previous simulations, radiative and mechanical feedback from the protostar on the accretion flow are not treated self-consistently.

Similar results have been found by Abel, Bryan & Norman (2000). Their simulation is based on a 3-D Adaptive Mesh Refinement (AMR), covering comoving scales from 128 kpc down to 1 pc and follows the collapse of primordial molecular clouds and their subsequent fragmentation within a cosmologically representative volume. The authors find

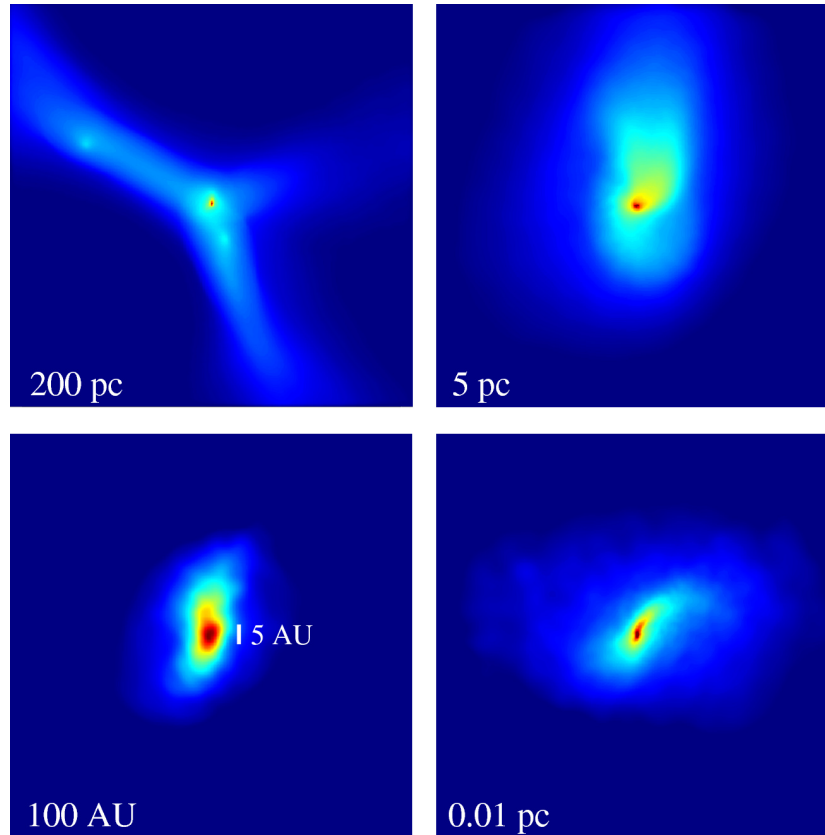


Figure 10. Projected distribution for a first star cosmological simulation at $z \approx 19$. The physical side length is indicated in each panel. See Yoshida et al. (2006) for details.

that these molecular clouds, of mass $M_{cloud} \approx 10^5 M_{\odot}$, will eventually form a cold (≈ 200 K) region at the center of the halo. Within this cold region a quasi-hydrostatic contracting clump with mass $\approx 200 M_{\odot}$ and density $n > 10^5 \text{ cm}^{-3}$ (and as high as $\approx 10^8 \text{ cm}^{-3}$) is found. The authors speculate that more than one clump could be found in the same object and that their number is likely to be proportional to the total amount of cooled gas. Clearly, the ability of these clumps to form stars is closely related to the strength of feedback processes (see Sec. 4). In addition, they suggest that the formation of a disk and its fragmentation, found by Bromm, Coppi & Larson (1999, 2002), is related to their highly idealized initial conditions (top-hat spheres that initially rotate as solid bodies on which smaller density fluctuations are imposed). But, although the process that leads to the formation of dense clumps in the two simulations is different, the final result is quite

similar, with very dense, massive protostellar clumps out of which the first star will eventually form. See Fig. 10 for a typical simulation of Pop III star formation.

It should be noted that the fragmentation and the thermal evolution depend strongly on the geometry of the clouds. For filamentary clouds the gravitational contraction is slower and the compressional heating rate is lower than for spherical ones. Hence, for the filamentary cloud the isothermality breaks down at higher density, leading to a smaller mass of the final clumps. Nakamura & Umemura (2001) have studied the collapse and fragmentation of a filamentary cloud using a two-dimensional hydrodynamic simulation, finding that the mass of the resulting clumps depends on the initial density of the collapsing cloud: filaments with low initial density ($n < 10^5 \text{ cm}^{-3}$) tend to fragment into dense clumps before the cloud becomes optically thick to the H_2 lines and the H_2 cooling with the three-body reaction is effective. This would result in clumps much more massive than some tens M_\odot . However, relatively dense filaments result in clumps of a few M_\odot (the result is in practice somewhat ambiguous as proper “initial conditions” are rarely known). The more effective H_2 cooling with the three-body reaction allows the filament to contract up to $n \approx 10^{12} \text{ cm}^{-3}$, when it becomes optically thick to H_2 lines and the radial contraction stops.

As the first stars form in regions of the universe corresponding to peaks of the large-density field, a significant contribution to the local overdensity comes from large wavelength fluctuations. Thus, simulations that take into account this effect are needed to properly study the formation of the first stars. Gao et al. (2007) have run a variety of SPH simulations (from cosmological scales down to densities at which the gas is no more optically thin to molecular hydrogen lines, i.e. $\approx 10^{10} \text{ cm}^{-3}$) to investigate whether there is a significant scatter in the properties of primordial star-forming clouds and whether they depend on redshift. They find that the formation path of primordial stars is similar in all simulations, independently on redshift and environment. The only difference is that the timescale of the formation is much shorter at high redshift. Moreover, the star-forming clouds exhibit a variety of morphologies and different accretion rates. In general though, at the end of the simulation, none of the clouds have fragmented and stars of more than a few tens of solar masses can be expected, although nothing more precise can be said on the mass of the first stars.

It should be noted that SPH simulations that do not resolve the Jeans mass at any time might suffer from the problem called artificial fragmentation, which, if not properly addressed, can induce errors in the determination of the mass of the stars and their Initial Mass Function (IMF). A relatively new technique, the particle splitting (Kitsionas

& Whitworth 2002), has been used by Martel, Evans & Shapiro (2006) to investigate the artificial fragmentation of a molecular cloud.

O’Shea & Norman (2007) have run AMR simulations with the code ENZO to study systematic effects in the formation of primordial protostellar cores. As previous studies, they find no evidence of fragmentation in any of their simulations, suggesting that Pop III stars forming in halos of $\sim 10^5 - 10^6 M_{\odot}$ form in isolation. The minimum mass of halos hosting Pop III stars ($\sim 10^5 M_{\odot}$), as well as other bulk halo properties, is independent on redshift.

Small mass clumps can be obtained when the collapse of a cloud is driven by HD or atomic cooling rather than molecular cooling. For example, Uehara & Inutsuka (2000) find that, including HD cooling, fragmentation of primordial gas can produce clumps as small as $0.1 M_{\odot}$, but more typically of few $\times M_{\odot}$ (Johnson & Bromm 2006; Yoshida, Omukai & Hernquist 2007). Thus, any physical process promoting HD formation might induce the formation of metal-free, small mass stars. Possible locations for such stars are relic H II regions (Johnson & Bromm 2006; Yoshida, Omukai & Hernquist 2007), shocked gas during merger of halos (Vasiliev & Shchekinov 2007), regions shocked by protostellar jets (Machida et al. 2006), SN explosions (Johnson & Bromm 2006) or during structure formation (Vasiliev & Shchekinov 2005; Johnson & Bromm 2006), in presence of cosmic rays (Jasche, Ciardi & Enßlin 2007; Stacy & Bromm 2007). Omukai (2001) argues that, in the absence of molecular hydrogen (which can be easily dissociated by feedback effects, Sec. 4), sufficiently massive clouds can start dynamical collapse by Ly α emission, two-photon emission and H $^-$ free-bound emission and continue to collapse almost isothermally at several thousand K along the “atomic cooling track”, until the clump mass is possibly reduced to about $0.03 M_{\odot}$. In conclusion, depending on the cooling mechanism, a clump of $M_{clump} \approx 10^2 - 10^3 M_{\odot}$ (H_2 cooling) or $M_{clump} \approx 0.1 - few \times 10 M_{\odot}$ (H or HD cooling) forms out of the collapsing molecular cloud.

Once a clump has reached densities of the order of $n \approx 10^8 \text{ cm}^{-3}$, the three-body formation of molecular hydrogen becomes dominant, the assumption of optically thin cooling begins to break down and radiative transfer effects become important. Tracking the subsequent evolution of these clumps is a very challenging problem, as it requires the simultaneous solution of the hydrodynamic equations and of line radiative transfer. In their pioneering work, Omukai & Nishi (1998) studied the contraction of protostellar clumps into stars, for various masses and initial conditions, by means of 1-D hydrodynamical calculations (see Fig. 11 for a summary of their results). Coincidentally, some of their initial conditions are very close to the final state of Abel, Bryan &

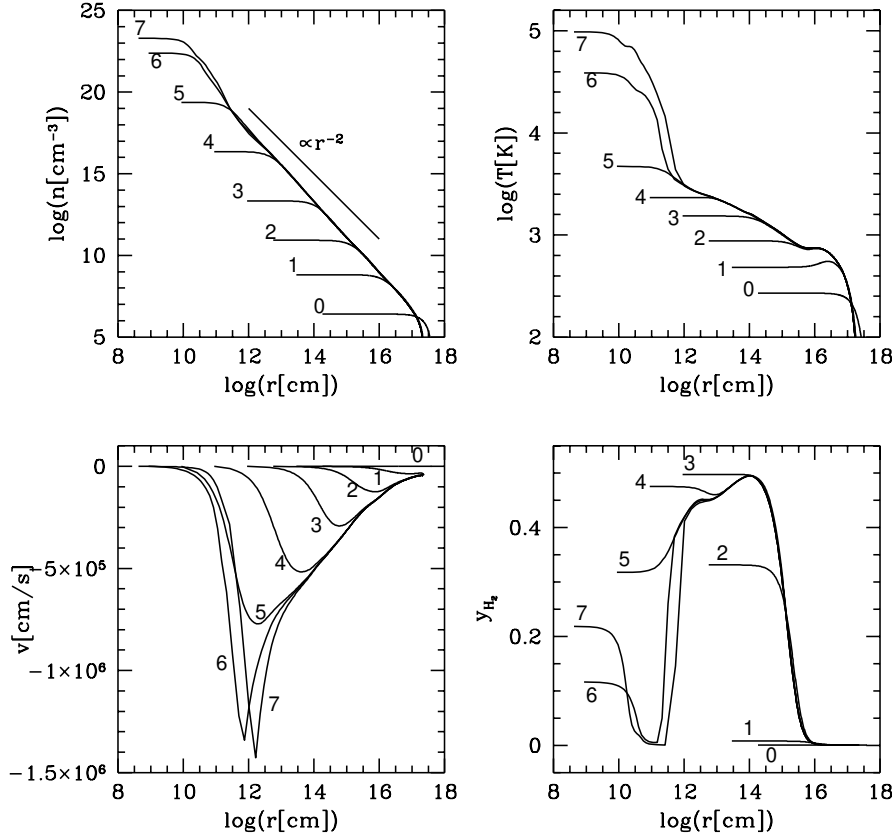


Figure 11. Evolutionary sequence for a contracting protostellar clump. Gas number density (upper left panel), temperature (upper right), velocity (lower left) and H_2 concentration (lower right) as a function of radial distance. (0) Initial conditions. (1) After 5.7×10^5 yr three-body processes are active in the central region and temperature inversion occurs: (2) 8.5×10^3 yr after (1). The cloud becomes optically thick to some lines: (3) 2.8×10^2 yr after (2). The central region becomes fully molecular: (4) 12 yr after (3). The central region becomes optically thick to H_2 CIA continuum: (5) 0.32 yr after (4). In the midst of dissociation: (6) 2.4×10^{-2} yr after (5). Shortly after the core formation: (7) 4.1×10^{-2} yr after (6). Final state. See Omukai & Nishi (1998) for details.

Norman (2000). The authors find that the evolution of a gravitationally unstable clump proceeds in a highly non-homologous fashion, with the central parts collapsing first. This runaway phase is induced by H_2 line radiation cooling up to densities of $n \approx 10^{14} \text{ cm}^{-3}$, and by H_2 collision-induced emission at higher densities. The resulting gas temperature is nearly constant at several 10^2 K and the innermost region of $\approx 1 M_\odot$ becomes fully molecular due to the three-body reaction. At densities

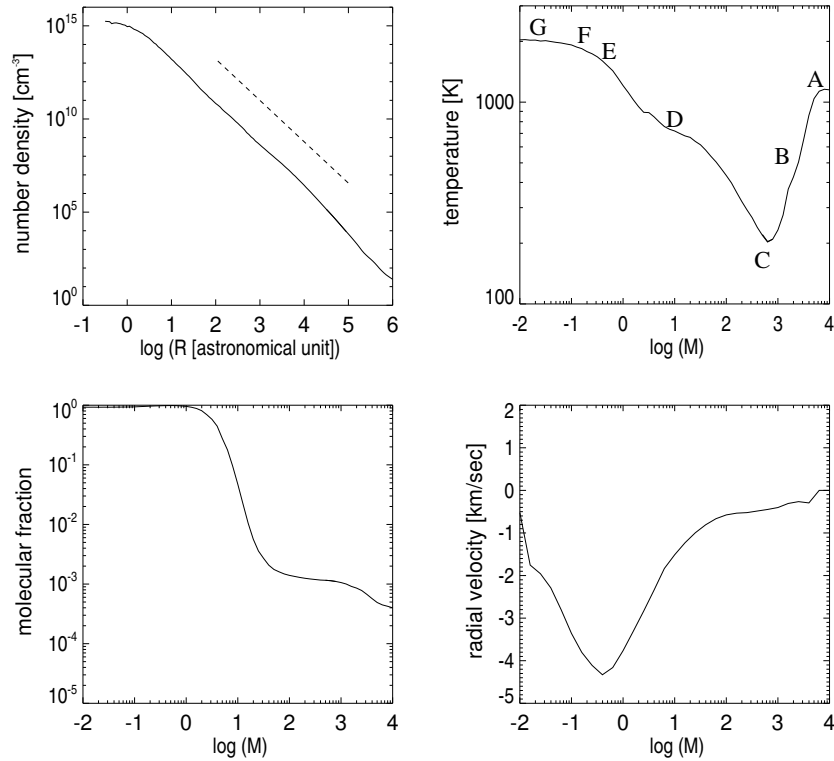


Figure 12. Radial profiles for density, temperature, molecular fraction, and infall velocity of a protostellar clump of primordial composition collapsing at redshift $z \approx 19$. The density is plotted as a function of distance from the center, whereas the other three quantities are plotted as a function of enclosed gas mass. The density profile is close to the power law $\propto R^{-2.2}$. The characteristic features in the temperature profile (marked AG) are described in Yoshida et al. (2006).

$n \approx 10^{16} \text{ cm}^{-3}$ the clump becomes optically thick to collision-induced absorption and H_2 dissociation works as an effective cooling agent. Finally, lacking further cooling mechanisms, at $n \approx 10^{22} \text{ cm}^{-3}$, a *small hydrostatic core of mass $\approx 10^{-3} M_\odot$ is formed. The core mass is highly independent of initial conditions.*

The same results have been confirmed by other authors (e.g. Ripamonti et al. 2002; Machida et al. 2006). Among them, Yoshida et al. (2006) and Yoshida, Omukai & Hernquist (2007) pushed 3-D simulations up to number densities of $\approx 10^{18} \text{ cm}^{-3}$, by improving in both physics implementation (a treatment of the regime in which the gas is optically thick to H_2 lines which allows to reach such densities) and resolution (which allows to reach a particle mass of 60 times the Earth mass and scale of about 1 AU). The run-away collapse of the internal

core is followed down to the scales of the central $1 M_{\odot}$ fully molecular core and the $0.01 M_{\odot}$ which is completely opaque to H_2 lines. No indication of fragmentation is found. Their results are quantitatively summarized in Fig. 12 in terms of the gas density, H_2 fraction, temperature and velocity profiles, which can be readily compared with earlier semi-analytical results obtained by Omukai & Nishi (1998) and discussed in Fig. 11. In spite of some minor discrepancies, the degree of agreement between the two widely different methods is outstanding.

As the core is surrounded by a large amount of reservoir gas (corresponding to the mass of the initial clump), in the absence of any effect quenching accretion, the protostar can grow by several orders of magnitude in mass by accreting the envelope matter. It has yet to be firmly established whether standard mechanisms proposed to halt the infall continue to work under primordial conditions: the radiation force could be opacity limited; bipolar flows need some magnetohydrodynamic acceleration process, and therefore seem to be excluded by the weak primordial magnetic field (e.g. Gnedin, Ferrara & Zweibel 2000; Langer, Puget & Aghanim 2003; Banerjee & Jedamzik 2005; Langer, Aghanim & Puget 2005).

The mass accretion rate onto the protostar can be written as $\dot{M}_{acc} \sim c_s^3/G$ (Stahler, Shu & Taam 1980), where c_s is the isothermal sound speed of the protostellar clump. Thus, the mass accretion rate is higher for protostars formed by atomic cooling because of the higher temperature of the protostellar clump, although the mass available for accretion is smaller. The evolution of zero-metal protostars in the main accretion phase has been recently studied by Omukai & Palla (2001) under a constant mass accretion rate of $4.4 \times 10^{-3} M_{\odot} \text{ yr}^{-1}$. The high accretion rate used, combined with a low opacity of the infalling gas due to the lack of dust grains, implies a milder effect of radiation pressure by protostellar photons and a higher inflow momentum. In fact, fast accreting protostars enter a phase of rapid expansion at a mass of $\approx 300 M_{\odot}$ when the luminosity becomes close to the Eddington limit. This event may determine the onset of a powerful stellar wind driven by radiation pressure that can effectively quench further accretion. The effect of a time-dependent accretion rate, initially as high as $\approx 10^{-2} M_{\odot} \text{ yr}^{-1}$ and rapidly decreasing once the stellar mass exceeds $M_{\star} \approx 90 M_{\odot}$, has been studied by Omukai & Palla (2003). They find that if $\dot{M}_{acc} < \dot{M}_{crit} \approx 4 \times 10^{-3} M_{\odot} \text{ yr}^{-1}$, stars with mass $\gg 100 M_{\odot}$ can form, provided there is sufficient matter in the parent clumps. For $\dot{M}_{acc} > \dot{M}_{crit}$ instead, the maximum mass limit decreases with \dot{M}_{acc} . In the context of cosmological simulations, a large scatter in the mass accretion rates ($10^{-4} - 10^{-2} M_{\odot}/\text{yr}$) is found, with a general trend of lower accretion rates at higher redshift (O’Shea & Norman 2007). Although

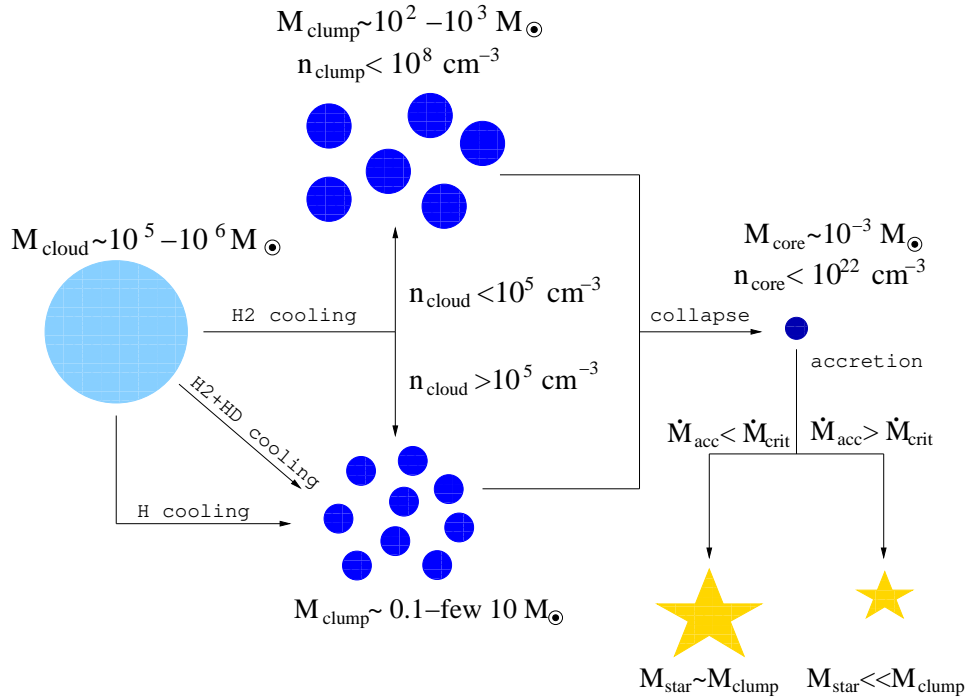


Figure 13. Summary of the relevant physical processes and possible evolution paths for Pop III star formation.

this points toward a *minimum mass of Pop III stars* $\gg 1 M_{\odot}$, the *upper limit remains uncertain*. Similar numbers ($10^{-4} - 10^{-1} M_{\odot}/\text{yr}$) are obtained by Yoshida et al. (2006), who also estimate a final stellar mass of 60-100 M_{\odot} .

An ingredient which has so far received little attention but which could be quite important to determine the final mass of the first stars, is rotation of the infalling envelope. If protostellar clumps are rotating above a critical value of the rotational energy, which is found to be about 10^{-5} times the gravitational energy (Machida et al. 2007), fragmentation of the clump might occur. Under the conditions prevailing at the time of first stars formation, such value is not implausible and as a result a non-negligible fraction of this ancient stellar population might be constituted by binary or multiple systems. In addition, as pointed out by Tan & McKee (2004), rotation might also lead to dramatic differences in the way the H II region breaks out of the infalling envelope and in radiation pressure effects. Radiation pressure, in particular, appears to be the dominant mechanism for suppressing infall, becoming dynamically important around 20 M_{\odot} .

Table I. Classification of stars. The columns indicate: the name of the stellar type, their typical metallicity Z and mass M_* , their formation mechanism or site.

Name	Z	$M_* [M_\odot]$	Formation
Pop IIIa	0	$\gtrsim 100$	minihalos, H_2 cooling
Pop IIIb	0	$\gtrsim 10$	HD, H cooling
Pop II.5	$\lesssim Z_{crit}$	$\gtrsim 10$	pre-enriched SF sites
Pop II	$> Z_{crit}$	local IMF	metal enriched SF sites

As previously mentioned, primordial magnetic fields seem to be extremely weak. But during the collapse magnetic pressure increases more rapidly than gas pressure. For this reason, although the initial magnetic field is small, it can be amplified by 10 orders of magnitude and thus affect the formation of a star. Machida et al. (2006) use 3-D magneto-hydrodynamical (MHD) simulations to follow the collapse of a slowly rotating spherical cloud of $5 \times 10^4 M_\odot$ with central number density n_c , permeated by a uniform magnetic field. They find that if the initial field is $> 10^{-9}(n_c/10^3 \text{cm}^{-3})^{2/3}$ G, a protostellar jet forms blowing away 3-10% of the accreting matter and reducing the final mass of the star. Studies in this area are still in their infancy and definite conclusions have to await for more detailed calculations. To summarize, *if $\dot{M}_{acc} < \dot{M}_{crit}$ protostellar cores can accrete all the matter of the parent clumps and possibly become very massive stars of $M_* \sim M_{clump}$; otherwise accretion is less efficient and $M_* \ll M_{clump}$.* In Fig. 13 a summary of the relevant physical processes and possible paths for Pop III star formation is sketched. A possible classification scheme of Pop III and Pop II stars has been recently agreed upon at the First Stars III Conference held in Santa Fe (O’Shea et al. 2008). A slightly modified version of such classification is reported in Tab. I. Here III, II.5 and II indicate a metallicity sequence, while (differently from the original classification), *a* and *b* indicate a temporal sequence, i.e. first and second generation of Pop III stars.

3.1.1. Initial Mass Function

As we have seen above, recent studies seem to indicate that the first stars were massive. Nevertheless, as the primordial fragmentation process is very poorly understood, the distribution of masses with which stars are formed, the so-called IMF, is still very uncertain. The determination of the IMF is also of basic importance because, although the luminosities of galaxies depend primarily on stars of masses $\approx 1 M_\odot$,

metal enrichment and feedback effects on galactic scales depend on the number of stars with masses above $\approx 10 M_{\odot}$.

For many years, beginning with Schwarzschild & Spitzer (1953), there have been speculations in the literature that the IMF was dominated by massive stars at early times. More recently, Larson (1998) has proposed a modified Salpeter IMF for the first stars. If we define N as the number of stars formed per logarithmic mass interval, the standard parameterization of the Larson IMF reads:

$$dN/d\log M_{\star} \propto (1 + M_{\star}/M_c)^{-1.35}, \quad (15)$$

where M_c is a characteristic mass scale, related to the Jeans mass, and more in general to the scale at which there is a transition from a chaotic regime dominated by non-thermal pressure on larger scales to a regular regime dominated by thermal pressure on smaller scales. As the Jeans mass depends on temperature and pressure of a star-forming cloud as $T^2 p^{-1/2}$, a variable mass scale M_c naturally arises with a higher value at earlier times. The essential effect of this type of variability would be to alter the relative number of low-mass to large-mass stars formed, with an *IMF biased toward massive stars at high redshift*.

If indeed the mass of the clumps originating the protostars depends on the density of the collapsing cloud, as discussed earlier, this could produce a bimodal IMF with peaks of $\approx 10^2$ and $1 M_{\odot}$ (Nakamura & Umemura 2001). A similar IMF would arise in a scenario in which the first very massive stars create intense radiation fields which deplete the H_2 content inside their parent clouds, decreasing, as mentioned earlier, the subsequent fragmentation mass scale. The resulting IMF would be bimodal, with a high-mass peak at $\approx 40 M_{\odot}$ and a low-mass peak at $\approx 0.3 M_{\odot}$ (Omukai & Yoshii 2003). The high-mass portion of the IMF is a very steep function of mass, with a power-law index of -4; thus, although some of the first stars are very massive, their typical mass scale is smaller. A Larson IMF with an upper cut off of $\sim 100 M_{\odot}$ seems to be favored also by theoretical models of the Pop III to Pop II transition (see below) which include constraints from the NICMOS UDFs field (Bouwens et al. 2005) and the WMAP satellite (Spergel et al. 2003).

On the contrary, it has been known since the work of Salpeter (1955) that the present-day IMF of stars in the solar neighborhood can be approximated by a declining power-law for masses above $1 M_{\odot}$, flattening below $0.5 M_{\odot}$, and possibly even declining below $0.25 M_{\odot}$ (Scalo 1986, 1998; Kroupa 2001). While the behavior of the IMF at the lowest masses remains uncertain because of the poorly known mass-luminosity relation for the faintest stars, above $\approx 1 M_{\odot}$ there is a consensus on the universality of the power-law part of the IMF, with

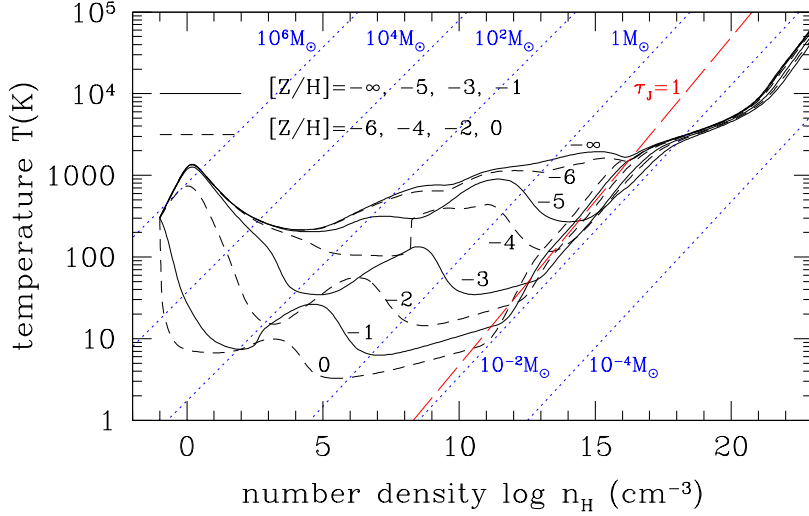


Figure 14. Temperature evolution of prestellar clouds with different metallicities. Those with metallicities $[Z/H]=-\infty$ ($Z=0$), -5 , -3 , and -1 (-6 , -4 , -2 , and 0) are shown by solid (dashed) lines. Only the present-day CMB is considered as an external radiation field. The lines for constant Jeans mass are indicated by thin dotted lines. The positions where the central part of the clouds becomes optically thick to continuum self-absorption is indicated by the thin solid line. The intersection of the thin solid line with each evolutionary trajectory corresponds to the epoch when the cloud becomes optically thick to the continuum. To the right of this line, the clouds are optically thick and there is little radiative cooling. See Omukai et al. (2005) for details.

$dN/d\log M_\star \propto M_\star^{-1.35}$ (von Hippel et al. 1996; Hunter et al. 1997; Massey 1998).

Following the early study by Yoshii & Sabano (1980), it has been proposed (Bromm et al. 2001; Schneider et al. 2002; Bromm & Loeb 2003; Santoro & Shull 2006; Smith & Sigurdsson 2007) that *the mechanism inducing a transition from a top-heavy to a more conventional IMF is metal enrichment*. In fact, it is only when metals change the composition of the gas that further fragmentation occurs producing stars with significantly lower masses. Bromm et al. (2001) have numerically studied the effect of metals on the evolution of the gas in a collapsing dark matter minihalo, using an SPH simulation, for two different values of metallicity. They have shown that fragmentation of the gas cloud proceeds very differently in the two cases and concluded that there exists a critical metallicity, Z_{cr} , which marks a transition from a high-mass to a low-mass fragmentation mode. The value of Z_{cr} is estimated to be $10^{-4} - 10^{-3} Z_\odot$. These values should be taken as a

first order approximation since the model does not include some key cooling agents, such as H_2 , other molecules and dust grains. Santoro & Shull (2006), though, found similar values including cooling from CII, OI, SiII and FeII lines and from H_2 . The same values are found by Smith & Sigurdsson (2007) using the code ENZO to follow the formation and fragmentation of clouds starting from cosmological initial conditions. Schneider et al. (2002) though have investigated the problem including a much larger number (> 500) of chemical reactions. Using the 1-D code described in Omukai (2000), they have studied the fragmentation properties of a gravitationally unstable gas cloud for different initial metallicities in the range $0 - 1 Z_\odot$. Including the effect of H_2 and molecular cooling as well as the presence of dust grains in the thermal evolution, they concluded that the transition between the two fragmentation modes takes place for metallicities in the range $10^{-6} - 10^{-4} Z_\odot$. This critical threshold is almost two orders of magnitude lower than that found by Bromm and collaborators because the fragmentation properties of a gas cloud with $Z = Z_{\text{cr}}$ depend on the fraction of metals depleted onto dust grains rather than on the metals present in the gas phase (Schneider et al. 2003). A more recent study by Omukai et al. (2005), which includes also the chemistry of D previously neglected, confirms the above results (see Fig. 14). The equation of state provided by the authors at different metallicities has been used in SPH simulations of primordial star formation by Tsuribe & Omukai (2006) and Clark, Glover & Klessen (2008). Both simulations confirm the results of the 1-D calculations (see also Tsuribe & Omukai 2008) but show also that, if substantial rotation or elongation of the collapsing core is present, fragmentation can happen at metallicities $Z > 10^{-6} Z_\odot$ (Tsuribe & Omukai 2006) or even lower.

Finally, Omukai & Palla (2003) have considered the effect of heavy elements with abundances in the range $Z = 5 \times 10^{-5} - 5 \times 10^{-3} Z_\odot$ on the accretion process. The main evolutionary features of protostars are similar to those of metal-free objects, except that the value of \dot{M}_{crit} increases for metal-enriched protostars. Since the accretion rate is lower in a slightly polluted environment, the condition $\dot{M}_{\text{acc}} < \dot{M}_{\text{crit}}$ is expected to be more easily met and the formation of massive stars is favored, provided the clump mass is large enough.

3.2. EMISSION SPECTRUM

The metal-free composition of *the first stars* restricts the stellar energy source to proton-proton burning rather than to the more efficient CNO cycle. Consequently, they *are hotter and have harder spectra than their present-day counterparts of finite metallicity*. These unique physical

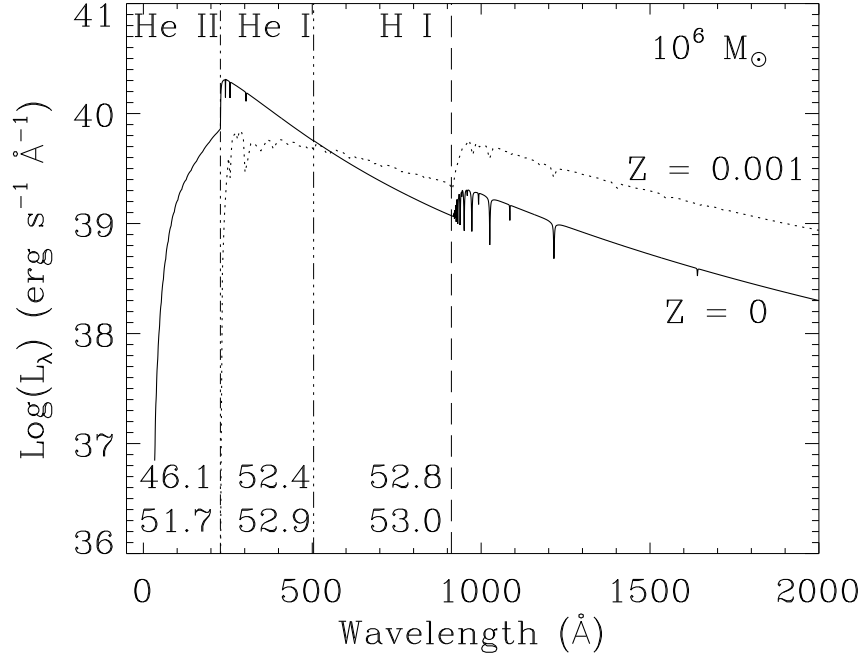


Figure 15. Synthetic spectra of Pop II and Pop III clusters of $10^6 M_{\odot}$ with a Salpeter IMF. The numbers in the lower left corner, near each continuum mark, represent the rate (in units of photons s^{-1}) of ionizing photons production (log) for that continuum (Tumlinson & Shull 2000).

characteristics enhance the ionizing photon production of Pop III stars, particularly in the He II continuum, in which they produce up to $\approx 10^5$ times more photons than Pop II (see Fig. 15 for a comparison of Pop II and Pop III emission spectra). If, in addition, the first stars were also massive, they would be even hotter and have harder spectra. Bromm, Kudritzki & Loeb (2001) find that metal-free stars with mass above $300 M_{\odot}$ resemble a blackbody with an effective temperature of $\approx 10^5$ K, with a production rate of ionizing radiation per stellar mass larger by ≈ 1 order of magnitude for H and He I and by ≈ 2 orders of magnitude for He II than the emission from Pop II stars. In the less extreme case of metal-free stars with masses $< 100 M_{\odot}$, Tumlinson, Shull & Venkatesan (2003) predict that the H-ionizing photon production takes twice as long as that of Pop II to decline to 1/10 of its peak value. Nevertheless, due to the redward stellar evolution and short lifetimes of the most massive stars, the hardness of the ionizing spectrum decreases rapidly,

leading to the disappearance of the characteristic He II recombination lines after ≈ 3 Myr in instantaneous bursts (Schaerer 2002, 2003).

Models of emission spectra from primordial stars have been calculated by different authors for stars with masses up to $\approx 50 M_{\odot}$ (Brocato et al. 2000 and Cassisi, Castellani & Tornambè 1996 in the implementation of Ciardi et al. 2001), $\approx 100 M_{\odot}$ (Tumlinson & Shull 2000; Tumlinson, Shull & Venkatesan 2003) and $\approx 1000 M_{\odot}$ (Bromm, Kudritzki & Loeb 2001; Marigo et al. 2003). In particular, Marigo et al. (2003) have carried out extensive evolutionary calculations over a large range of stellar masses ($0.7 M_{\odot} \leq M_{\star} \leq 1000 M_{\odot}$), covering the H- and He-burning phases and allowing for a moderate overshooting from convective cores, but neglecting rotation. Additionally, for very massive stars ($M_{\star} > 120 M_{\odot}$), they apply recent mass-loss rate prescriptions for the radiation-driven winds at very low metallicities and the amplification of the loss rate caused by stellar rotation. Nevertheless, the above studies are based on some strong simplifying assumptions; e.g. all the stars are assumed to be on the Zero Age Main Sequence (ZAMS) (i.e. stellar evolution is neglected) and nebular continuum emission is not included. In particular, this last process cannot be neglected for metal-poor stars with strong ionizing fluxes, as it increases significantly the total continuum flux at wavelengths redward of $\text{Ly}\alpha$ and leads in turn to reduced emission line equivalent widths (Schaerer 2002, 2003). Nebular emission has been included in a more complete and extended study by Schaerer (2002, 2003), who presents realistic models for massive Pop III stars and stellar populations based on non-LTE model atmospheres, recent stellar evolution tracks and up-to-date evolutionary synthesis models, including also different IMFs. For more recent tabulated emission rates refer also to Heger & Woosley (2008). In Table II we have summarized the emission properties of Pop III stars. The numbers have been derived integrating the ionizing photon rate in the absence of stellar winds given in Schaerer (2002) over different IMFs, i.e. Salpeter, Larson and Gaussian.

3.3. FINAL FATE

As the pp-chain is never sufficiently efficient to power massive stars, stars of initial zero metallicity contract until central temperatures $\geq 10^8$ K are reached and CNO seed isotopes are produced by the triple- α process. As a consequence of their peculiar behavior in hydrogen burning, the post-main sequence entropy structure of stars of zero initial metallicity is different from that of stars having a metallicity above $10^{-5} Z_{\odot}$. A major uncertainty in the evolution of these stars is mass loss. Although radiative mass loss is probably negligible for stars

Table II. ZAMS Properties of Pop III stars. The columns show: the IMF type; the IMF mass interval [M_{\odot}]; the characteristic (central) mass scale for the Larson (Gaussian) IMF [M_{\odot}]; rms deviation for the Gaussian IMF [M_{\odot}]; logarithm of $H\text{ I}$ -, $He\text{ I}$ -, $He\text{ II}$ -ionizing and H_2 -dissociating photons per baryon in Pop III stars.

IMF	ΔM	M_c	σ_c	H I	He I	He II	H ₂
Salpeter	1-100			4.235	3.919	2.010	4.374
Salpeter	1-500			4.355	4.070	2.750	4.469
Salpeter	10-100			4.705	4.410	2.518	4.799
Salpeter	10-500			4.753	4.483	3.175	4.833
Salpeter	50-500			4.869	4.632	3.540	4.925
Larson	1-100	5		4.505	4.201	2.342	4.622
Larson	1-100	10		4.578	4.280	2.454	4.686
Larson	1-100	50		4.703	4.420	2.698	4.791
Larson	1-500	5		4.604	4.331	3.056	4.699
Larson	1-500	10		4.670	4.404	3.160	4.757
Larson	1-500	50		4.782	4.533	3.402	4.851
Larson	1-500	100		4.808	4.567	3.490	4.872
Larson	10-100	50		4.778	4.500	2.781	4.856
Larson	10-500	50		4.822	4.576	3.447	4.887
Larson	10-500	100		4.834	4.594	3.518	4.895
Larson	50-500	100		4.865	4.636	3.629	4.920
Gaussian	1-500	50	5	4.835	4.568	2.659	4.902
Gaussian	1-500	50	10	4.832	4.564	2.697	4.900
Gaussian	1-500	100	10	4.887	4.634	3.370	4.949
Gaussian	1-500	100	20	4.885	4.632	3.354	4.947
Gaussian	10-500	50	5	4.835	4.568	2.659	4.902
Gaussian	10-500	50	10	4.832	4.564	2.697	4.900
Gaussian	10-500	100	10	4.887	4.634	3.370	4.949
Gaussian	10-500	100	20	4.885	4.632	3.354	4.947
Gaussian	50-500	100	10	4.887	4.634	3.370	4.949
Gaussian	50-500	100	20	4.885	4.632	3.357	4.947

of such low metallicity, they still might lose an appreciable fraction of their mass because of nuclear-driven pulsations. Smith & Owocki (2006) started from the observational evidence that nebulae around luminous blue variables (LBV) and LBV candidates (e.g. η Car) show high ejecta masses, to discuss the possibility that the mass loss during the evolution of very massive stars may be dominated by optically thick, continuum-driven outbursts or explosions, rather than by steady

line-driven winds. Unlike the latter, the former may be independent of metallicity and play an important role in the evolution of Pop III stars. In any case, recent theoretical analysis on the evolution of metal-free stars predict that their fate can be classified as follows (see also the comprehensive paper by Heger & Woosley 2008):

- Stars with masses $10 M_{\odot} \lesssim M_{\star} \lesssim 40 M_{\odot}$ proceed through the entire series of nuclear burnings accompanied by strong neutrino cooling: hydrogen to helium, helium to carbon and oxygen, then carbon, neon, oxygen and silicon burning, until finally iron is produced. When the star has built up a large enough iron core, exceeding its Chandrasekhar mass, it collapses, followed by a supernova explosion (Woosley & Weaver 1995). In particular, stars with $M_{\star} \gtrsim 30 M_{\odot}$ would eventually collapse into a Black Hole (BH) (Woosley & Weaver 1995; Fryer 1999).
- For stars of $40 M_{\odot} \lesssim M_{\star} \lesssim 100 M_{\odot}$ the neutrino-driven explosion is probably too weak to form an outgoing shock. A BH forms and either swallows the whole star or, if there is adequate angular momentum, produces a jet which could result in a Gamma Ray Burst (GRB; Fryer 1999).
- Stars with $M_{\star} \gtrsim 100 M_{\odot}$ (see e.g. Portinari, Chiosi & Bressan 1998) form large He cores that reach carbon ignition with masses in excess of about $45 M_{\odot}$. It is known that after helium burning, cores of this mass will encounter the electron-positron pair instability, collapse and ignite oxygen and silicon burning explosively. If explosive oxygen burning provides enough energy, it can reverse the collapse in a giant nuclear-powered explosion (the so-called Pair Instability Supernova, PISN) by which the star would be partly or completely (if $M_{\star} \gtrsim 140 M_{\odot}$) disrupted (Fryer, Woosley & Heger 2001). The onset of a PISN though depends whether the star can retain enough of its initial mass to have a helium core bigger than about $64 M_{\odot}$ at the end of the core He-burning phase, or rather lose the mass during the previous stages of its evolution (Meynet, Ekström & Maeder 2006). For even more massive stars ($M_{\star} \gtrsim 260 M_{\odot}$) a new phenomenon occurs as a sufficiently large fraction of the center of the star becomes so hot that the photo-disintegration instability is encountered before explosive burning reverses the implosion. This uses up all the energy released by previous burning stages and accelerates the collapse leading to the prompt formation of a massive BH, and, again, either a complete collapse or a jet-powered explosion (Bond, Arnett and Carr 1984;

Fryer, Woosley & Heger 2001; Ohkubo et al. 2006; Suwa et al. 2007a).

- At even higher masses ($M_{\star} \gtrsim 10^5 M_{\odot}$) the evolution depends on the metallicity (Fuller, Woosley & Weaver 1986): if $Z < 0.005$ the star collapses to a BH as a result of post-Newtonian instabilities without ignition of the hydrogen burning; for higher metallicities it explodes, as it could generate nuclear energy more rapidly from β -limited cycle.

A summary of the final fate of Pop III stars is sketched in Fig. 16.

3.4. BLACK HOLES AND GAMMA RAY BURSTS FROM THE FIRST STARS

As discussed in the previous Section, metal-free (and also moderately metal-poor) stars more massive than approximately $260 M_{\odot}$ collapse completely to BHs. Similar arguments apply to stars in a lower mass window ($30 M_{\odot} - 140 M_{\odot}$), which are also expected to end their evolution as BHs. If this is the case, a numerous population of Intermediate Mass Black Holes (IMBHs) – with masses $M_{\bullet} \approx 10^2 - 10^3 M_{\odot}$, between those of stellar and SuperMassive Black Holes (SMBHs) – may be the end-product of those episodes of early star formation and offer a possible observable of primordial stars. As these pre-galactic BHs become incorporated through a series of mergers into larger and larger halos, they sink to the center because of dynamical friction, accrete a fraction of the gas in the merger remnant to become supermassive, form a binary system, and eventually coalesce.

Volonteri, Haardt & Madau (2003) thoroughly studied this scenario including a number of physical ingredients such as gas accretion, hardening of the IMBH binary and triple interactions. Their results show that this hierarchical growth can reproduce the observed luminosity function of optically selected quasars in the redshift range $1 < z < 5$. A prediction of the model is that a population of “wandering” black holes in galactic halos and in the IGM should exist (and possibly observed), contributing around 10% of the present day total black hole mass density, $4 \times 10^5 M_{\odot} \text{ Mpc}^{-3}$ (a similar study has been performed by Islam, Taylor & Silk 2003). IMBHs that have not yet ended up in SMBHs could also be either (*i*) en route toward galactic nuclei, thereby accounting for the X-ray-bright off-center sources detected locally by ROSAT¹⁸, or (*ii*) constituting the dark matter candidates composing the entire baryonic halos of galaxies (Schneider et al. 2002). A possible

¹⁸ <http://wave.xray.mpe.mpg.de/rosat>

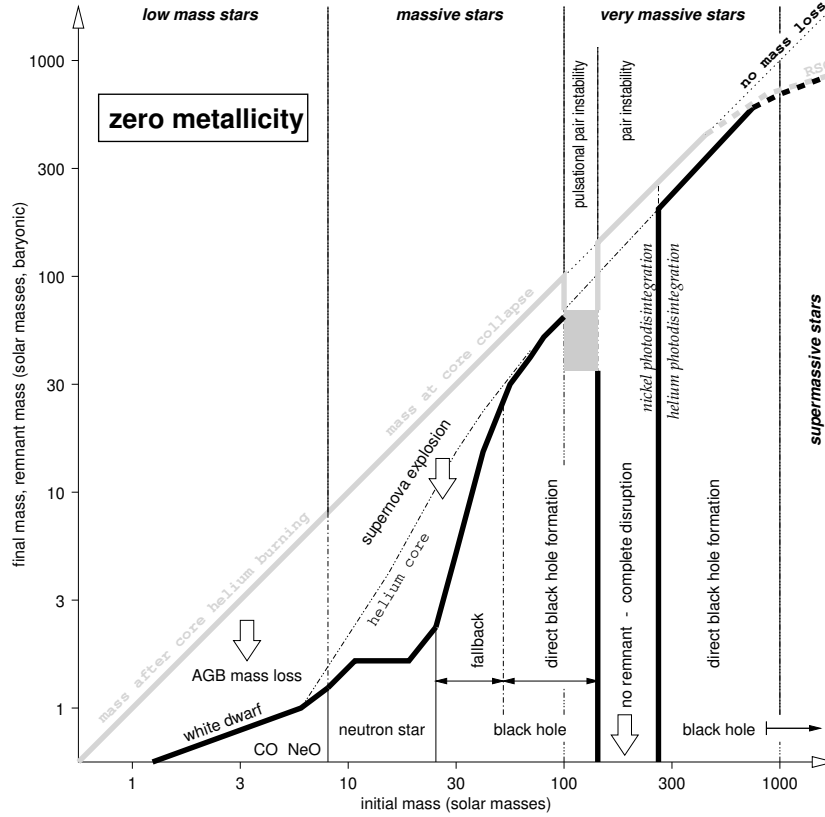


Figure 16. Initial-final mass function of Pop III stars (Heger & Woosley 2002). The horizontal axis gives the initial stellar mass. The y -axis gives the final mass of the collapsed remnant (thick black curve) and the mass of the star at the beginning of the event producing that remnant (thick gray curve). Since no mass loss is expected from Pop III stars before the final stage, the gray curve is approximately the same as the line of no mass loss (dotted). Exceptions are $\approx 100 - 140 M_{\odot}$ where the pulsational pair-instability ejects the outer layers of the star before it collapses, and above $\approx 500 M_{\odot}$ where pulsational instabilities in red supergiants may lead to significant mass loss (dashed). The hydrogen-rich envelope and parts of the helium core (dash-double-dotted curve) are ejected in a supernova explosion.

method to constrain the existence and nature of BHs at $z > 6$ would be with the next generation of X-ray and NIR space telescopes, that could detect BHs down to masses of $10^5 - 10^6 M_{\odot}$ (Salvattera, Haardt & Volonteri 2007).

Once a proto-BH has formed into the stellar core, accretion continues through a disk. It is widely accepted, though not confirmed, that magnetic fields drive an energetic jet (Fig. 17) which produces a burst of TeV neutrinos (Linke et al. 2001; Mészáros, & Waxman 2001; Schneider, Guetta & Ferrara 2002) by photon-meson interaction,

and eventually breaks out of the stellar envelope appearing as a GRB. Based on recent numerical simulations and neutrino emission models, the expected neutrino diffuse flux from these Pop III GRBs could be within the capabilities of present and planned detectors as **AMANDA**¹⁹ (Antartic Muon And Neutrino Detector Array) and **IceCube**²⁰. High-energy neutrinos from Pop III GRBs could dominate the overall flux in two energy bands, $10^4 - 10^5$ GeV and $10^5 - 10^6$ GeV, of neutrino telescopes. The enhanced sensitivities of forthcoming detectors in the high-energy band (**AMANDA-II**, **IceCube**) will provide a fundamental insight into the characteristic explosion energies of Pop III GRBs, and will constitute a unique probe of the IMF of the first stars. Based on such results, Pop III GRBs could be associated (e.g. Schneider, Guetta & Ferrara 2002; Arefiev, Priedhorsky & Borozdin 2003) with a new class of events detected by **BeppoSax**²¹, the Fast X-ray Transients (FXTs), bright X-ray sources with peak energies in the 2–10 keV band and durations between 10 s and 200 s (e.g. Heise et al. 2001). Iocco et al. (2007) though, using updated models of Pop III star formation history and neutrino emission yields show that the planned generation of neutrino telescope will not be able to detect the contribution from Pop III stars and that, in any case, this would be highly contaminated by the contribution from Pop II stars.

3.5. KEY OBSERVATIONS

Despite the efforts made in the past decades, the search for zero-metallicity stars has been proven unfruitful as no Pop III star has been detected yet. The first very low metallicity star, with a logarithmic abundance relative to solar of $[\text{Fe}/\text{H}] = -4.5$ ²², was identified more than 15 years ago (Bessel & Norris 1984). Since then, more stars with $-4.5 < [\text{Fe}/\text{H}] < -2$ have been detected (McWilliam et al. 1995; Beers et al. 1998; Norris, Ryan & Beers 2001; Carretta et al. 2002). The record was established by Christlieb et al. (2002), who measured an abundance of $[\text{Fe}/\text{H}] = -5.3$ in HE0107-5240, a star with a mass of $\approx 0.8 M_{\odot}$. Does the existence of this star suggest that Pop III also contained low-mass and long-lived objects? To answer this question, we should be able to infer the metallicity of the gas cloud out of which HE0107-5240 formed from the abundance of the elements observed on its surface. In particular, the observed abundance pattern in elements heavier than Mg (which

¹⁹ <http://amanda.berkeley.edu/www/amanda.html>

²⁰ <http://icecube.wisc.edu/>

²¹ <http://www.asdc.asi.it/bepposax/>

²² In the usual notation, $[\text{X}/\text{H}] = \log(\text{X}/\text{H}) - \log(\text{X}/\text{H})_{\odot}$.

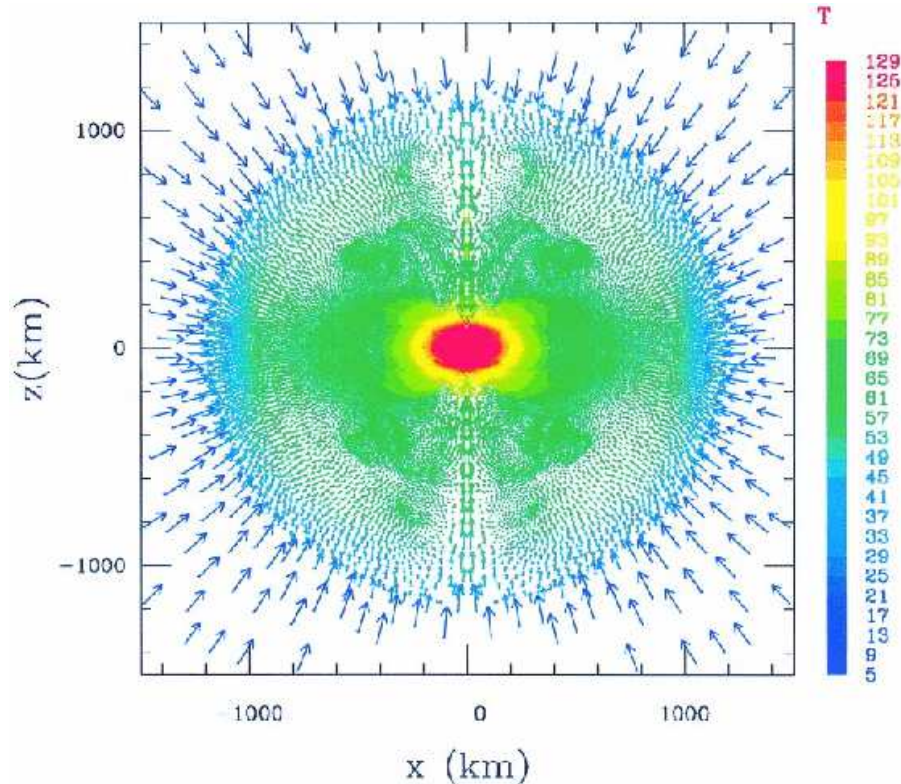


Figure 17. Collapse of a $300 M_{\odot}$ Pop III star (Fryer, Woosley & Heger 2001). The proto-BH 0.5 s before BH formation is shown. Color denotes temperature in 10^9 K, and the vectors represent the direction and magnitude of the particle velocity. At this time, the proto-BH has a mass of roughly $78 M_{\odot}$ and size of 1100 km. The inner core first forms a black hole, but as soon as it collapses, the entire proto-BH (which is $90 M_{\odot}$ at collapse) quickly accretes onto the BH.

cannot be synthesized in the interior of a $0.8 M_{\odot}$ star) is a distinct signature of the previous generation of stars.

HE0107-5240 is very iron-deficient but overabundant in C, N and O (Bessel et al. 2004; Christlieb et al. 2004). The origin of these light elements can be twofold: (i) either they were already present in the parent gas cloud out of which the star was born, or (ii) their origin is due to a post-formation mechanism, such as mass transfer from a companion star, self-enrichment from the star itself or accretion due to repeated passage through the Galactic disk (for a thorough discussion of these issues we refer to Christlieb et al. 2004). In the first scenario, the gas cloud out of which the star formed would have had to be pre-enriched to a metallicity as high as $Z = 10^{-2} Z_{\odot}$. This metallicity is significantly higher than Z_{cr} and low-mass stars can form. Moreover,

Umeda & Nomoto (2005) have shown that if the polluter is a zero-metallicity star with mass in the range $\approx 25 - 130 M_{\odot}$ exploding as a sub-luminous Type-II SN, a good fit of the observed abundance pattern can be obtained (although some problems remain with the updated oxygen abundance; Bessel et al. 2004; Christlieb et al. 2004). In the second scenario, only the elements heavier than Mg, which cannot be synthesized in the interior of such a low-mass star, were already present before its formation. The composition of these elements can be equally well reproduced by the predicted elemental yields of either an intermediate mass star that exploded as SN (Christlieb et al. 2002; Limongi, Chieffi & Bonifacio 2003; Weiss et al. 2004; Iwamoto et al. 2005) or of a $200 - 220 M_{\odot}$ star that exploded as a PISN (Schneider et al. 2003). Thus, HE0107-5240 may have formed from a gas cloud which had been pre-enriched by such supernovae up to an estimated metallicity of $10^{-5.5} \leq Z/Z_{\odot} \leq 10^{-5.1}$. These values fall within the proposed range for Z_{cr} .

A second very iron deficient star (HE1327-2326, with $[\text{Fe}/\text{H}] = -5.4$) with an overabundance of C and N has been detected by Frebel et al. (2005). Differently from HE0107-5240, which is a giant and has evolved off the main-sequence, HE1327-2326 is relatively unevolved.

The most massive star is the Pistol star, with an estimated initial mass of $200 - 250 M_{\odot}$ (Figer et al. 1998). Although there are no indications that the star is a binary, it might have recently experienced a rejuvenation through a merger with another star. Figer (2005) has investigated the presence of very massive stars in the Arches cluster, which has an estimated age of 2-2.5 Myr. Thus, stars with masses above $\sim 150 M_{\odot}$ should still be visible if they were formed. The typical mass function would predict 18 stars with masses greater than $130 M_{\odot}$, but none were found, suggesting a firm upper limit for the star masses of $150 M_{\odot}$. Also Oey & Clarke (2005), based on a statistical analysis of OB associations, find that, if the IMF has a slope close to a Salpeter, it would be extremely unlikely to have stars with masses greater than $120-200 M_{\odot}$.

As a novel strategy to search for Pop III stars, Scannapieco, Schneider & Ferrara (2003) have suggested that at least some intermediate redshift Ly α -emitting galaxies might have their flux powered by Pop III stellar clusters. In Fig. 18 the isocontours in the Ly α luminosity-redshift plane indicate the probability to find Pop III star-hosting galaxies in a given sample of Ly α emitters for various feedback efficiencies, E_g . Such objects populate a well defined region of the Ly α -redshift plane, whose extent is governed by the feedback strength. Furthermore, their fraction increases with redshift, independently of the assumed feedback strength, suggesting that Ly α emission from already observed high- z

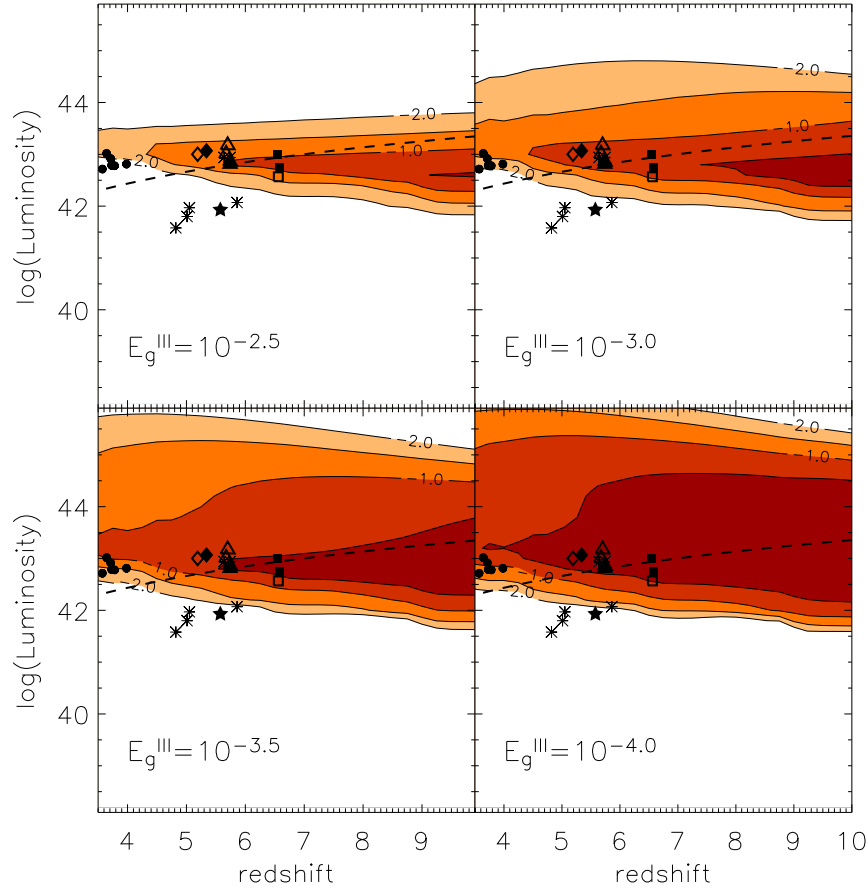


Figure 18. Fraction of Pop III star-hosting galaxies as a function of Ly α luminosity and redshift. Isocontours of fractions $\geq 10^{-2}$, $10^{-1.5}$, 10^{-1} and $10^{0.5}$ are shown for a burst-mode star formation. Each panel is labeled by the assumed feedback parameter E_g value. For reference, the dashed line gives the luminosity corresponding to an observed flux of $1.5 \times 10^{-17} \text{ ergs cm}^{-2} \text{ s}^{-1}$, and the various points correspond to observed galaxies (see details in Scannapieco, Schneider & Ferrara 2003).

sources can be due to Pop III stars. Hence, collecting large data samples to increase the statistical leverage may be crucial for detecting the elusive first stars.

Confirmation of the presence of Pop III stars in the Ly α emitters can come from follow-up spectroscopy. Tumlinson and collaborators (Tumlinson, Giroux & Shull 2001; Tumlinson, Shull & Venkatesan 2003) have suggested that the harder ionizing spectrum expected from metal-free stars would result in stronger He II recombination lines. Their

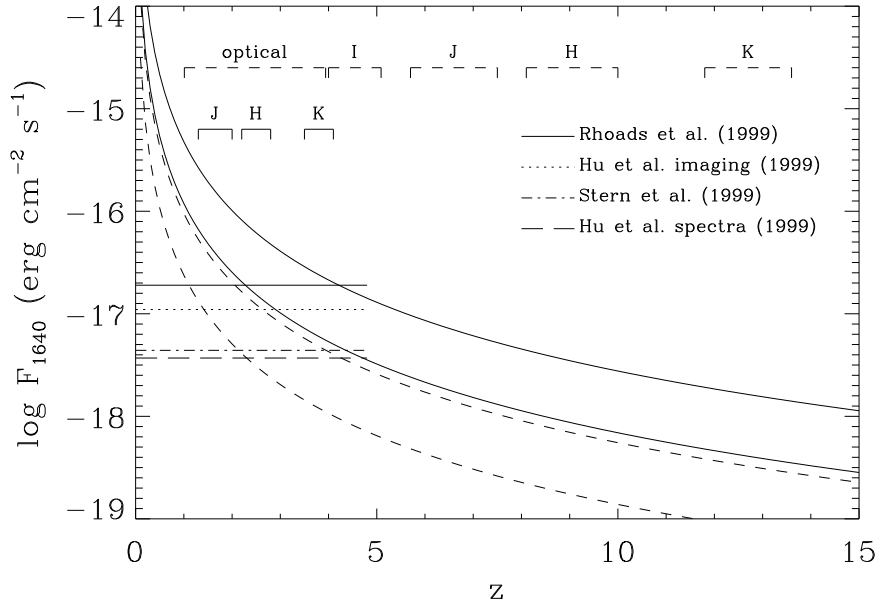


Figure 19. Flux of He II $\lambda 1640$ line as a function of the source redshift. The different lines refer to different models for the time evolution of the stellar ionizing radiation. The horizontal lines show the limits of the current Ly α emission-line surveys. At the top, the ranges of redshift probed by the He II $\lambda 1640$ (above) and $\lambda 4686$ (below) lines for optical and infrared searches are marked. See Tumlinson, Giroux & Shull (2001) for details.

calculations indicate that line fluxes of the He II $\lambda 1640$ and $\lambda 4686$ are sufficiently large to be detected by narrow-band and spectroscopic searches for high-redshift emission-line sources (see Fig. 19). Together with measurements of the H α emission line, the He II recombination lines can be used also to infer the ratio of the He II to H I ionizing photons (Oh, Haiman & Rees 2001).

Nagao et al. (2008) performed a photometric search of Pop III stars by looking at galaxies with strong emission both in Ly α and He II $\lambda 1640$ in the redshift intervals $3.93 < z < 4.01$ and $4.57 < z < 4.65$. As none of the observed dual emitters could be identified with a galaxy hosting a Pop III star, an upper limit of $5 \times 10^{-6} \text{ M}_{\odot} \text{ yr}^{-1} \text{ Mpc}^{-3}$ to the Pop III SFR has been set.

In addition to He lines, also H $_2$ lines could be used to observe the first stars. For example, H $_2$ lines (principally $J = 5 - 3(v = 0)$, $J = 2 - 0(v = 0)$ and $\Delta v = 1$ lines) emitted by collapsing primordial clouds, although not observable from an individual object, could pro-

duce cumulative fluxes in the sub-mJy level, marginally observable with ASTRO-F²³ and ALMA²⁴ (Atacama Large Millimeter Array). If HD is an important coolant as discussed in the previous Section, then additional line emission might be observed. In this case, the lines emitted during the collapse would show a double-peak feature, with the higher peak associated with the H₂ $J = 2 - 0(v = 0)$ transition and the lower peak with the HD $J = 4 - 3(v = 0)$ transition (Kamaya & Silk 2002; Kamaya & Silk 2003). A similar strategy has been proposed by Ripamonti et al. (2002), who suggest that the sum of the H₂ infrared line and continuum emission radiation produced during the collapse and accretion on a small hydrostatic protostellar core could be detected by JWST. In contrast with the above studies, Mizusawa, Nishi & Omukai (2004), who include in their calculation the emission of H₂ lines both in the collapse and in the accretion phase, find that observation of such lines with forthcoming facilities will be highly improbable.

While direct observations of the early stars are very difficult (if not impossible) to obtain, one can search for evidence of their past existence with other observable. Such evidence can in particular be seen in binary systems, where one of the components is a sub-solar-mass star and the other was a larger mass star. The presently observed spectrum of the lower-mass companion would exhibit the chemical signature of the larger-mass companion. The high frequency of carbon-enhanced stars found among very metal-poor stars in the halo of our Galaxy provides a constrain on the past IMF and indicates that it was different from the present and shifted toward higher masses (e.g. Lucatello et al. 2005). These findings are consistent with an early prediction by Hernandez & Ferrara (2001) of an upward shift of the characteristic stellar mass with redshift based on an analysis of the observational data of Galactic metal poor stars. Such mass increases above the Jeans mass fixed by the increase of the CMB temperature with redshift.

Ballerio, Matteucci & Chiappini (2006) though reach a different conclusion. They have studied the effect of Pop III star metal pollution on the chemical evolution of the Milky Way, focusing their analysis on α -elements, carbon, nitrogen and iron, finding that the effect of Pop III stars is negligible and it is not possible to prove or disprove their existence based on chemical abundance in the Milky Way. Moreover, their analysis favors a constant or slightly varying IMF to a strongly variable one. Along the same lines, Damped Lyman Alpha (DLA) systems have been searched for the nucleosynthetic ashes of Pop III stars. Erni et al. (2006) compare the chemical enrichment pattern of

²³ <http://www.ir.isas.ac.jp/ASTRO-F/index-e.html>

²⁴ <http://www.alma.nrao.edu>

the most metal-poor DLAs with predictions from different explosive nucleosynthesis models and find that the observed abundance pattern favors massive (10-50 M_{\odot}) metal-free supernovae/hypernovae. Pair-instability SNe seem to be excluded; however, given the metallicity level of DLAs ($\approx 10^{-2}Z_{\odot}$), this is not surprising as it is likely that the gas in these systems has already been enriched by a large number of stellar populations.

Signatures of Pop III stars might be seen in puzzling observations of the abundance of lithium isotopes (e.g. Asplund et al. 2006). While ${}^7\text{Li}$ is produced both in BBN and through cosmic ray (CR) spallation, ${}^6\text{Li}$ is produced only via the second process. On this basis a correlation between ${}^6\text{Li}$ abundance and metallicity is expected. Two problems arise: (i) ${}^7\text{Li}/\text{H}$ abundance observed in metal-poor halo stars is $\sim 10^{-10}$, i.e. much lower than expected from BBN alone ($\sim 4.5 \times 10^{-10}$); (ii) ${}^6\text{Li}$ abundance does not correlate with metallicity and rather shows a plateau that extends to low metallicity values. Different scenarios have been proposed to explain the plateau (CR in shocks during the formation of the Galaxy, decay of relic particles during BBN, production in connection with gamma rays, initial burst of cosmological CRs) without overproducing ${}^7\text{Li}$. A tentative solution has been found by Rollinde, Vangioni & Olive (2006) who have calculated the production of ${}^6\text{Li}$ from CR produced by Pop III and Pop II stars using a prescription for the cosmic SN rate. However, the models makes extreme and somewhat unphysical assumptions concerning the cosmic star formation history and it is not clear to what extent it can reproduced the metallicity distribution function of halo stars. Useful reviews for readers interested in the subject can be found in Coc et al. (2004) and Steigman (2005).

Jimenez & Haiman (2006) explain with the presence of 10%-30% of metal-free stars at $z \sim 3 - 4$, four puzzling observations that cannot be accounted for with a more normal stellar population: (i) the significant UV emission from LBGs at $\lambda < 912 \text{ \AA}$; (ii) the strong Lyman- α emission from extended blobs at $z = 3.1$ with little or no associated apparent ionizing continuum; (iii) a population of $z \sim 4.5$ galaxies with a very wide range of Lyman- α equivalent width emission lines; (iv) strong HeII emission line in a composite of LBGs.

GRBs have been proposed as possible tools to study the high- z universe and, in principle, a fraction of them could be triggered by Pop III progenitors. To produce a GRB though, a star needs to lose its outer H envelope. As the mass loss from Pop III stars is not expected to be significant, mass transfer to a companion star in binaries could help. If Pop III binaries are common, Pop III star formation at high- z

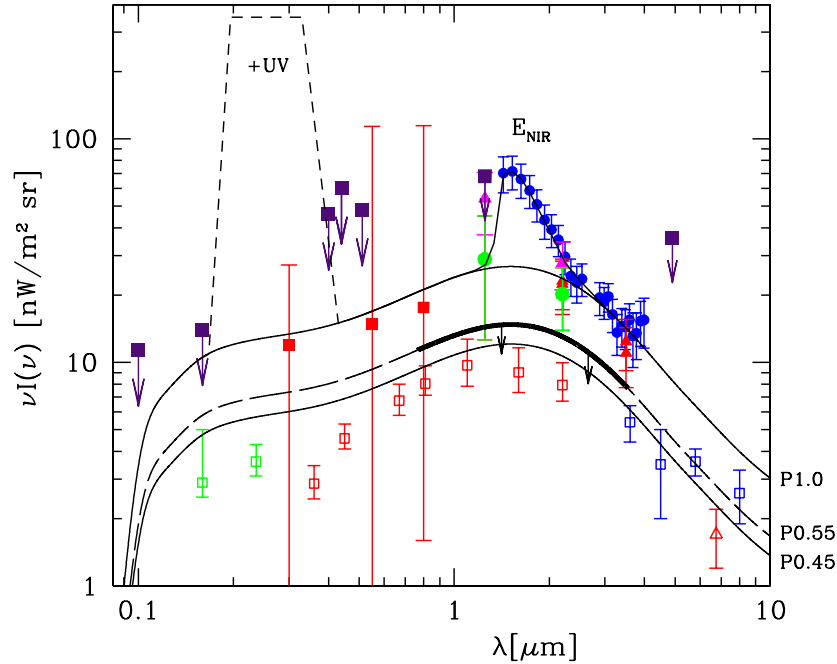


Figure 20. Extragalactic background light data compilation from various IR and UV experiments. Also shown are (lower) limits coming from galaxy counts (open symbols). Lines denote different theoretical models (for details see Aharonian et al. 2006).

could be probed by SWIFT²⁵ (Bromm & Loeb 2006). Belczynski et al. (2007) find that, although, about 10% of Pop III binaries lose the H envelope, only 1% acquire sufficient angular momentum to produce a GRB. Thus, it will be extremely difficult for SWIFT to detect GRBs from Pop III binaries.

In the last years the alleged discovery of an excess in the near IR background (an updated compilation on the extragalactic background light measurements is shown in Fig. 20) and of its fluctuations above the “normal” galaxy contribution claimed by Matsumoto et al. (2005; but see, e.g., Aharonian et al. 2006 for a different view), has produced considerable excitement given the fact that the excess could be interpreted as an imprint of redshifted light of the first (massive) stars,

²⁵ <http://www.swift.psu.edu/xrt/>

(Santos, Bromm & Kamionkowski 2002; Salvaterra & Ferrara 2003a; Madau & Silk 2005; Kashlinsky 2005). In addition, the emission from metal-free stars is needed to explain the level of fluctuations in the same background, at least at the shortest wavelengths. In fact, clustering of unresolved Pop III stars can account for the entire signal at almost all the $\approx 1 - 30$ arcsec scales probed by observations in the J band, while their contribution fades away at shorter frequencies and becomes negligible in the K band, where “normal” galaxies are dominant (Magliocchetti, Salvaterra & Ferrara 2003; Cooray et al. 2004; Kashlinsky et al. 2004; Kashlinsky et al. 2005; Cooray et al. 2007). The new measurements of fluctuations with the IRAC instrument on board of *Spitzer* and the associated analysis confirm that the anisotropies on scales $\sim 0.5' - 10'$ must be of extragalactic origin (Kashlinsky et al. 2007a). Salvaterra et al. (2006) find that Pop III stars can contribute only less than 40% to the NIRB and that the fluctuations can be reproduced by the clustering of Pop II hosting galaxies at $z > 5$. That the fluctuations must arise from a population of sources at those redshifts is confirmed also by Kashlinsky et al. (2007b), although they find that such sources should be much brighter per unit mass than the present stellar population.

Dwek, Arendt & Krennrich (2005) also noticed that explaining the excess with Pop III contribution only, would require uncomfortably high formation efficiencies. In fact, more than 5% of all baryons must be processed into Pop III stars and, to avoid excessive metal pollution, they should end up in IMBHs with steep UV/X-ray spectra (not to overproduce the present-day soft X-ray background). In addition, if the excess in the NIRB were of extragalactic origin (rather than due to zodiacal light), its $\gamma - \gamma$ interactions with γ -ray photons emitted by blazars would produce a distinct absorption feature in the spectra of these sources. Dwek, Krennrich & Arendt (2005) show that, if the NIRB excess were due to Pop III stars it would be difficult to reproduce the absorption-corrected spectra of some observed distant TeV blazars.

A substantial IR background could arise from Pop III stars not only due to the direct emission associated with these stars, but also due to indirect processes that lead to free-free and Ly α emission from the ionized nebulae or H II regions surrounding the stars. In view of more recent observations though, a substantial contribution to the near IR background for Pop III stars seems to be excluded. Salvaterra & Ferrara (2006) find that if this is the case, a large fraction (in some case all) of *Spitzer* counts (at $3.5 \mu\text{m}$ and $4.5 \mu\text{m}$; Fazio et al. 2004) at the faintest fluxes is due to galaxies at $z > 8$, but worse, the number of J-dropout and Ly α emitters identified in NICMOS (Bouwens et al. 2005)

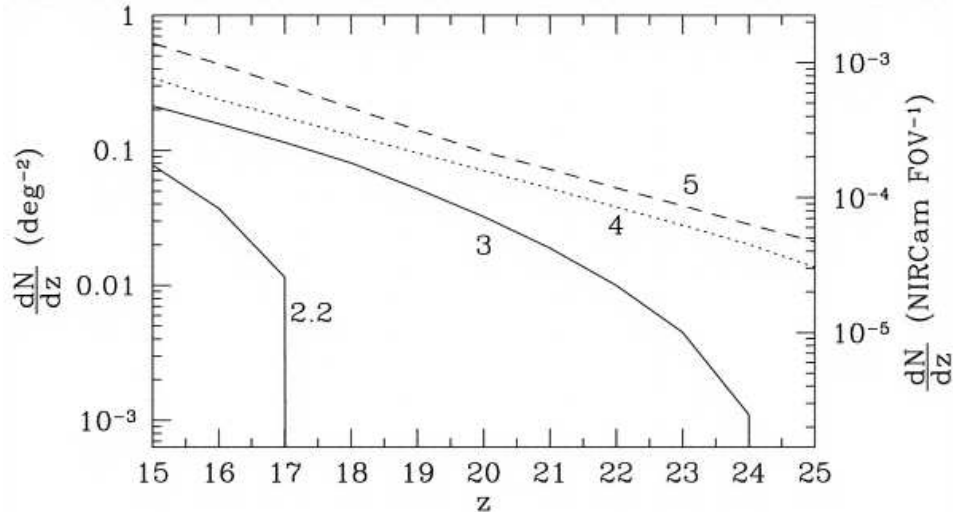


Figure 21. Predicted surface density of PISNe on the sky per unit redshift as a function of redshift for four different observing wavelengths (labeled in μm), assuming that survey images reach 1 mag below maximum light, after Weinmann & Lilly (2005).

and ZEN (Willis & Courbin 2005) deep surveys would be overpredicted by a factor of thousands.

An additional NIRB contribution could come from supernovae (although this is usually minor) and high redshift quasars. The latter could give a substantial contribution if Pop III were indeed very massive and ended up as IMBH (Cooray & Yoshida 2004). In this case though they would probably overestimate the measured soft X-ray background (Salvaterra, Haardt & Ferrara 2005).

Regardless of the precise contribution from primordial stars to the IR background, they would leave enough photons to provide a large optical depth for high-energy photons from high- z GRBs. Observations of their spectra could thus provide information on the emission from the first stars (Kashlinsky 2005).

JWST could observe the upper mass range of pair instability supernovae from the first stars, which would provide, in addition to an observational proof of the existence of very massive metal-free stars, stringent constraints on the understanding of primordial star formation and IMF (Wise & Abel 2005). Although PISN are bright enough to be detected by JWST, Weinmann & Lilly (2005) claim that their rate is so small ($0.2\text{-}4 \text{ deg}^{-2} \text{ yr}^{-1}$) that either a dedicated wide-angle search or a serendipitous search is needed. The numbers quoted by the latter authors are less optimistic than previous estimates ($0\text{-}2200 \text{ deg}^{-2} \text{ yr}^{-1}$;

e.g. Cen 2003a; Mackey, Bromm & Hernquist 2003; Wise & Abel 2005) because very approximate light curves were adopted. Although, as noted by Scannapieco et al. (2005), the light curves used by Weinmann & Lilly (2005) contain a normalization error, the numbers derived are in agreement with those derived adopting the correct light curves (see Fig. 21). In any case, Smith et al. (2007) reported the detection of the peculiar Type II SN 2006gy which could be the first SN powered by a pair-instability explosion.

If indeed the first stars were very massive and left BH remnants, then gravitational waves emitted during each collapse (Schneider et al. 2000; Fryer, Holz & Hughes 2002; Buonanno et al. 2005; Sandick et al. 2006; Suwa et al. 2007b) would be seen as a stochastic background, whose predicted spectral strain peaks in the frequency range $5 \times 10^{-4} - 5 \times 10^{-3}$ Hz (where it has a value $10^{-20} - 10^{-19}$ Hz $^{-1/2}$) and might be detected by LISA²⁶(Laser Interferometer Space Antenna). Similarly, the coalescence of massive black hole binaries due to galaxy mergers has also been considered as a source of low-frequency gravitational radiation (Wyithe & Loeb 2003c; Sesana et al. 2004; Belczynski, Bulik & Rudak 2004). Several discrete mHz massive black hole sources detectable by LISA are likely to originate at redshifts $z > 7$, while the advanced LIGO²⁷ should detect at least several events per year with high signal to noise ratio ($\gtrsim 10$). Core collapse SN from primordial stars would produce a gravitational wave background that peaks at 30-100 Hz (compared to 300-500 Hz from a normal mode of star formation) and is within the sensitivity of planned interferometers as LIGO, BBO (Big Bang Observatory) and DECIGO (DECi-hertz Interferometer Gravitational wave Observatory) (Sandick et al. 2006). Using an improved spectrum, Suwa et al. (2007b) find that the range of observability is 0.1-1 Hz.

4. Feedback Effects

Once the first sources have formed, their mass deposition, energy injection and emitted radiation can deeply affect the subsequent galaxy formation process and influence the evolution of the IGM via a number of so-called “feedback” effects. The word “feedback” is by far one of the most used in modern cosmology, where it is applied to a vast range of situations and astrophysical objects. However, for the same reason, its meaning in the context is often unclear or fuzzy. Generally speaking, the concept of feedback invokes a *back reaction of a process on itself or on the causes that have produced it*. Secondly, the character of feedback

²⁶ <http://lisa.jpl.nasa.gov>

²⁷ <http://www.ligo.caltech.edu>

Table III. Classification of different feedback effects.

NEGATIVE		
<i>Radiative</i>	<i>Mechanical</i>	<i>Chemical</i>
1. Photoionization/evaporation	1. Blowout/blowaway	1. Fragmentation
2. H ₂ Photodissociation	2. Impinging shocks	
3. Photoheating filtering	3. Preheating	
POSITIVE		
<i>Radiative</i>	<i>Mechanical</i>	<i>Chemical</i>
1. In front of H II regions	1. Behind shocks	
2. Inside relic H II regions	2. Shell fragmentation	
3. X-ray background		

can be either *negative or positive*. Finally, and most importantly, the idea of feedback is intimately linked to the possibility that *a system can become self-regulated*. Although some types of feedback processes are disruptive, the most important ones in astrophysics are probably those that are able to drive the systems towards a steady state of some sort. To exemplify, think of a galaxy which is witnessing a burst of star formation. The occurrence of the first supernovae will evacuate/heat the gas thus suppressing the subsequent SF process. This feedback is then acting back on the energy source (star formation); it is of a negative type, and it could drive the SF activity in such a way that only a sustainable amount of stars is formed. However, feedback can fail to produce such regulation either in small galaxies, where the gas can be ejected by a handful of SNe, or in cases when the star formation timescale is too short compared to the feedback timescale. In the spirit of the present review we will only discuss feedback occurring at high redshifts and hence shaping the first structures.

Although a rigorous classification of the various effects is not feasible, they can be divided into three broad classes: *radiative*, *mechanical* and *chemical* feedback. In the first class fall all those effects associated, in particular, with ionization/dissociation of hydrogen atoms/molecules; the second class is produced by the mechanical energy injection of massive stars in form of winds or SN explosions; and chemical feedback is instead related to the postulated existence of a critical metallicity governing the cosmic transition from very massive stars to “normal” stars.

Attempting a classification of all proposed feedback effects is almost desperate, due to the large number of applications and definitions, often discordant, present in the literature. Nevertheless, we offer in Table III a working classification aimed essentially at organizing the material discussed in this Section. Whereas the radiative feedback is intimately connected with cosmic reionization, chemical feedback is instead strongly dependent on the history of metal enrichment of the universe. Although reionization and metal enrichment could then be analyzed as aspects of feedback, given their importance and the large amount of literature on these subjects, we have reserved a separate discussion for them in Sec. 5.

4.1. RADIATIVE FEEDBACK

Radiative feedback is related to the ionizing/dissociating radiation produced by massive stars or quasars. This radiation can have local effects (i.e. on the same galaxy that produces it) or long-range effects, either affecting the formation and evolution of nearby objects or joining the radiation produced by other galaxies to form a background. In spite of the different scenarios implied, the physical processes are very similar.

Photoionization/evaporation

The collapse and formation of primordial objects exposed to a UV radiation field can be inhibited or halted for two main reasons: *(i)* cooling is considerably suppressed by the decreased fraction of neutral hydrogen, and *(ii)* gas can be photoevaporated out of the host halo. In fact, the gas incorporated into small mass objects that were unable to cool efficiently, can be boiled out of the gravitational potential well of the host halo if it is heated by UV radiation above the virial temperature. Such effects are produced by the same radiation field and act simultaneously. For this reason, it is hard to separate their individual impact on the final outcome. The problem has been extensively studied by several authors (e.g. Thoul & Weinberg 1996; Nagashima, Gouda & Sugiura 1999; Barkana & Loeb 1999; Susa & Kitayama 2000; Chiu, Gnedin & Ostriker 2001; Kitayama et al. 2000, 2001; Machacek, Bryan & Abel 2001; Haiman, Abel & Madau 2001; Susa & Umemura 2004b; Ahn & Shapiro 2007; Whalen et al. 2007). In particular, Susa & Kitayama (2000) and Kitayama et al. (2000, 2001), assuming spherical symmetry, solve self-consistently radiative transfer of photons, non-equilibrium H₂ chemistry and gas hydrodynamics of a collapsing halo. They find that at weak UV intensities ($J < 10^{-23}$ erg s⁻¹ cm⁻² sr⁻¹ Hz⁻¹), objects as small as $v_c \sim 15$ km s⁻¹ are able to collapse, owing to both self-shielding of the gas and H₂ cool-

ing. At stronger intensities though, objects as large as $v_c \sim 40 \text{ km s}^{-1}$ can be photoevaporated and prohibited from collapsing, in agreement with previous investigations based on the optically thin approximation (Thoul & Weinberg 1996). Similar results have been found by Susa & Umemura (2004b) by means of a 3-D hydrodynamic simulation which incorporates the radiative transfer of ionizing photons. Also the 3-D hydrodynamic simulation of Machacek, Bryan & Abel (2001) confirms that the presence of UV radiation delays or suppresses the formation of low mass objects. In contrast with these studies, Dijkstra et al. (2004), applying the 1-D code by Thoul & Weinberg (1996) to $z > 10$ objects, find that objects as small as $v_c \sim 10 \text{ km s}^{-1}$ can self-shield and collapse because the collisional cooling processes at high redshift are more efficient and the amplitude of the ionizing background is lower. The second condition might not always apply, as the ionizing flux at high redshift is dominated by the direct radiation from neighboring halos rather than the background (Ciardi et al. 2000).

The photoevaporation effect might be particularly important for Pop III objects, as their virial temperatures are below the typical temperatures achieved by a primordial photoionized gas ($T \approx 10^4 \text{ K}$). For such an object, the ionization front gradually burns its way through the collapsed gas, producing a wind that blows backwards into the IGM and that eventually evaporates all the gas content. According to recent studies (Haiman, Abel & Madau 2001; Shapiro, Iliev & Raga 2004; Whalen et al. 2007) these sub-kpc galactic units were so common to dominate the absorption of ionizing photons. This means that estimates of the number of ionizing photons per H atom required to complete reionization should not neglect their contribution to absorption. As Fig. 22 (Shapiro, Iliev & Raga 2004) shows, the number of ionizing photons absorbed per initial minihalo atom, ξ , increases gradually with time; in addition, it depends on the ionizing spectrum assumed. For the hard QSO spectrum, the ionization front is thicker and penetrates deeper into the denser and colder parts of the halo, increasing the rate of recombinations per atom, compared to stellar type sources. However, this same pre-heating effect shortens the evaporation time, ultimately leading to a rough cancellation of the two effects and the same total ξ as for a black-body spectrum with $T = 5 \times 10^4 \text{ K}$ (mimicking a low metallicity Pop II stellar emission). An even lower ξ is needed for a black-body spectrum with $T = 10^5 \text{ K}$ (more typical of a Pop III stellar emission), because of an increased evaporation vs. penetration ability. Thus, overall, Pop III stellar sources appear significantly more efficient than Pop II or QSO sources in terms of the total number of ionizing photons needed to complete the photoevaporation process. It should be noted though that the typical timescales for photoevaporation are

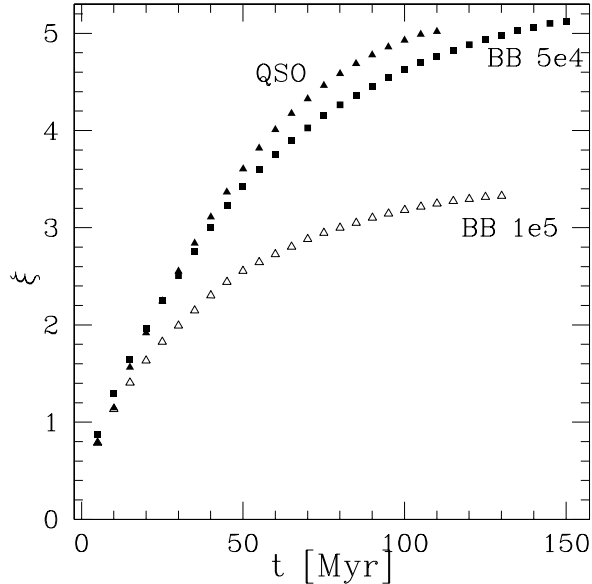


Figure 22. Evolution of the cumulative number of ionizing photons absorbed per initial minihalo atom for a QSO and two black-body spectra with $T = 5 \times 10^4$ K and $T = 10^5$ K, as labelled (see Shapiro, Iliev & Raga 2004 for detailed definitions).

larger than the lifetime of massive Pop III stars, and thus minihalos generally survive photoevaporation (Alvarez, Bromm & Shapiro 2006). The degree of photoevaporation also depends sensitively on the evolution stage of halos, with diffuse halos with central densities below few cm^{-3} being completely photoevaporated, while more evolved halos generally retaining their core (Whalen et al. 2007).

H₂ Photodissociation

As intergalactic H₂ is easily photodissociated, a soft-UV background in the Lyman-Werner bands could quickly build up and have a negative feedback on the gas cooling and star formation inside small halos (Haiman, Rees & Loeb 1997; Ciardi, Ferrara & Abel 2000; Ciardi et al. 2000; Haiman, Abel & Rees 2000; Ricotti, Gnedin & Shull 2002; Mackey, Bromm & Hernquist 2003; Yoshida et al. 2003a; Wise & Abel 2008; Johnson, Greif & Bromm 2008). In addition to an external background, the evolution of structures can also be affected by internal dissociating radiation. In fact, once the first generation of stars has formed in an object, it can affect the subsequent star formation process by photodissociating molecular hydrogen in star forming clouds (Omukai & Nishi 1999; Nishi & Tashiro 2000; Glover & Brand 2001;

Oh & Haiman 2002). In particular, Nishi & Tashiro (2000) show that if the molecular cloud has a metallicity smaller than about $10^{-2.5} Z_{\odot}$, a single O star can seriously deplete the H_2 content so that subsequent star formation is almost quenched. Thus, it seems plausible that stars do not form efficiently before the metallicity becomes larger than about 10^{-2} solar. On the other hand, Susa & Umemura (2006) performed hydrodynamic simulations coupled to radiative transfer of ionizing and dissociating photons finding that, if a star forming cloud exceeds the threshold density of $\sim 10^2 \text{ cm}^{-3}$ and is at a distance $> 30 \text{ pc}$ from a $120 M_{\odot}$ Pop III star, it can survive negative feedback as the H_2 shell formed in front of the ionization front is able to shield the cloud. This suggests that in typical primordial star forming conditions secondary star formation can actually take place.

Machacek, Bryan & Abel (2001) find that the fraction of gas available for star formation in Pop III objects of mass M exposed to a flux with intensity J_{LW} in the Lyman-Werner band is $\sim 0.06 \ln(M/M_{th})$, where the mass threshold, M_{th} , is given by:

$$(M_{th}/M_{\odot}) = 1.25 \times 10^5 + 8.7 \times 10^5 \left(\frac{J_{LW}}{10^{-21} \text{ erg}^{-1} \text{ cm}^{-2} \text{ Hz}^{-1}} \right). \quad (16)$$

An AMR simulation by O’Shea & Norman (2007b) confirms that the formation of small mass, primordial objects in the presence of a Lyman-Werner flux is delayed (although not completely suppressed because enough H_2 is retained in the core), and, as a result, the virial mass of the halo at the time of the collapse is increased compared to a case when no dissociating flux is present (see Fig. 23). The same problem has been analyzed by Susa & Umemura (2004a) by means of three-dimensional SPH calculations, where radiative transfer is solved by a direct method and the non-equilibrium chemistry of primordial gas is included. They find that star formation is suppressed appreciably by UVB, but baryons at high-density peaks are self-shielded, eventually forming some amount of stars. Similarly, a 1-D radiation-hydrodynamical simulation by Ahn & Shapiro (2007) suggests that minihalos down to total masses of $10^5 M_{\odot}$ are able to self-shield against dissociating radiation from a nearby massive Pop III star and form dense cold clouds at their center, also due to shock-induced molecule formation. Their results though suffer from unphysical geometric effects due to the 1-D configuration and are not reproduced by the 2-D simulations by Whalen et al. (2007), who find that shock-induced molecule formation plays no role. Nevertheless, they confirm that a LW flux does not exert a strong feedback on collapse of minihalos.

The negative feedback described above could be counterbalanced by the *positive feedback* of H_2 re-formation, e.g. in front of H II regions,

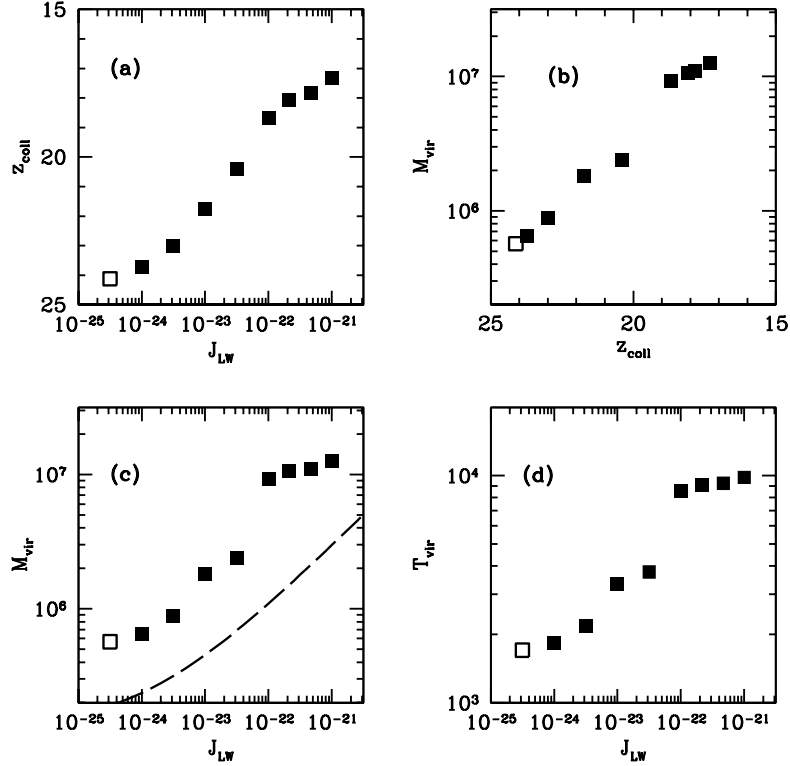


Figure 23. Mean halo quantities for several simulations with the same cosmic realization but a range of Lyman-Werner molecular hydrogen photodissociating flux backgrounds (O’Shea & Norman 2007). Panel (a): halo collapse redshift vs. J_{LW} . Panel (b): halo virial mass vs. collapse redshift. Panel (c): halo virial mass vs. J_{LW} . Panel (d): virial temperature vs. J_{LW} . The $J_{21} = 0$ “control” results are shown as an open square (it is at $\log J_{LW} = -24.5$ in the panels which are a function of J_{LW}). In the bottom panel, the dashed line corresponds to the fitting function for threshold mass by Machacek, Bryan & Abel (2001).

inside relic H II regions, once star formation is suppressed in a halo and ionized gas starts to recombine (Ricotti, Gnedin & Shull 2001, 2002; Mashchenko, Couchman & Sills 2006; Abel, Wise & Bryan 2007; Johnson, Greif & Bromm 2007), in cooling gas behind shocks produced during the ejection of gas from these objects (Ferrara 1998). Ricotti, Gnedin & Shull (2002) study the formation/dissociation of H_2 by means of hydrodynamics simulations coupled with a radiative transfer scheme following the propagation of ionizing and dissociating radiation. Their main result is that the above positive feedback is usually able to counterbalance the effect of H_2 dissociation. As a consequence, the formation of small mass galaxies is not suppressed, as found by other authors.

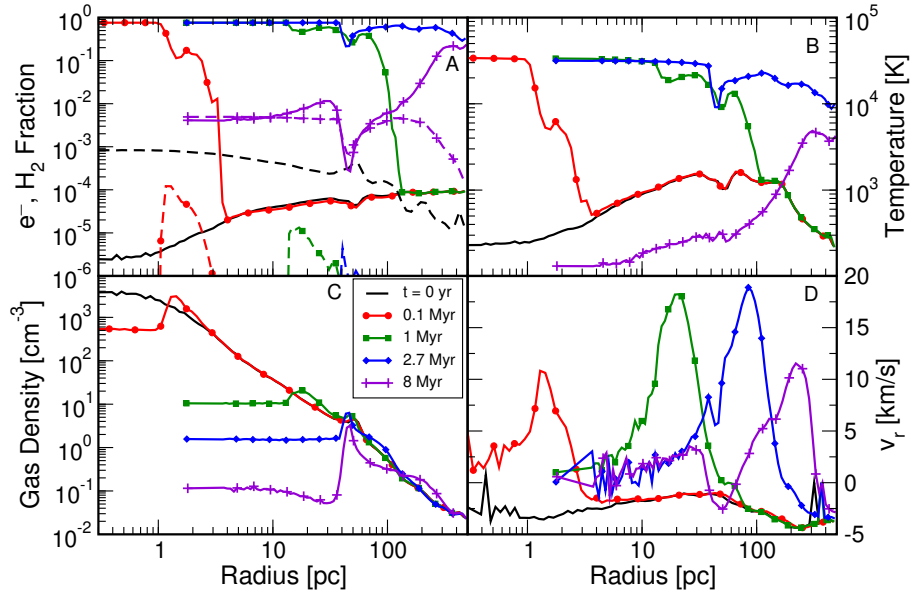


Figure 24. Mass weighted radial profiles around the position of a star with mass $M_* = 100 M_\odot$. Panel A: electron number fraction (solid) and H_2 mass fraction (dashed) for 5 different times, 0, 0.1, 1, 2.7, and 8 Myr after the star is born. The star dies at 2.7 Myr. Panel B: temperature. Panel C: gas density. Panel D: radial velocity. (Abel, Wise & Bryan 2007).

Cen (2005) has also proposed that supersonic collisions of cold atomic gas clouds, which were originally minihalos and accreted into larger halos, can shock heat and compress the gas, which then cools and forms H_2 molecules. This would enhance the star formation process. Thus, a second burst of star formation might take place also in the small objects where it has been suppressed by H_2 dissociation. H_2 production could also be promoted by an X-ray background, which would increase the fractional ionization of protogalactic gas. Such a positive feedback, though, is not able to balance UV photodissociation in protogalaxies with $T_{\text{vir}} < 2000$ K (Haiman, Abel & Rees 2000; Glover & Brand 2003). Kuhlen & Madau (2005) have simulated with the code ENZO the effect of the X-ray radiation produced by the first quasar on the surrounding medium. They find that the net effect of X-ray is to reduce the gas clumping with the consequence of suppressing gas infall at overdensities $\delta < 2000$, but at higher overdensities molecular cooling is increased, although this is not enough to overcome heating in the proximity of the quasar. Similar arguments apply to cosmic rays (e.g. Shchekinov & Vasiliev 2004; Jasche, Ciardi & Enßlin 2007; Stacy & Bromm 2007).

An example of positive feedback can be seen in Figure 24.

Photoheating filtering

Cosmic reionization might have a strong impact on subsequent galaxy formation, particularly affecting low-mass objects. In fact, the heating associated with photoionization causes an increase in the temperature of the IGM gas which will suppress the formation of galaxies with masses below the Jeans mass. As Gnedin (2000b) has pointed out, one can expect that the effect of reionization depends on the reionization history, and thus is not universal at a given redshift. More precisely, one should introduce a “filtering” scale, k_F , (or, equivalently, filtering mass M_F) over which the baryonic perturbations are smoothed as compared to the dark matter, yielding the approximate relation $\delta_b = \delta_{dm} e^{-k^2/k_F^2}$. The filtering mass as a function of time is related to the Jeans mass by:

$$M_F^{2/3} = \frac{3}{a} \int_0^a da' M_J^{2/3}(a') \left[1 - \left(\frac{a'}{a} \right)^{1/2} \right]. \quad (17)$$

Note that at a given moment in time the two scales can be very different. Also, in contrast to the Jeans mass, the filtering mass depends on the full thermal history of the gas instead of the instantaneous value of the sound speed, so it accounts for the finite time required for pressure to influence the gas distribution in the expanding universe. The filtering mass increases from roughly $10^7 M_\odot$ at $z \approx 10$ to about $10^9 M_\odot$ at redshift $z \approx 6$, thus efficiently suppressing the formation of objects below that mass threshold. Of course such result is somewhat dependent on the assumed reionization history.

An analogous effect is found inside individual H II regions around the first luminous sources. Once an ionizing source turns off, its surrounding H II region Compton cools and recombines. Nonetheless, the “fossil” H II regions left behind remain at high adiabats, prohibiting gas accretion and cooling in subsequent generations of Pop III objects (Oh & Haiman 2003). A similar entropy floor could be obtained by heating the gas with Ly α photons (Ciardi & Salvaterra 2007) or x-ray photons (Oh & Haiman 2003), although the latter mechanism would also promote H₂ formation which in turn would increase the cooling (Kuhlen & Madau 2005). The suppression of minihalos formation in photoionized regions is increased if the clustering of the sources is considered (e.g. Kramer, Haiman & Oh 2006). O’Shea et al. (2005), on the other hand, find that it is possible for a primordial star to form within an H II region (similar results are found by Nagakura & Omukai 2005 by means of 1-D hydrodynamical calculation which include also the effect of HD). By means of an Eulerian adaptive mesh refinement simulation they find that the enhanced electron fraction within the

H II region catalyzes H₂ formation that leads to faster cooling in the subsequent star forming halos, although the accretion rate is much lower. A similar result is found by Abel, Wise & Bryan (2007) who, via a hydrodynamic simulation with radiative transfer, follow the formation of a first star and its H II region, and the consequent collapse inside it of a second star. They also argue that an entropy floor in relic H II regions is present, but not as high as discussed by Oh & Haiman (2003), because the typically high density gas does not get very heated. This is confirmed by Mesinger, Bryan & Haiman (2006), who use a hydrodynamic simulation to study the collapse of minihalos inside H II regions. They find that there exist a critical intensity for the UV flux such that for lower values H₂ formation is enhanced, while for higher star formation is reduced. This critical value is a function of the gas density.

Haiman & Bryan (2006) interpret the low value of the Thomson scattering optical depth inferred by the 3-yr (confirmed by the 5-yr) WMAP release as an evidence for the efficiency of radiative feedback on small mass object formation. In fact, the ionizing photon production efficiency in these objects must have been low in order to not overproduce the optical depth. Nevertheless, a comprehensive conclusion on the impact of radiative feedback effects is still impossible, given the large number of different assumptions, approximations and parameters used in the (sometimes specific) studies present in the literature. With the only aim to give a flavor of the large discrepancies, in Fig. 25 we compare various predictions on the mass of halos affected by radiative feedback (in some of the forms discussed above). There we show the results of Ciardi et al. (2000) (long dashed-dotted line), Kitayama et al. (2000) (dotted), Kitayama et al. (2001) (short dashed and long dashed), Dijkstra et al. (2004) (solid) and Yoshida et al. (2003) (short dashed-dotted); obviously, the comparison is far from exhaustive. Here we simply summarize the main features addressed in those papers, while for the details we refer the reader to them. Ciardi et al. (2000) have derived the minimum mass a halo must have to self-shield against an incident UV flux (in addition to the background, the contribution from the direct flux from nearby objects is included). They have studied the non-equilibrium multifrequency radiative transfer of the incident spectrum in the approximation of a homogeneous gas layer composed of H, H⁻, H⁺, He, He⁺, He⁺⁺, H₂, H₂⁺ and free electrons. Kitayama et al. (2000) have studied the collapse of primordial objects in the presence of an UV background radiation, by means of a 1-D spherical hydrodynamical calculation combined with a treatment of the radiative transfer of photons. An analogous, but more refined calculation, has

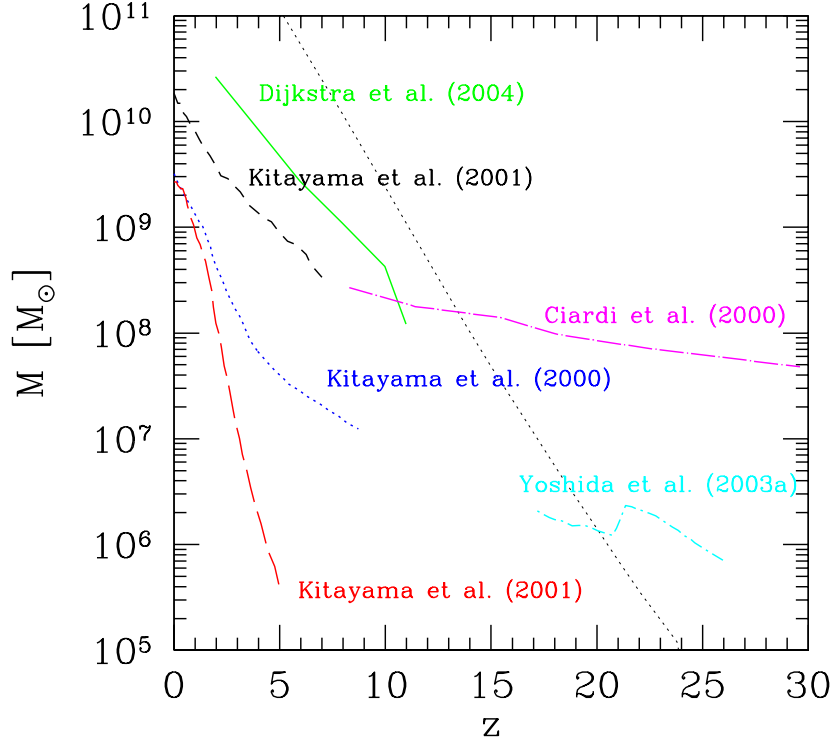


Figure 25. Mass of halos affected by radiative feedback in the formulation of Ciardi et al. (2000) (long dashed-dotted line), Kitayama et al. (2000) (dotted), Kitayama et al. (2001) (short dashed and long dashed), Dijkstra et al. (2004) (solid) and Yoshida et al. (2003a) (short dashed-dotted). The straight dotted line corresponds to the formation redshift of $3\text{-}\sigma$ peaks in a Λ CDM model. For details refer to the text and the above papers.

been performed by Kitayama et al. (2001), for different assumptions for the incident flux. The curve of Dijkstra et al. (2004) is the mass corresponding to the case in which the presence of an external ionizing flux reduces the gas infall of a factor of 2. The calculations are performed by means of a 1-D spherically symmetric hydrodynamic code. Finally, Yoshida et al. (2003a) derive the minimum mass of halos that host gas clouds in their N-body/SPH simulations, which include the non-equilibrium evolution of the relevant species.

In summary, *the presence of a UV flux delays the collapse and cooling of small mass halos and the amount of cold gas available primarily depends on the intensity of the flux and the mass of the halo. Some controversy though still exists on the efficiency of such feedback.*

4.2. MECHANICAL FEEDBACK

In addition to the radiative feedback, the mechanical feedback associated with mass and energy deposition from the first stars, can deeply affect the subsequent SF process in several ways.

Blowout and Blowaway

Depending on the mass and the dark matter content of galaxies, SN and multi-SN events might induce partial (*blowout*) or total (*blowaway*) gas removal from the galaxy itself, regulating the SF (e.g. Mac Low & Ferrara 1999; Nishi & Susa 1999; Ferrara & Tolstoy 2000; Springel & Hernquist 2003; Bromm, Yoshida & Hernquist 2003; Silk 2003; Wada & Venkatesan 2003; Greif et al. 2007; Whalen et al. 2008). It is found that only objects with masses $M \lesssim 5 \times 10^6 M_\odot$ can experience a complete blowaway, while larger objects have lower mass ejection. Thus, quenching SF in galaxies by ejecting large fractions of their gas is very difficult. These results have been substantiated and confirmed by Mori, Ferrara & Madau (2002) who have performed a three-dimensional hydrodynamic simulation, using a nested grid method to follow the evolution of explosive multi-SN events in an object of total mass of $10^8 M_\odot$ at $z = 9$, representing a $2\text{-}\sigma$ fluctuation of the density power spectrum. They find that, depending on the stellar distribution, less than 30% of the available SN energy is converted into kinetic energy of the escaping material, the remainder being radiated away. It appears that mechanical feedback is less efficient than expected from simple energetic arguments, as off-nuclear SN explosions drive inward-propagating shocks that tend to collect and pile up cold gas in the central regions of the host halo (see Fig. 26). Thus, also relatively low-mass galaxies at early epochs may be able to retain a considerable fraction of their gas and continue forming stars. A variant of this study, using the SPH method and considering a single supernova explosion in Pop III objects at higher redshift, has been carried out by Bromm, Yoshida & Hernquist (2003). These authors find that the more energetic PISN explosions ($M_\star = 250 M_\odot$; $E \approx 10^{53}$ erg) lead to a blowaway (this has been later confirmed by Greif et al. 2007 for a PISN with mass $M_\star = 250 M_\odot$ and $E \approx 10^{53}$ erg), while the lower explosion energy corresponding to a single Type II SN ($E \approx 10^{51}$ erg) leaves much of the halo intact. Nevertheless, the extent to which such feedback can operate depends sensitively on the initial configuration of the medium surrounding the explosion site and the ionization front expansion around a massive progenitor star can significantly aid gas evacuation by SN blastwaves (Kitayama & Yoshida 2005), as can be seen in Fig. 27.

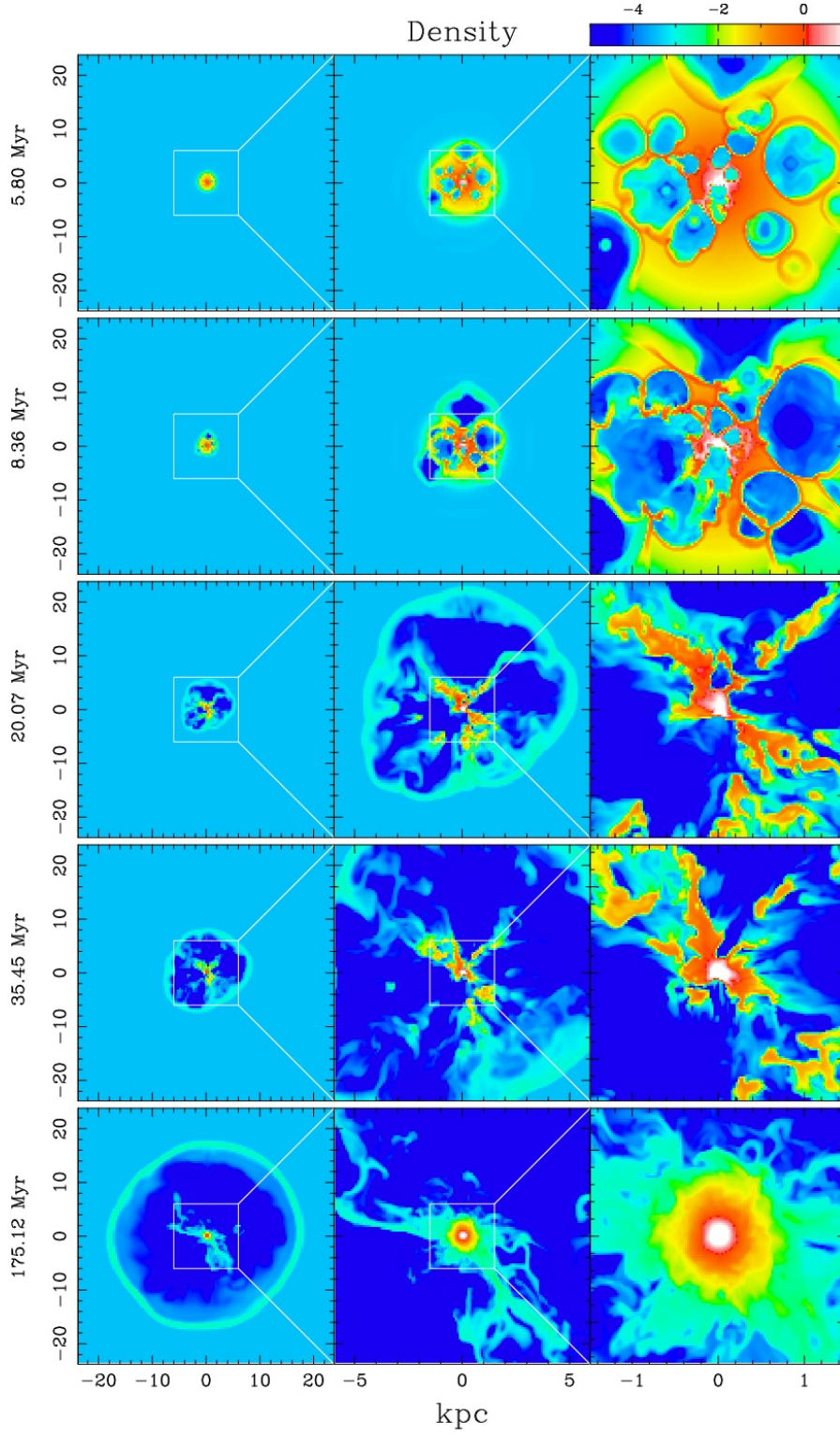


Figure 26. Snapshots of the simulated logarithmic gas number density due to SN explosions (at five different elapsed times) in a halo with mass $M = 10^8 h^{-1} M_\odot$ at redshift $z = 9$ (Mori, Madau & Ferrara 2002). The three panels in each row show the spatial density distribution in the $X - Y$ plane on the nested grids. The left, middle, and right panels in each row correspond to the spatial resolution levels.

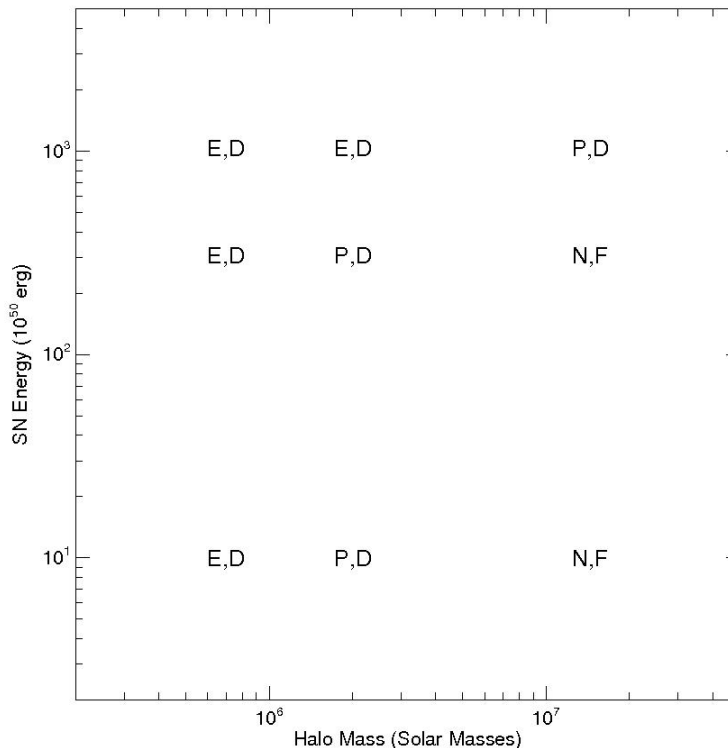


Figure 27. Eventual fate of a halo given the indicated explosion energy. The first letter refers to the final state of the halo prior to the explosion (E: photoevaporated; P: partly ionized, defined as the I-front not reaching the virial radius; N: neutral, or a failed H II region). The second letter indicates outcome of the explosion (D: destroyed, or F: fallback). See Whalen et al. (2008) for details.

Following the ejection of gas, H₂ formation is favored in cooling gas behind the shocks, possibly balancing H₂ dissociation, as discussed in the previous Section (Ferrara 1998). This process should be accessible to observations, as the re-formed H₂ emits mid-IR roto-vibrational lines (as for example the restframe 2.2 μm) detectable by JSWT (Ciardi & Ferrara 2001).

In some cases, SN explosions could promote star formation. In fact, following an explosion, the interstellar gas is swept up and a dense shell is formed immediately behind the radiative shock front at radius R_{sh} . When the dense shell gets dynamically overstable, it breaks into fragments, some of which will contract and eventually form stars (see e.g. Vishniac 1983; McCray & Kafatos 1987; Nakano 1998; Tsujimoto, Shigeyama & Yoshii 1999; Reynoso & Mangum 2001; Mackey, Bromm & Hernquist 2003; Salvaterra, Ferrara & Schneider 2003). Shell expansion tends to suppress (stabilize) the growth of density pertur-

bations owing to stretching, hence counteracting the self-gravity pull. The instantaneous maximum growth rate is:

$$\omega = -\frac{3\dot{R}_{sh}}{R_{sh}} + \left[\left(\frac{\dot{R}_{sh}}{R_{sh}} \right)^2 + \left(\frac{\pi G \rho_0 R_{sh}}{3c_{s,sh}} \right)^2 \right]^{1/2}, \quad (18)$$

where $c_{s,sh} = (kT_{sh}/\mu m_H)^{1/2}$ is the sound speed in the shell and ρ_0 the ambient gas density. Instability occurs only if $\omega > 0$, or

$$\frac{\dot{R}_{sh}}{R_{sh}} < \frac{1}{8^{1/2}} \frac{\pi G \rho_0 R_{sh}}{3c_{s,sh}} \propto \frac{t_{cross}}{t_{ff}^2}, \quad (19)$$

where $t_{cross} \sim R_{sh}/c_{s,sh}$ is the crossing time in the shell and t_{ff} is the free-fall time. Furthermore, if the fragment mass is not much larger than the Jeans mass, the $\omega > 0$ condition translates into $\dot{R}_{sh}/R_{sh} < 1/t_{ff}$. Instability occurs only if $\dot{R}_{sh}/R_{sh} < t_{cross}/t_{ff}^2$, where R_{sh} is the shell radius, t_{cross} is the crossing time in the shell and t_{ff} is the free-fall time. Hence, large shell velocity-to-radius ratios inhibit the formation of gravitationally unstable fragments. Under some conditions (see e.g. Salvaterra, Ferrara & Schneider 2003) the above instability criterion is satisfied and (typically low-mass) stars are formed as a result of shell fragmentation.

Impinging Shocks

The formation of a galaxy can be inhibited also by the effects of shocks from neighboring objects, causing heating, evaporation and/or stripping of the baryonic matter (Scannapieco, Ferrara & Broadhurst 2000). In the former scenario (mechanical evaporation), the gas in a forming galaxy is heated above its virial temperature by the shock. The thermal pressure of the gas then overcomes the dark matter potential and the gas expands out of the halo, preventing galaxy formation. Only if the cooling time of the collapsing cloud is shorter than its sound crossing time, will the gas cool before it expands out of the gravitational well and continue to collapse. In the latter scenario, the gas may be stripped from a collapsing perturbation by a shock from a nearby source. In this case, the momentum of the shock is sufficient to carry the gas with it, emptying the halo of its baryons and preventing a galaxy from forming.

In practice, the short cooling times for most dwarf-scale collapsing objects suggest that the baryonic stripping scenario is almost always dominant. This mechanism has the largest impact in forming dwarfs in the $\lesssim 10^9 M_\odot$ range, which is sufficiently large to resist photoevaporation by UV radiation, but too small to avoid being swept up by nearby

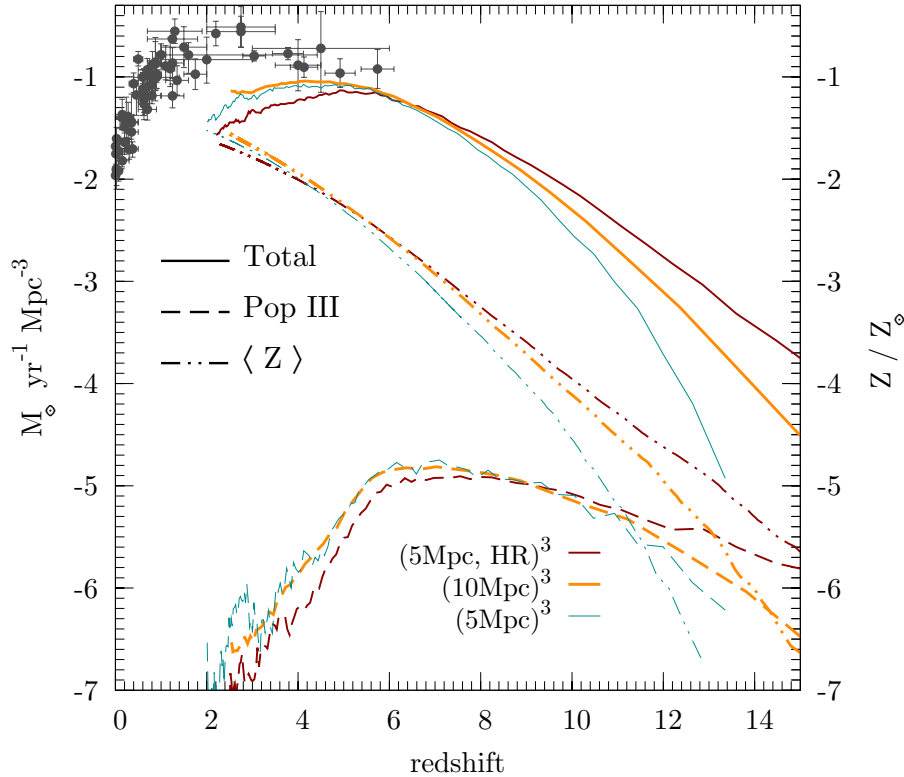


Figure 28. Predicted evolution of Pop II (solid lines) and Pop III (dashed) cosmic star formation rates, and mass-averaged metallicity (dot-dot-dashed) from Tornatore, Ferrara & Schneider (2007). The results of three simulation runs at different resolution are shown for each quantity. As a reference, low-redshift measurements (points) taken from Hopkins (2004) are reported.

outflows. Sigward, Ferrara & Scannapieco (2005) studied this problem by means of numerical simulations, finding that, if the forming galaxy is virialized, the impinging shock has a negligible effect on its evolution, while, if it is in the turnaround stage, up to 70% of its gas content can be stripped away.

4.3. CHEMICAL FEEDBACK

The concept of chemical feedback is relatively recent, having been first explored by Bromm et al. (2001) (following the early study by Yoshii & Sabano 1980) and Schneider et al. (2002), and subsequently discussed by Schneider et al. (2003), Mackey, Bromm & Hernquist (2003) and others.

According to the scenario outlined in Sec. 3, the first stars forming out of gas of primordial composition might be very massive, with masses $\approx 10^2 - 10^3 M_\odot$. The ashes of these first supernova explosions pollute with metals the gas out of which subsequent generations of low-mass Pop II/I stars form, driving a transition from a top-heavy IMF to a “Salpeter-like” IMF when locally the metallicity approaches the critical value $Z_{cr} = 10^{-5 \pm 1} Z_\odot$ (Schneider et al. 2002, 2003). The uncertainty in the value of the critical metallicity is due to the role of dust cooling, which has been only recently quantitatively assessed by Schneider et al. (2006b). In brief, metals depleted onto dust grains enable fragmentation to solar or sub-solar mass scales already at metallicities $Z = 10^{-6} Z_\odot$; on the contrary, in the absence of dust grains, even at $Z = 0.01 Z_\odot$ metals diffused in the gas-phase lead to fragment mass scales which are still of the order of 100 solar masses.

Thus, the cosmic relevance of Pop III stars and the transition to a Pop II/I star formation epoch depends on the efficiency of metal enrichment from the first stellar explosions, the so-called chemical feedback, which is strictly linked to the number of Pop III stars that explode as PISN, the metal ejection efficiency, transport and mixing in the IGM. Depending on the strength of the chemical feedback Pop III star formation could last for a very short time and their contribution to the ionizing photon production could be negligible (see e.g. Ricotti & Ostriker 2004a for a discussion). It is very likely though that the transition occurred rather smoothly because the cosmic metal distribution is observed to be highly inhomogeneous: even at moderate redshifts, $z \approx 3$, the clustering properties of C IV and Si IV QSO absorption systems are consistent with a metal filling factor $< 10\%$, showing that metal enrichment is incomplete and inhomogeneous (see Sec. 5).

As a consequence, the use of the critical metallicity as a global criterion is somewhat misleading because chemical feedback is a *local process*, with regions close to star formation sites rapidly becoming metal-polluted and overshooting Z_{cr} , and others remaining essentially metal-free. Thus, Pop III and Pop II star formation modes could have been coeval, and detectable signatures from Pop III stars could be found well after the volume-averaged metallicity has become larger than critical.

In a seminal paper Scannapieco, Schneider & Ferrara (2003) studied, using an analytical model of inhomogeneous structure formation, the separate evolution of Pop III/Pop II stars as a function of star formation and wind efficiencies. Their main finding was that, essentially independent of the free parameters of the model, Pop III stars continue to contribute appreciably to the star formation rate density at much lower redshift. These findings have been now confirmed by

additional numerical work (Tornatore, Ferrara & Schneider 2007) and are summarized in Fig. 28, where the relative contribution of Pop III and Pop II to the cosmic star formation is shown along with the mean IGM metallicity evolution. Due to inefficient heavy element transport by outflows and slow "genetic" transmission during hierarchical growth, large fluctuations around the average metallicity arise; as a result Pop III star formation continues down to $z = 2.5$, but at a low peak rate of $10^{-5} \text{ M}_{\odot} \text{ yr}^{-1} \text{ Mpc}^{-3}$ occurring at $z \approx 6$ (about 10^{-4} of the Pop II one). This finding has important implications for the development of efficient strategies for the detection of Pop III stars in primeval galaxies, as discussed previously. A similar result has been found by Wyithe & Cen (2007).

5. Cosmic Reionization and IGM Metal Enrichment

Although cosmic reionization has received great attention in the last decade due to the availability of high- z absorption line studies and progresses in the CMB experiments, the nature of the ionizing sources, the reionization history and its effect on structure formation remain unclear and highly debated. This is mostly due to uncertainties in the modeling of several physical issues: properties of first stars and quasars, ionizing photon production and radiative transfer, just to mention a few. Whatever their nature, only a fraction of the emitted ionizing photons is able to escape from their production site and reach the IGM. Thus, the knowledge of the escape fraction is crucial for any theoretical modeling of the reionization process. The same stars that produce the ionizing radiation are expected to pollute the IGM with heavy elements. In the following we will discuss the present understanding of the above processes.

5.1. ESCAPE FRACTION

The first attempt to derive a value of the escape fraction, f_{esc} , for a Milky Way-type galaxy dates to Dove & Shull (1994), who assumed a smoothly varying H I galactic distribution and OB associations located in the Galactic plane. By integrating the fraction of Lyman continuum (Lyc) photons that escapes the disk over the adopted luminosity function of OB associations, they estimated $f_{esc} \approx 14\%$. Dove, Shull & Ferrara (2000) later improved the calculation by solving the time-dependent transfer problem of stellar radiation through evolving superbubbles. Their main result is that the shells of the expanding superbubbles quickly trap ionizing photons, so that most of the radiation

escapes only after the superbubbles have broken out of the Galaxy, when however the ionizing power of the central stellar cluster has already largely faded away. This results in an escape fraction roughly a factor of 2 lower than the one obtained by Dove & Shull (1994), although the exact value depends on the star formation history. An even more refined approach is the one by Fujita et al. (2003), in which the effects of repeated supernova explosions, including the formation and evolution of superbubbles, are modeled using a hydrodynamical simulation. They confirm that the shells can trap ionizing radiation very effectively until the bubbles start to accelerate, causing the shells to fragment. The values found for f_{esc} are roughly consistent with the Dove, Shull & Ferrara (2000) estimates. All the above studies model the idealized case of a smoothly varying H I distribution and sources positioned on the Galactic plane. A more realistic case would give a higher value of the escape fraction. The effects of gas density inhomogeneities have been studied by Ciardi, Bianchi & Ferrara (2002) for a Milky Way-type galaxy. To this aim, a comparison between a smooth Gaussian distribution and an inhomogeneous fractal one has been made, including realistic assumptions for the position and emission properties of the ionizing stellar sources based on the available data, and the 3-D radiative transfer of ionizing photons. While a fractal interstellar medium results in an escape fraction roughly constant over a wide range of ionization rates, in a Gaussian distribution f_{esc} decreases with decreasing rates. Based on a model that provides a good fit to the observed size distribution of H I holes in nearby galaxies, Clarke & Oey (2002) derive a simple relationship between the star formation rate and the interstellar porosity of a galaxy. This gives a critical star formation rate for which the porosity is of the order of 1. The authors expect high escape fractions only in galaxies whose star formation rates exceed the critical value, as for example Lyman Break Galaxies (LBGs).

Additional theoretical works (Ricotti & Shull 2000; Wood & Loeb 2000; Fujita et al. 2003) have extended the analysis to include high-redshift galaxies, for which the escape of Ly α photons can be modified by geometrical effects (i.e. disk vs. spheroidal systems) and by the higher mean galactic Interstellar Medium (ISM) density. Ricotti & Shull (2000) use models of smoothly distributed gas in hydrostatic equilibrium and estimate f_{esc} by integrating the escaping radiation of each single OB association over the luminosity function of the OB associations. They perform a parametric study to understand the dependence of f_{esc} on redshift, mass, star formation efficiency, stellar density distribution and OB association luminosity function. Generally speaking, the escape fraction decreases as the object virialization redshift or mass become larger or the rate of Ly α photons emitted smaller. Their analysis

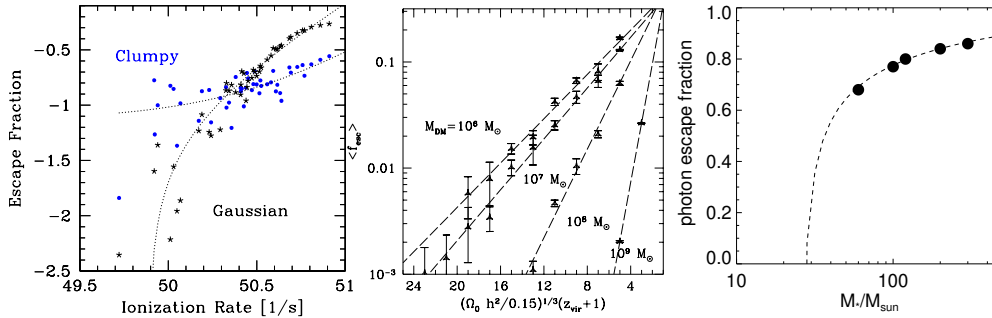


Figure 29. Left panel: Escape fraction as a function of the ionization rate for a clumpy (circles) and a Gaussian (asterisks) density distribution (Ciardi, Bianchi & Ferrara 2000). Central panel: Redshift evolution of the escape fraction for different masses of the host dark matter halo (Ricotti & Shull 2000). Right panel: Evolution of the escape fraction as a function of the mass of the first, massive star (Yoshida et al. 2007).

is confined to objects with $M \approx 10^{6-9} M_\odot$, but a similar result is found by Wood & Loeb (2000) for objects with $M \approx 10^{9-12} M_\odot$. They improved on the previous calculation by following the propagation of ionizing photons with a 3-D radiation transfer code and considering also a case of a two-phase medium. They find that the escape fraction is enhanced in a clumpy ISM. Although the derived escape fraction is lower than 1% at $z \approx 10$ for stellar sources, for miniquasars, which have higher luminosities and harder spectra, f_{esc} can be $\gtrsim 30\%$ at the same redshift. The higher escape fraction expected for quasars suggests that, if sufficiently abundant, they might have played a crucial role in the reionization of the IGM (see next Section). A similar trend with the mass and the virialization redshift of the galaxies is found for single metal-free very massive stars (Kitayama et al. 2004), by means of 1-D hydrodynamic code coupled with radiative transfer. In contrast with the above works, Fujita et al. (2003), in the previously mentioned paper, find $f_{esc} > 20\%$ at $z > 5$. This reversed trend would be due to the fact that ionizing photons escape more easily from high-redshift disks because the gas distribution is highly stratified under the strong gravitational potentials of the compact, high-redshift halos, and this allows quick acceleration of the superbubbles. The same trend is found by Razoumov & Sommer-Larsen (2006) who find that f_{esc} increases from 1-2% at $z = 2.39$ to 6-10% at $z = 3.6$ by postprocessing high-resolution simulations of galaxies with radiative transfer. A value of few % for galaxies with $M > 10^{11} M_\odot$ and $SFR \approx 1 - 5 M_\odot \text{ yr}^{-1}$

over the redshift range 3 – 9 is found by Gnedin, Kravtsov & Chen (2008) by means of AMR simulations with on-the-fly radiative transfer. Escape fractions larger than 70% as high as 100% (depending on the mass of the star and the hosting halo) are instead expected from very massive stars at high redshift (Whalen, Abel & Norman 2004; Alvarez, Bromm & Shapiro 2006; Yoshida et al. 2007). Thus, *the majority of theoretical models converge on values $f_{esc} < 15\%$ (the number though depends e.g. on mass of the host object, redshift, gas distribution), but a clear consensus has not yet been reached, although the first, relatively- or very-massive stars seem to have $f_{esc} > 70\%$ and as high as 100%*. For an example of the dependence of the escape fraction see Fig. 29.

5.2. HYDROGEN REIONIZATION

It is commonly believed that the reionization process proceeds through different stages. According to the terminology introduced by Gnedin (2000a), during the initial, pre-overlap stage, the hydrogen throughout the universe is neutral except for isolated H II regions due to individual sources. Following is the overlap stage, during which individual H II regions overlap and reionize the low-density, diffuse intergalactic gas. Some neutral hydrogen remains in dense clumps which are then slowly reionized during the post-overlap stage. The epoch of complete reionization, z_{ion} , is somewhat dependent on the definition of “complete”. A possible definition could be the redshift at which the mean free path to the ionizing radiation is of the order of the Hubble radius, or the time derivative of the mean free path has a peak. A more practical definition, associated with a quantity more easily measurable, is that z_{ion} corresponds to the epoch when the volume weighted neutral hydrogen fraction becomes $< 10^{-3}$. Increasing attention has been dedicated to the theoretical modeling of the reionization process, adopting semi-analytical (from the pioneering Shapiro & Giroux 1987; Fukugita & Kawasaki 1994; Miralda-Escudé & Rees 1994 and Tegmark, Silk & Blanchard 1994 to the more recent Haiman & Loeb 1997; Madau, Haardt & Rees 1999; Valageas & Silk 1999; Cojazzi et al. 2000; Chiu & Ostriker 2000; Miralda-Escudé, Haehnelt & Rees 2000; Wyithe & Loeb 2003a; Cen 2003a; Liu et al. 2004; Furlanetto, Zaldarriaga & Hernquist 2004a; Furlanetto & Oh 2005; Benson et al. 2006; Choudhury & Ferrara 2006; Cohn & Chang 2007) perturbative or semi-numerical (e.g. Zhang, Hui & Haiman 2007; Mesinger & Furlanetto 2007) and numerical approaches (e.g. Gnedin & Ostriker 1997; Gnedin 2000a; Ciardi et al. 2000; Razoumov et al. 2002; Ciardi, Stoehr & White 2003; Ciardi, Ferrara & White 2003; Ricotti & Ostriker 2004a; Sokasian et al. 2003; Iliev et al. 2006a; Trac & Cen 2007; Croft & Altay 2008). Two

main ingredients are required for a proper modeling of the reionization process: *(i) a reliable model of galaxy formation and (ii) an accurate treatment of the radiative transfer of ionizing photons.*

Despite many applications of hydrodynamical simulations to the structure formation process, much of our current understanding comes from semi-analytical models, based on simplified physical assumptions. These models have the advantages of allowing a larger dynamic range and of being fast enough to explore a vast range of parameters. Their main disadvantage is that no information on the spatial distribution of structures is provided. For this reason a new method has recently been developed that combines N-body simulations of the dark matter component, with semi-analytical models predicting galactic properties “a posteriori” (e.g. Kauffmann et al. 1999). The limitation of the above methods is related to the resolution of the N-body simulations, which turns out to be critical in studies of the reionization process. In fact, the resolution must be high enough to follow the formation and evolution of the objects responsible for producing the bulk of the ionization radiation. At the same time, a large simulation volume is required to have a region with “representative” properties and to avoid biases due to cosmic variance. It should be noted, however, that although the contribution of small mass objects to the ionizing photon production might be negligible due to feedback effects, they are nevertheless sinks of ionizing radiation (e.g. Barkana & Loeb 2002 and references therein). Thus, any numerical simulation which is not able to resolve these objects is likely to underestimate the gas clumping factor, and consequently the recombination rate, resulting in an earlier reionization epoch. These minihalos introduce a substantial cumulative opacity to ionizing radiation, unless they are photoevaporated by UV radiation quickly enough (Barkana & Loeb 2002; Shapiro, Iliev & Raga 2004; see previous Section). Ciardi et al. (2006) demonstrated by means of numerical simulations of cosmic reionization including minihalos, that, depending on the details of the minihalo formation process, their effect can delay complete reionization by $\Delta z \sim 0 - 2$.

At the present state, while the evolution of dark matter structures is well understood, the treatment of the physical processes that govern the formation and evolution of the luminous objects (e.g. heating/cooling of the gas, star formation, feedback) is more uncertain. In particular, no study treats the entire range of the feedback effects that can influence the galaxy formation process (see previous Section). A first attempt to treat self-consistently a number of feedback effects ranging from the mechanical energy injection to the H₂ photodissociating radiation produced by massive stars has been done by Ciardi et al. (2000), followed by the more recent Ricotti, Gnedin & Shull (2002) and Yoshida et al.

(2003a), but the complexity of the network of processes makes their implementation not trivial.

The next challenge for this kind of study is to develop accurate and fast radiative transfer schemes that can be then implemented in cosmological simulations. The full solution of the seven dimension radiative transfer equation (three spatial coordinates, two angles, frequency and time) is still well beyond our computational capabilities and, although in some specific cases it is possible to reduce its dimensionality, for the reionization process no spatial symmetry can be invoked. Thus, an increasing effort has been devoted to the development of radiative transfer codes based on a variety of approaches and approximations (e.g. Umemura, Nakamoto & Susa 1999; Razoumov & Scott 1999; Abel, Norman & Madau 1999; Gnedin 2000a; Ciardi et al. 2001; Gnedin & Abel 2001; Sokasian, Abel & Hernquist 2001; Cen 2002; Maselli, Ferrara & Ciardi 2003; Whalen & Norman 2006; Mellema et al. 2006a; Qiu et al. 2006; Rijkhorst et al. 2006; Susa 2006; Pawlik & Schaye 2008; for a comparison between different codes see Iliev et al. 2006b). The first attempt to include the radiative transfer in simulations of the reionization process has been done by Gnedin & Ostriker (1997). Ideally, radiative transfer codes should be eventually coupled with a hydrodynamic simulation. Although such an implementation has already been attempted by Gnedin (2000a), the Local Optical Depth approximation adopted for radiative transfer is less accurate for optical depths $\gtrsim 1$ and therefore may not be suitable to describe in detail the entire reionization history. A similar implementation, with the Optically Thin Variable Eddington Tensor approximation for radiative transfer, is used by Ricotti & Ostriker (2004a). Although in some respect these two works improve on previous calculations (they couple radiative transfer with hydrodynamic simulations and include some feedback effects), their conclusions might be affected by possible uncertainties introduced by the small cosmic volumes (maximum box size of $4 h^{-1}$ Mpc) considered (see e.g. Barkana & Loeb 2004 for a discussion of box dimension in simulations of cosmic reionization). Iliev et al. (2006a) have in fact clearly shown that only boxes larger than $20\text{-}30 h^{-1}$ Mpc can properly describe the global reionization process, while smaller boxes exhibit a large scatter. For this reason, boxes with such dimensions are needed (see Trac & Cen 2007 for a self-consistent calculation on large boxes). The largest simulations run (applied to the study of high- z QSOs spectra) have $1280 h^{-1}$ Mpc side (Kohler, Gnedin & Hamilton 2007), but the resolution is very poor and results from smaller simulations are used to include the effect of scales below the resolution limit.

An illustrative example of models of the reionization process is shown in Fig. 30. The Figure refers to the simulations by Ciardi, Stoehr

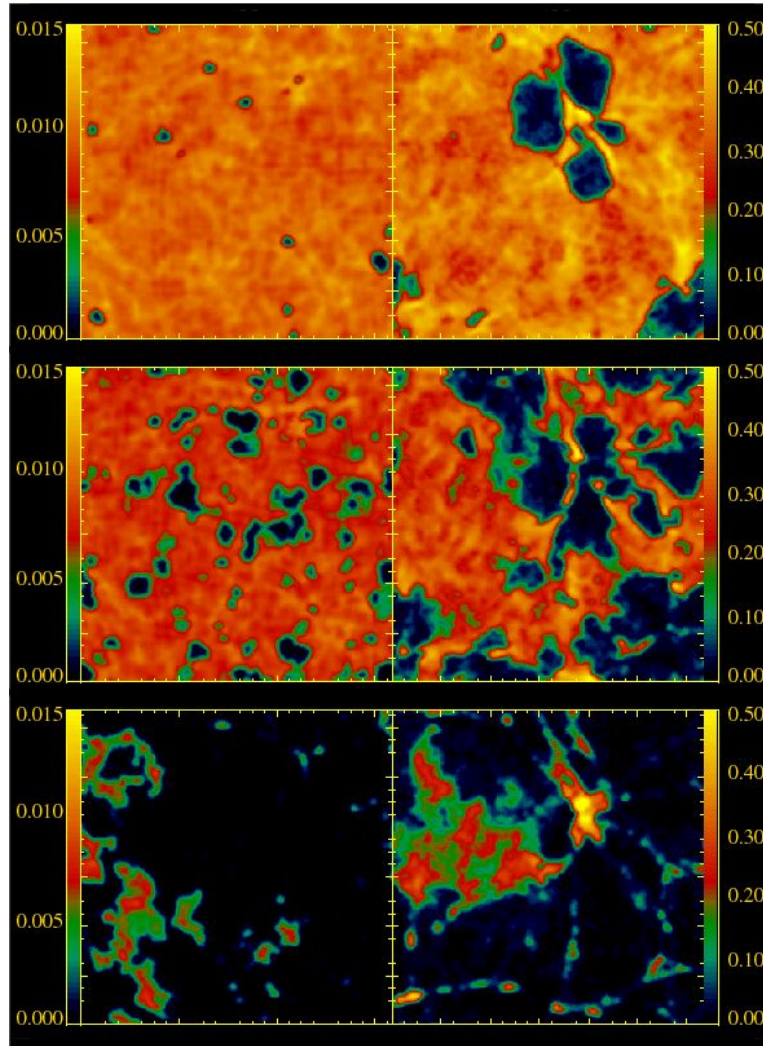


Figure 30. Reionization maps showing the redshift evolution of the number density of neutral hydrogen in the field ($L = 20h^{-1}$ Mpc comoving; left panels) and in a protocluster environment ($L = 10h^{-1}$ Mpc comoving; right panels). From top to bottom the redshift of the simulations is 15.5, 12 and 9 (Ciardi, Stoehr & White 2003; Ciardi, Ferrara & White 2003).

& White (2003), employing a combination of high resolution N-body simulations, a semi-analytical model of galaxy formation and the radiative transfer code CRASH (Ciardi et al. 2001; Maselli, Ferrara & Ciardi 2003). The maps are indicative of how the reionization process is affected by the environment: although in a protocluster environment the ionizing photon production per unit mass is higher at high redshift

than in a field region, as the high-density gas, more common in a protocluster, is more difficult to ionize and recombines much faster, filaments of neutral gas are still present after the field region is almost completely ionized.

The reionization process is affected not only by the environment, but also by the scale considered. In fact, while on scales of order of few Mpc reionization might be complete, on larger scales it could still be quite inhomogeneous due to the large scatter in the abundance of star-forming galaxies at early epochs (Barkana & Loeb 2004). A useful mathematical tool to study such complex topology is constituted by the Minkowski functionals (Gleser et al. 2006) of isodensity surfaces which can be used to discriminate among different reionization histories. In general, we expect that the properties of the H II regions depend on many poorly constrained quantities. McQuinn et al. (2007) have investigated this issue by means of radiative transfer simulations on large scales, including small scale physics via analytic prescriptions. They find that the morphology of H II regions is similar for fixed values of the mean ionization fraction, with other parameters playing a secondary role (the next most important dependence is on the nature of the ionizing sources, with larger and more spherical regions for rarer sources). Clearly topology of the H II regions, clustering of sources and the clumpiness of the IGM are key issues to understand reionization in detail. These have been investigated by Furlanetto & Oh (2005). Their main result is that the radiation background at any point evolves through a series of discrete jumps until it saturates at the mean free path, when a region becomes recombination-limited; afterwards the evolution proceeds very slowly. Towards the end of reionization fluctuations in the mean free path within large contiguous H II regions dominates over the clustering of the sources. However, Liu et al. (2006) noted that if the UVB evolves rapidly the following facts can be explained without invoking a fluctuating UVB at $z \sim 6$: rapid increase and large scatter in the Gunn-Peterson optical depth, long-tail distribution of the transmitted flux, long dark gaps in spectra.

The nature of the sources responsible for the IGM reionization is still the subject of a lively debate, but most theoretical models adopt stellar type sources, including a variety of spectra and IMF. These have to be constrained on the basis of the available observations: (i) the value of the IGM temperature from the Ly α forest at $z \approx 2 - 4$ (e.g. Bryan & Machacek 2000; Ricotti, Gnedin & Shull 2000; Schaye et al. 2000b; McDonald et al. 2001; Meiksin, Bryan & Machacek 2001; Zaldarriaga, Hui & Tegmark 2001); (ii) the abundance of neutral hydrogen at $z > 6$ from the spectra of high-redshift QSOs or galaxies (e.g. Fan et al. 2000, 2001, 2003, 2006) and (iii) the measurements of the Thomson scattering

optical depth (e.g. Kogut et al. 2003; Spergel et al. 2003; Page et al. 2007; Nolta et al. 2008). A simple scenario in which the IGM reionized early ($z_{ion} > 10$, as suggested by the last condition) and remains so thereafter, is ruled out as the IGM would reach an asymptotic thermal state too cold compared to observations (Theuns, Schaye & Haehnelt 2000; Hui & Haiman 2003; Wyithe & Loeb 2003b).

The most attractive scenario requires an enhanced ionizing photon emission at high redshift (compared to the low redshift), obtained either through a higher ionizing photon production (metal-free stars and/or top-heavy IMF), star formation efficiency or escape fraction. A suitable combination of these parameters allows an early enough reionization and matches the measured Thomson scattering optical depth (e.g. Cen 2003b; Ciardi, Ferrara & White 2003; Ciardi, Stoehr & White 2003; Haiman & Holder 2003; Onken & Miralda-Escudé 2004; Sokasian et al. 2003, 2004; Wyithe & Loeb 2003b; Iliev et al. 2006a; but see also Ricotti & Ostriker 2004a). Following feedback and metal enrichment, it is plausible that the ionizing photon production drops, resulting in a partial/total recombination of the IGM, followed by a second reionization at $z \approx 6$, produced by more standard sources (Wyithe & Loeb 2003a; Cen 2003a; but see also Oh & Haiman 2003 who propose that the ionizing photon production is regulated by gas entropy rather than by a transition from Pop III to Pop II stars) or more simply resulting in a temporary slight decrease of the ionizing flux (Tumlinson, Venkatesan & Shull 2004). Such reionization history might also help in releasing the tight constraint posed by the IGM temperature at $z \approx 3$ on the reionization redshift. The contribution to cosmic reionization from very massive metal-free stars is still very uncertain. In fact, to produce a number of ionizing photons sufficient to substantially ionize the IGM, there would be an over production of metals (e.g. Ricotti & Ostriker 2004a; Rozas, Miralda-Escudé & Salvador-Sol'e 2006) and the transition from Pop III to Pop II stars would occur early on (Fang & Cen 2004). It has been proposed that while very massive metal-free stars would form in metal-free halos with $T_{vir} < 10^4$ K, larger metal-free halos would host metal-free stars with masses $< 100 M_{\odot}$. In this case, it is found (Greif & Bromm 2006) that, due to the impact of radiative feedback, the contribution of very massive Pop III stars to reionization (and metal enrichment, see Section 5.4) is not substantial as their formation terminates at relatively high redshift. The formation of lower mass Pop III stars would stop at lower redshift due to metal enrichment and feedback, and their contribution to reionization would be more important. This picture is supported by Schneider et al. (2006a). Using a semi-analytic model to follow the formation and evolution of dark matter halos, coupled with a self-consistent treatment of chemical

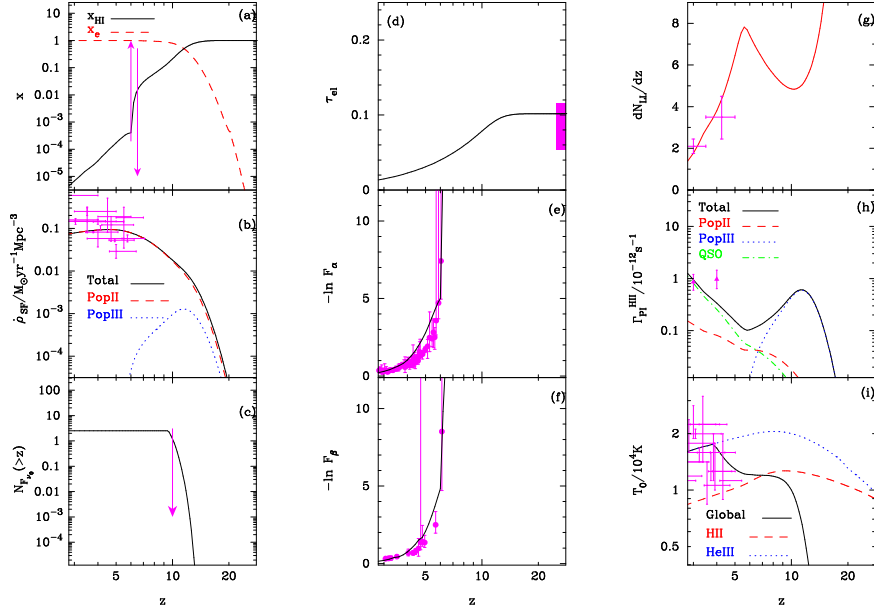


Figure 31. The best-fitting model Choudhury & Ferrara (2006). The panels show the redshift evolution of: (a) the volume-averaged electron and HI fraction. The arrows show an observational lower limit from QSO absorption lines at $z = 6$ and upper limit from Ly α emitters at $z = 6.5$; (b) the cosmic star formation history, with the contribution of Pop III and Pop II stars. (c) the number of source counts above a given redshift, with the observational upper limit from NICMOS HUDF; (d) the electron scattering optical depth, with observational constraints from 3-yr WMAP data; (e) Ly α effective optical depth; (f) Ly β effective optical depth; (g) the evolution of Lyman-limit systems; (h) photoionization rates for neutral hydrogen, with estimates from numerical simulations; (i) temperature evolution of the mean density IGM. For the data sources, see the original paper.

and radiative feedback, they find that the constraints imposed by the NICMOS observations (Bouwens et al. 2005) can be fulfilled together with those imposed by WMAP only if Pop III stars have a slightly top-heavy IMF, but masses $< 100 M_{\odot}$. A similar result is found by Daigne et al. (2004) and Choudhury & Ferrara (2006). The last paper presents a comprehensive model of reionization which satisfies simultaneously all the available constraints set by different observations (see caption of Fig. 31 for a complete list). Although many details might be modified by future observations, a solid conclusion seems to be that reionization has been a gradual and long-lasting event which was started by Pop III stars at $z \approx 15$, it was 90% complete at $z \approx 9$ and completed only with the help of Pop II stars and quasars at $z \approx 7$.

Following the first year release of WMAP data, that implied a high value for the Thomson scattering optical depth, several alternative

processes/contributions to enhance the high redshift ionizing photon emission have been proposed. For example, a component of a non-scale-free isocurvature power spectrum in addition to the more standard scale-free adiabatic power spectrum, would induce an earlier structure formation and yield an efficient source of early star formation, down to $z \approx 10$, without violating the existing constraints from the Lyman- α forest observations (Sugiyama, Zaroubi & Silk 2004). The same effect could be obtained with non-Gaussian density fluctuations (Chen et al. 2003). If magnetic fields generated in the early universe had a strength $B \gtrsim 0.5$ nG (consistent with BBN and CMB constraints that set an upper limit to the comoving amplitude of ~ 10 nG at 1 Mpc scale), they would as well induce additional density perturbation on small scales (Tashiro & Sugiyama 2006a). A contribution could also come from globular clusters, for which a high escape fraction is expected (Ricotti 2002). An enhancement of the ionizing photon production caused by an increased/earlier formation of low mass galaxies, though, would crucially depend on the efficiency of feedback effects and their ability to partially/completely suppress star formation in primordial objects (see previous Section). Moreover, e.g. Ricotti, Gnedin & Shull (2002) have shown that even for the case of weak feedback, small galaxies can only partially reionize the IGM. More specifically, reionization begins earlier with the inclusion of small galaxies (with the consequence of raising the value of the Thomson scattering optical depth), but their influence is limited by Jean-mass filtering in the ionized regions and the time of overlap is dictated by the efficiency of the higher mass halos (Iliev et al. 2007a). In more exotic scenarios, loops formed from a cosmic string network would induce structure formation at earlier times (Olum & Vilenkin 2006).

In addition to stellar-type sources, a contribution to the UV photon budget could also come from other sources. In particular, high- z quasars, if present, can produce a substantial amount of ionizing photons (e.g. Madau, Haardt & Rees 1999; Valageas & Silk 1999; Miralda-Escudé, Haehnelt & Rees 2000; Wyithe & Loeb 2003a; Ripamonti, Mapelli, Zaroubi 2008), thanks to their higher luminosity and escape fraction. Madau et al. (2004), for example, have shown that miniquasars powered by intermediate-mass black holes (the remnants of the first generation of massive stars) could produce a significant amount of ionizing photons at $z > 15$, under a number of plausible assumptions for the amount of gas accreted onto the black holes and their emission spectrum. On the other hand, as the recombination rate and hence the required emissivity to reionize the IGM, increase both with redshift and with the luminosity of the sources (Miralda-Escudé, Haehnelt & Rees 2000), this might reduce the effectiveness

of reionization by luminous quasars. Another crucial question about QSOs is their relatively short lifetime, which might effectively limit the growth of their ionized regions. In addition, Salvaterra, Haardt & Ferrara (2005) find that, unless primordial quasars are extremely X-ray quiet (to avoid exceeding the observed soft X-ray background), their contribution to reionization is only secondary.

Also more energetic photons, e.g. X-ray photons, can contribute to the IGM reionization (Oh 2001; Venkatesan, Giroux & Shull 2001; Madau et al. 2004; Ricotti & Ostriker 2004b). This component could come from early quasars, but also from thermal emission from the hot supernova remnants, or inverse Compton scattering of soft photons by relativistic electrons accelerated by supernova explosions (Oh 2001). As X-rays have much larger mean free paths, compared to photons from stellar spectra (the mean free path for a 1 keV X-ray photon is 10^5 times larger than for a 13.6 eV photon), and their escape fraction is ≈ 1 , they can permeate the IGM relatively uniformly. But only if redshifted X-rays are taken into account, their contribution to reionization can be substantial (e.g. Ricotti & Ostriker 2004b).

Another possible contribution to reionization at high redshift could come from decaying particles and neutrinos. While massive active neutrinos (Sciama 1990; Scott, Rees & Sciama 1991) have been excluded by current cosmological data (see Spergel et al. 2003 for the latest results), a decaying sterile neutrino does not violate existing astrophysical limits on the cosmic microwave and gamma ray backgrounds and could partially ionize the IGM. While Hansen & Haiman (2004) find that a decaying sterile neutrino could account for the observed Thomson scattering optical depth, Mapelli & Ferrara (2005) conclude that it must have played only a minor role in the reionization process. But there is no lack of other decaying particle-physics candidates; e.g. cryptons, R-parity violating gravitinos, moduli dark matter, superheavy dark matter particles, axinos and quintessinos. Chen & Kamionkowski (2004) have studied these particles, deriving the channels in which most of the decay energy ionizes and heats the IGM gas and those in which most of the energy is instead carried away (e.g. photons with energies $100 \text{ keV} < E < 1 \text{ TeV}$). They find that decaying particles can indeed produce an optical depth consistent with the WMAP results, but they produce new fluctuations in the CMB temperature-polarization power spectra. The amplitude of such fluctuations generally violates current constraints for decay lifetimes that are less than the age of the universe, while it is usually consistent with the data if the lifetime is longer (but see also Kasuya & Kawasaki 2004, who find that also particles in a short lifetime are consistent with the WMAP data. In a subsequent version of the paper they favor longer lifetimes to be consistent the WMAP3

results). Avelino & Barbosa (2004) have shown that a contribution to reionization from the decay products of a scaling cosmic defect network could help to reconcile a high optical depth with a low redshift of complete reionization. Finally, it has been proposed (Sethi & Subramanian 2005) that the primordial magnetic field energy could dissipate into the IGM by ambipolar diffusion and by generating decaying magneto hydrodynamics turbulence. These processes can modify the thermal and ionization history of the IGM and contribute to the Thomson scattering optical depth.

Neither X-rays nor decaying particles alone produce a fully ionized IGM, but the IGM may have been warm and weakly ionized prior to full reionization by stars and quasars. This scenario would also alleviate constraints on structure formation models with low small-scale power, such as those with a running or tilted scalar index, or warm dark matter models, which, alone, would not provide enough ionizing photons (e.g. Haiman & Holder 2003; Somerville, Bullock & Livio 2003; Yoshida et al. 2003b; Yoshida et al. 2003c).

5.3. HELIUM REIONIZATION

The stellar sources that ionize hydrogen can as well produce singly ionized helium, through photons with energies $h\nu > 24.6$ eV. Moreover, as these two species have comparable recombination rates, their reionization history is very similar. On the other hand, He II reionization requires harder photons ($h\nu > 54.4$ eV), either from massive Pop III stars (Venkatesan, Tumlinson & Shull 2003), from quasars (Madau, Haardt & Rees 1999; Miralda-Escudé, Haehnel & Rees 2000; Wyithe & Loeb 2003a; Madau et al. 2004; Ricotti & Ostriker 2004b) or from thermal emission from shock-heated gas in collapsed cosmic structures (Miniati et al. 2004). This last contribution would be comparable to the QSO one at $z \approx 3$ and dominating at $z > 4$, in terms of He II ionizing photons. Since H I and He I do not absorb a significant fraction of photons with energy higher than 54.4 eV, the problem of He II reionization can be decoupled from that of the other two species.

The He II Ly α absorption is generally much stronger than the H I Ly α absorption, by a factor $\eta = N(\text{He II})/N(\text{H I}) \sim 4\tau_{\text{HeII}}/\tau_{\text{HI}}$, where the second equality is valid for optically thin lines. The larger strength of He II arises because it is harder to photoionize than H I (although the number of helium atoms is smaller than hydrogen atoms by a factor of ≈ 10), owing to lower fluxes and cross sections at its ionizing threshold. In addition, He III recombines ≈ 5.5 times faster than H II and He II (this number becomes ≈ 5.9 when including the increase in the electron density due to the ionization of helium). This suggests,

supported by semi-analytical (Madau, Haardt & Rees 1999; Miralda-Escudé, Haehnelt & Rees 2000; Venkatesan, Tumlinson & Shull 2003; Wyithe & Loeb 2003a; Furlanetto & Oh 2008) and numerical (Sokasian, Abel & Hernquist 2001; Gleser et al. 2005; Paschos et al. 2008) calculations, that helium reionization occurred at $z \lesssim 5$, i.e. after completion of hydrogen reionization. The known population of quasars is sufficient to completely reionize He II before $z \approx 3$ (e.g. Miralda-Escudé, Haehnelt & Rees 2000), although this is subject to the assumed gas clumping and a contribution from high- z quasars (or other sources) could be needed (e.g. Madau, Haardt & Rees 1999). On the other hand, one might worry that the primordial contribution to He II ionizing photons may be too high and induce an almost simultaneous H I and He II reionization. Assuming a standard power-law spectrum for miniquasars, it is shown that only a small delay between the complete overlapping of H II and He III regions is expected. Thus if in addition to miniquasars Pop III stars and thermal emission from shock-heated gas also contributed to He II reionization in the early universe, one might expect a double reionization, a first time by the above sources, followed by recombination as Pop II stars with softer spectra took over, and then by a second overlap phase at $z \approx 3$, driven by the known population of quasars (e.g. Venkatesan, Tumlinson & Shull 2003; Wyithe & Loeb 2003a). Ricotti & Ostriker (2004b) find that reionization of He II from primordial black holes can be almost complete at $z \approx 15$. In their model, the full reionization at $z \approx 3$ is due to a hardening of the background radiation rather than QSO activity. The He III ionizing flux should fluctuate substantially because, in a random region of space, it is dominated by only a few active sources. This can produce optical depth fluctuations in the He II forest on scales comparable to the mean free path, $\approx 7000 \text{ km s}^{-1}$. These fluctuations may also be due, however, to the random fluctuations in the number of underdense voids in the IGM crossed by the line of sight. A strong proximity effect is also expected, and it is observed in the spectra of quasars for which the He II Ly α forest has been observed.

Associated with IGM reionization is also an increment of its temperature (e.g. Miralda-Escudé & Rees 1994; Theuns et al. 2002a; Ricotti & Ostriker 2004b). Because its cooling time is long, the low-density IGM retains some memory of when and how it was reionized. The post-ionization temperature is generally higher for harder spectra of the ionizing radiation, but it depends also on the type of source. While the IGM can be heated up to $T \approx 10,000 \text{ K}$ during hydrogen reionization, it can reach $T \approx 20,000 \text{ K}$ during helium reionization (see also Fig. 40).

5.4. IGM METAL ENRICHMENT

The same stars that ionize the IGM are responsible for its metal enrichment. Differently from their present counterparts, Pop III stars do not suffer strong stellar winds and thus the main contribution to the metal pollution comes from the later stages of their evolution. Wind-driven mass loss is believed to be metallicity-dependent, and a scaling law $\propto Z^{1/2}$ has been suggested for hot stars (Kudritzki 2000; Nugis & Lamers 2000). This scaling breaks down at $Z < 10^{-2} Z_{\odot}$, where the power-law becomes steeper (Kudritzki 2002). Marigo, Chiosi & Kudritzki (2003) have studied the mass loss by stellar winds for stars with initial masses in the range $120 - 1000 M_{\odot}$, including the two main mass loss driving processes, i.e. radiative line acceleration (e.g. Kudritzki 2002; Krtićka & Kubät 2006) and stellar rotation (Maeder & Meynet 2000). According to their calculations, wind mass-loss for stars with metallicity of $10^{-4} Z_{\odot}$ is significant only for very massive objects ($750 - 1000 M_{\odot}$). For a $1000 M_{\odot}$ non-rotating star, 17.33% (0.03%) of the initial mass is ejected via mass loss as helium (oxygen) during the stellar lifetime. A small amount of carbon and nitrogen is ejected as well. Several important effects are introduced if rotation is taken into consideration. First, chemical mixing is more efficient for lower metallicity for a given initial mass and velocity. This favors the evolution into the red supergiant stage, when mass loss is higher, and it enhances the metallicity of the surface of the star, boosting the radiatively driven stellar winds. Second, although metal-poor stars lose less mass to winds compared to their more enriched counterparts, they also lose less angular momentum, so that they have a larger chance of reaching the break-up limit (when the outer layers become unbound and are ejected) during the main sequence phase. Meynet, Ekström & Maeder (2006), including the above effects of rotation, find that a $60 M_{\odot}$ star, with $Z = 10^{-8}$ and initial velocity of 800 km/s can lose 22% of its mass. At $Z = 0$ though the mass loss is of the order of few percent (Ekström, Meynet & Maeder 2006). Finally, whereas pulsation-driven mass loss is important, if not dominant, at high metallicity, Baraffe, Heger & Woosley (2001) have shown that it is negligible at very-low metallicity. If indeed mass loss in very massive stars is dominated by optically thick, continuum-driven outbursts or explosions as suggested by Smith & Owocki (2006), nitrogen would be expelled, but no other heavy metal because these stars are not in advanced O, Si and subsequent burning stages. We can conclude then that, *as metal pollution from stellar winds is negligible for very-low metallicity stars, the main contribution to the IGM metal enrichment comes from those stars that end up their lives as PISN and core-collapse SNe* (see Fig. 16).

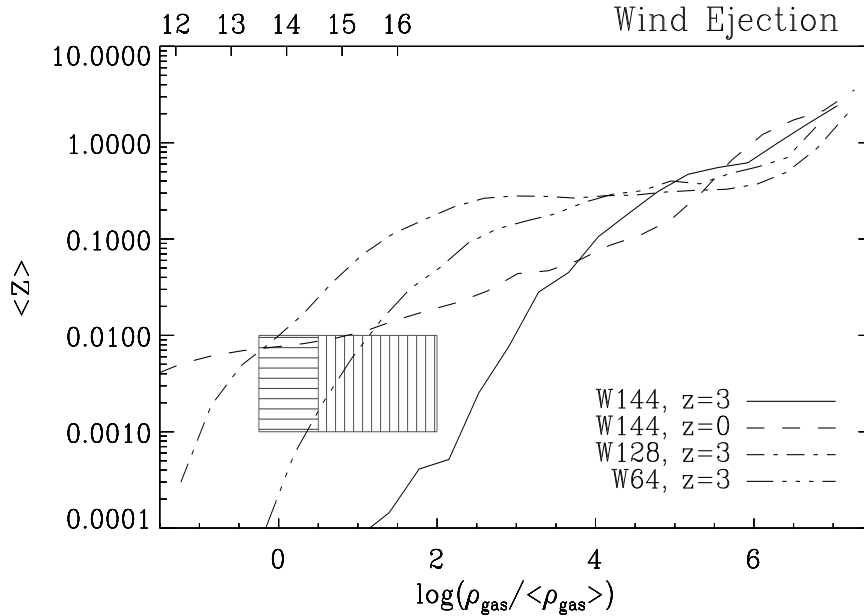


Figure 32. Mean metallicity vs. overdensity for three different simulations at $z = 3$ and for a simulation at $z = 0$ (see details in Aguirre et al. 2001c). The top axis is $\log N_{\text{HI}}$ of an absorber corresponding to the bottom-axis overdensity at $z = 3$. The vertically striped box outlines the approximate current constraints from the Ly α forest at $z \approx 3$, while the horizontally striped box shows an extension of these constraints to lower densities.

As metal factories (stars) are almost always associated with high density regions, in the absence of any efficient diffusion/transport mechanism, one would then expect a very strong density/metallicity correlation. Although such positive correlation is seen, it is not as strong as expected on the basis of the above naive assumption. However, a relation is predicted by simulations, as is clearly seen in Fig. 32 (Aguirre et al. 2001c). In any case, the observed large-scale clustering of metal absorbers encodes valuable information about the masses of the objects from which they were ejected. Likewise, as the maximal extent of each enriched region is directly dependent on the velocity at which the metals were dispersed, measurements of the small clustering of these absorbers is likely to constrain the energetics of their sources.

Different mechanisms have been suggested to remove metals from the galaxies in which they are produced, ranging from dynamical encounters between galaxies, to ram-pressure stripping, supernova-driven winds or radiation-pressure driven dust efflux. While dynamical removal undoubtedly occurs at some level, it is not clear if it can account

for the observed metallicity in the $z \approx 3$ IGM (Aguirre et al. 2001c; but see Gnedin 1998, who finds merging events as a dominant mechanism for transporting heavy elements into the IGM). The same argument applies to the ram-pressure stripping, which has a minor impact on the overall metallicity and filling factor as it occurs only in the densest and most polluted regions of space (Scannapieco, Ferrara & Madau 2002).

Metal ejection by galactic winds is one of the most popular mechanisms for the IGM pollution (e.g. Cen & Ostriker 1999; Aguirre et al. 2001b; Madau, Ferrara & Rees 2001; Scannapieco, Ferrara & Madau 2002; Qian & Wasserburg 2005; Scannapieco 2005; Pieri, Martel & Grenon 2006; Tornatore, Ferrara & Schneider 2007). Madau, Ferrara & Rees (2001) find that pre-galactic outflows from the same primordial halos that reionize the IGM, could also pollute it to a mean metallicity of $Z \gtrsim 10^{-3} Z_{\odot}$. The advantage of metals produced in these low-mass halos is that they can more easily escape from their shallow potential wells than those at lower redshift. In addition, the enriched gas had to travel much shorter distances between neighboring halos at these early times, and it might therefore have been easier to obtain non-negligible cosmic metal filling factors (see also Scannapieco 2005). Moreover, the velocities associated with these pre-galactic outflows are small enough to leave the thermal and structural properties of the IGM unperturbed, in contrast with stronger galaxy winds (with velocities $\gtrsim 200 - 300 \text{ km s}^{-1}$), which, although capable of enriching the IGM to the mean level observed, are likely to overly disturb it (e.g. Cen & Ostriker 1999; Aguirre et al. 2001b). Rayleigh-Taylor instabilities at the interfaces between the dense shell which contains the swept-up material and the hot, metal-enriched low-density bubble may contribute to the mixing and diffusion of heavy elements. The volume filling factor of the ejecta can be up to 30% or higher, depending on the star formation efficiency, with the majority of the enrichment occurring relatively early, $5 \lesssim z \lesssim 14$ (Madau, Ferrara & Rees 2001; Scannapieco, Ferrara & Madau 2002; Thacker, Scannapieco & Davis 2002), and a possibly large contribution from very massive stars (Qian & Wasserburg 2005). Such early enrichment model can explain quite well the observed redshift evolution of elemental abundances derived from QSO absorption line experiments, as seen from Fig. 33, where model predictions are compared with available data. Nevertheless, enrichment by outflowing galaxies is likely to have been incomplete and inhomogeneous. Oppenheimer & Davé (2006), via hydrodynamic simulations, find that momentum-driven winds from galaxies at $z < 5$ are able to reproduce the measured C IV over the range $z \sim 2 - 5$. Thus it seems that a very early generation of stars is not required to explain these observations. The worry remains that the hydrodynamical motions induced by the

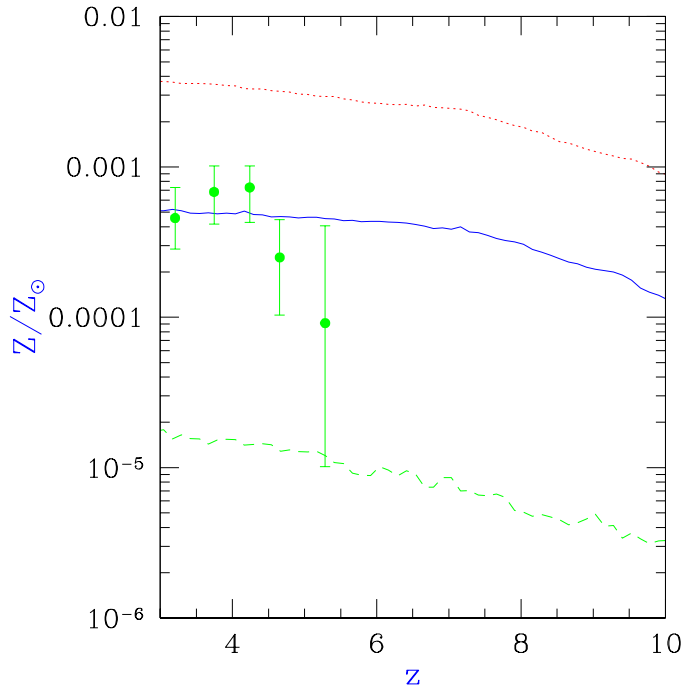


Figure 33. Metallicity evolution for low-density ($12 < \log N_{HI} < 15$) IGM. Points are the data of Songaila (2001); dotted, solid, and dashed lines are the predicted values for star formation efficiencies 0.5, 0.1, and 0.01, respectively (see Scannapieco, Ferrara & Madau 2002 for details).

outflow may spoil the nice agreement of Ly α absorption line statistics derived from studies in which these phenomena were not included. This problem has been convincingly washed out by the results of Bertone & White (2006), who, by combining N-body simulations and semi-analytical descriptions of the winds, find that winds do not sensibly alter the statistical properties of the Ly α forest.

But if indeed, as discussed in Sec. 3, the first stars were in the range for PISN and were produced, in the absence of feedback effects, in halos of masses of $M \approx 10^5 - 10^6 M_{\odot}$, the more energetic explosions would expel $\gtrsim 90\%$ of the stellar metals into a region of ≈ 1 kpc (Bromm, Yoshida & Hernquist 2003). Due to this burst-like initial SF episode, a large fraction of the universe could have been endowed with a metallicity floor $Z \gtrsim 10^{-4} Z_{\odot}$ already at $z \gtrsim 15$. Similarly, Matteucci & Calura (2005) find that ~ 110 PISN are enough to pollute a cubic comoving

Mpc to such metallicity floor. The authors find that, although it is easy for PISN to enrich the gas at high redshift, a contribution from Pop II stars is needed to reproduce the metallicity patterns observed in Ly α forest and in damped Ly α systems.

An alternative mechanism for the enrichment of the IGM is based on the *ejection of dust grains*, within which heavy elements are locked, by radiation pressure, along the lines suggested by Ferrara et al. (1991). Aguirre et al. (2001a) and Bianchi & Ferrara (2005), have investigated the IGM pollution caused by such a mechanism. An attractive feature of this model is that, unlike winds, enrichment by dust would not impact the thermal/structural properties of the IGM, as no shock waves are involved in the transport. According to this study, dust pollution can account for the observed level of C and Si enrichment of the $z \approx 3$ IGM, but not for all the chemical species observed in clusters at low redshift. Thus, the authors suggest a possible hybrid scenario in which winds expel gas and dust into galaxy halos but radiation pressure distributes the dust uniformly through the IGM. Of course, it is still to be demonstrated that grains are efficiently sputtered in the IGM and therefore can release their metals.

As discussed in Sec. 3, the presence of dust, as well as metals, can deeply affect the primordial star formation process. Thus, it is important to determine the dust production in the early universe. Recently, this issue has been discussed by Nozawa et al. (2003) and Schneider, Ferrara & Salvaterra (2004), which investigated the formation of dust grains in the ejecta of PISN and core-collapse SNe. The fraction of mass locked into dust grains is 2 – 5% of the progenitor mass for SN II and 15 – 30% for PISN; however, PISN dust depletion factors (fraction of produced metals locked into dust grains) are smaller (< 40%) than SN II ones. These conclusions depend very weakly on the thermodynamics of the ejecta, which instead affect considerably the grain formation epoch, composition and size distribution (Nozawa et al. 2003). Thus, if the first generation of stars were very massive, a *large amount of dust grains might be produced in the early universe*.

An additional problem is that our cosmic inventory of the cosmic metals associated with the observed star formation history is lacking a consistent fraction of heavy elements. This discrepancy is often referred to as the *missing metals* problem (see Pettini 2006 for the most recent review on the subject). One possibility is that missing metals escaped detection because they reside in the (hot) halos of the parent galaxies, as suggested by Ferrara, Scannapieco & Bergeron (2005) who found that up to 95% of the produced metals could be hidden in such a hot gas phase. Consistently with this hypothesis, Scannapieco et al. (2006) find that the correlation function of C IV absorbers favor a metal

enrichment mode in which metals are confined within bubbles with a typical radius of 2 Mpc around galaxies of mass $\approx 10^{12} M_{\odot}$. Note that this is not in contradiction with the fact that these metals could have been injected by early progenitors of these galaxies, as predicted by the pre-enrichment scenario.

5.5. KEY OBSERVATIONS

5.5.1. *Escape Fraction*

Observationally, a wide range of values for the escape fraction has been deduced, but it appears that – broadly speaking – relatively low values of f_{esc} are favored. For example, most of the detections of starburst galaxies with HUT²⁸ (Hopkins Ultraviolet Telescope) and FUSE²⁹ (Far Ultraviolet Spectroscopic Explorer) (Leitherer et al. 1995; Hurwitz, Jelinsky & Dixon 1997; Heckman et al. 2001) are consistent with $f_{esc} < 10\%$, although objects have been observed with $f_{esc} < 57\%$ (Hurwitz, Jelinsky & Dixon 1997). Tumlinson et al. (1999), based on H α images, derive a value of the escape fraction lower than 2%. However, absorption from undetected interstellar components could allow the true escape fractions to exceed these upper limits. Values of $f_{esc} \leq 10\%$ are found from the detection of flux beyond the Lyman limit in a composite spectrum of 29 LBGs at $z = 3.4$ (Steidel, Pettini & Adelberger 2001; Haehnelt et al. 2001). An $f_{esc} \lesssim 20\%$ would be compatible also with the observed UVB (Bianchi, Cristiani & Kim 2001). Fernández-Soto, Lanzetta & Chen (2003) found that, in a sample of 27 spectroscopically identified galaxies of redshift $1.9 < z < 3.5$ in the Hubble Deep Field, on average no more than 4% of the ionizing photons escape galaxies and even when all systematic effects are included, the data could not accommodate any escape fraction larger than 15%. A high value of f_{esc} has been measured only by Bland-Hawthorn & Maloney (1999; see Erratum 2001), who used optical line emission data for the Magellanic Stream to derive $f_{esc} \approx 45\%$. For a compilation of the existing measurements see Inoue, Iwata & Deharveng (2006). In conclusion, *observations of the escape fraction, with few exceptions, give $f_{esc} \leq 15\%$.*

5.5.2. *Gunn-Peterson Test*

The discovery of quasars at $z > 5.8$ (e.g. Fan et al. 2000, 2001, 2003, 2004; Goto 2006) are finally allowing quantitative studies of the high-redshift IGM and its reionization history. In particular, the detection of a Gunn-Peterson trough (Gunn & Peterson 1965) in the Keck³⁰ (Becker

²⁸ <http://praxis.pha.jhu.edu/hut.html>

²⁹ <http://fuse.pha.jhu.edu>

³⁰ <http://www2.keck.hawaii.edu>

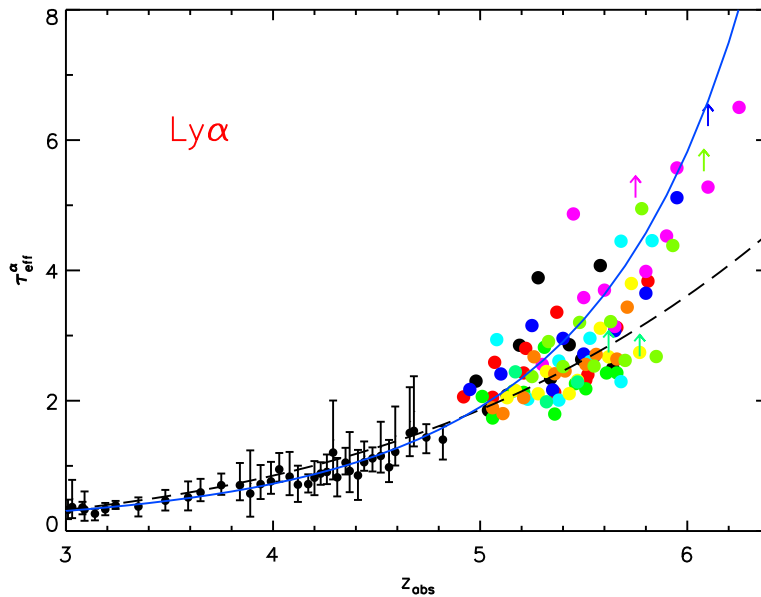


Figure 34. Evolution of the effective Ly α optical depth. Points correspond to data. The dashed line shows the best-fit at $z < 5.5$ (Fan et al. 2006), the solid line is calculated from the lognormal distribution of Ly α optical depths. For details see Becker et al. (2007).

et al. 2001) and VLT³¹ (Very Large Telescope) (Pentericci et al. 2002) spectra of the Sloan Digital Sky Survey quasars SDSS J1030-0524 at $z = 6.28$, and SDSS J1148+5251 at $z = 6.37$ (White et al. 2003) might indicate that the universe is approaching the reionization epoch at $z \approx 6$, consistent also with the dramatic increase in the neutral hydrogen optical depth at $z > 5.2$ observed by Djorgovski et al. (2001). However, while the theoretical optical depth distribution commonly used to measure the H I ionization rate gives a very poor fit to the observations, more accurate models of the density distribution (i.e. an inverted temperature-density relation, see Sec. 2) provide a better agreement and suggest that the measured dramatic increase might be explained other than with a reionization at $z \sim 6$ (Becker, Rauch & Sargent 2007). Analytical fits to the measured effective optical depth are shown in Fig. 34.

These observations suggest that the IGM is in the post-overlap stage (Barkana 2002). It should be noted, though, that an analysis of the same high redshift quasars which takes into account the observed dimension of the ionized region surrounding them, implies a neutral

³¹ <http://www.eso.org/projects/vlt>

fraction of $\gtrsim 0.1$, much higher than previous lower limits (Wyithe & Loeb 2004; Mesinger & Haiman 2004; Wyithe, Loeb & Carilli 2005; but see Oh & Furlanetto 2005 for a discordant view). The main uncertainty in the above estimates is the quasars lifetime. Also analyzing the QSOs and modeling their spectra separately, Mesinger & Haiman (2007) find a lower limit of 0.033. Maselli et al. (2007), using a combination of SPH simulations and radiative transfer and analyzing mock spectra along lines of sight through the simulated QSO environment, show that the observed dimension of the ionized region is typically 30% smaller than the physical one. This induces an overestimate of the neutral fraction, which they find to be < 0.06 . This value is consistent with that found by Yu & Lu (2005) using a semi-analytic model to describe the QSO's environment (including a clumping factor and the contribution to ionization from stars). A similar result has been found by Bolton & Haehnelt (2007a) for a variety of quasars lifetime and luminosity and including the treatment of He in their radiative transfer simulation. The bottom line is that, according to these studies, *the size of the observed ionized regions cannot put stringent limits on IGM ionized fraction*. Stronger constraints can be obtained considering the relative size of the ionized regions in the Ly α and Ly β (Bolton & Haehnelt 2007b). An additional complication follows from the location of QSOs in biased regions. In fact, as the extent of the H II regions produced by nearby galaxies can be substantial, their contribution should be included when using the H II regions from QSO to determine the abundance of H I in the IGM (e.g. Alvarez & Abel 2007; Lidz et al. 2007).

By itself, the detection of a Gunn-Peterson trough does not uniquely establish the fact that the source is located beyond the reionization epoch, since the lack of any observed flux could be equally caused by ionized regions with some residual neutral fraction, individual damped Ly α absorbers or line blanketing from lower column density Ly α forest absorbers. On the other hand, for a source located at a redshift beyond but close to reionization, the Gunn-Peterson trough splits into disjoint Lyman- α , - β and possibly higher Lyman series troughs, with some transmitted flux in between them, that can be detected for sufficiently bright sources and used to infer the reionization redshift (Haiman & Loeb 1999). Alternatively, metal absorption lines, rather than H ones, have been proposed to probe the pre-reionization epoch (Oh 2002). To this goal, one should select absorption-line probes which are still unsaturated when the IGM is predominantly neutral (this is possible for ions that are less abundant than H I or have smaller oscillator strengths), have ionization potentials similar to that of H, and that should lie redward of the Ly α wavelength (to avoid confusion with lower-redshift Ly α forest). This suggested experiment remains speculative as it is not

clear how it would be possible to have a highly neutral, but metal polluted IGM.

A recently suggested technique to study reionization is through the statistical analysis of QSO absorption spectra. In particular, the dark gap width distribution, together with the complementary leaks distribution (Fan et al. 2006; Gallerani, Choudhury & Ferrara 2006; Gallerani et al. 2007; Feng et al. 2008; Liu, Bi & Fang 2008) could help in discriminating between a late and an early reionization history, as for the former $>30\%$ of the line of sights to QSOs in the redshift range $5.7 < z < 6.3$ are expected to have dark gaps with widths $> 50\text{\AA}$, while none is expected for the latter (Gallerani, Choudhury & Ferrara 2006). In order to discriminate between different reionization histories though, a sample at higher redshift is required (Gallerani et al. 2007).

5.5.3. *Ly α Emitters*

Ly α emission has been crucial in determining the redshift of distant galaxies (e.g. Hu et al. 2002; Kodaira et al. 2003; Rhoads et al. 2003; Hu et al. 2004; Pelló et al. 2004; Kurk et al. 2004; Nagao et al. 2004; Stern et al. 2005; Wang, Malhotra & Rhoads 2005; Willis & Courbin 2005; Kashikawa et al. 2006), with the highest z Ly α emitter being at $z = 6.96$ (Iye et al. 2006; Ota et al. 2007; Stark et al. 2007b have found two possible gravitationally lensed candidates at $z \approx 10$) and it represents an invaluable tool to probe the high redshift universe and, possibly, the sources responsible for the IGM reionization. As Ly α is a resonant transition with a large cross section, even a small hydrogen neutral fraction in the intervening absorber can cause large opacity to Ly α photons from high- z sources. In particular, only the blue side of the Ly α line would be scattered away, while the red side would be observed, with a profile that depends on the ionization state of the IGM surrounding the galaxy or the presence of galactic winds (Miralda-Escudé 1998; Santos 2004). As a result of the absorption, the Ly α photons are scattered until they redshift out of resonance, resulting in a compact halo of Ly α light surrounding the source of the Ly α emission (Loeb & Rybicki 1999). Although the brightness of such diffuse Ly α component is very weak, this radiation is highly polarized and thus in principle detectable (Rybicki & Loeb 1999). If, on the contrary, the source is surrounded by a large H II region, the Ly α photons can avoid absorption, provided they redshift out of resonance before they reach the boundary of the H II region. Madau & Rees (2000) and Cen & Haiman (2000) (see also Cen 2003c) show that a sufficiently bright quasar placed at $z > 6$ can produce a Strömgren sphere large enough to render its Ly α emission line detectable, e.g. by JWST or Keck. Haiman (2002) has revisited this problem for a fainter source, showing that even for a galaxy as the one

discovered by Hu et al. (2002) a significant fraction of the emission line can remain observable. Moreover, if one considers the contribution to the formation of the H II region by neighboring galaxies, the prospect for observing a high- z galaxy are even better (Furlanetto, Hernquist & Zaldarriaga 2004), also prior to complete reionization (Wyithe & Loeb 2005). By means of numerical simulations of cosmological reionization, Gnedin & Prada (2004) show that it is possible to find galaxies at $z \approx 9$ (and possibly at $z > 10$) that are barely affected by the dumping wing of the Gunn-Peterson absorption. Later on, Mesinger, Haiman & Cen (2004) have shown that it should be possible to statistically extract relevant parameters, including the mean neutral fraction in the IGM and the radius of the local cosmological Strömngren region, from the flux distribution in the observed spectra of distant sources. Malhotra & Rhoads (2006) have estimated a lower limit for the volume average ionization fraction of 20-50% by assigning to each observed Ly α emitter a minimum H II region. The evolution in the luminosity function of Ly α emitters observed by Kashikawa et al. (2006) from $z = 5.7$ to $z = 6.5$ has been interpreted as due to a rapid evolution in the IGM ionization state. Dijkstra, Wyithe & Haiman (2007), though, argue that the observations are consistent with a mild or no evolution in the IGM transmission and can be explained with the evolution in the mass function of dark matter halos hosting Ly α emitters. Following an approach similar to that of Malhotra & Rhoads (2006) they estimate a volume averaged ionization fraction $> 80\%$.

5.5.4. *H I 21 cm Line Emission/Absorption*

It has long been known (e.g. Field 1959) that neutral hydrogen in the IGM and gravitationally collapsed systems may be directly detectable in emission or absorption against the CMB at the frequency corresponding to the redshifted H I 21 cm line (associated with the spin-flip transition from the triplet to the singlet ground state). Madau, Meiksin, & Rees (1997) first showed that 21 cm tomography could provide a direct probe of the era of cosmological reionization and reheating. In general, 21 cm spectral features will display angular structure as well as structure in redshift space due to inhomogeneities in the gas density field, hydrogen ionized fraction, and spin temperature. Several different signatures have been investigated in the recent literature: (i) fluctuations in the 21 cm line emission induced by the “cosmic web” (Tozzi et al. 2000), by the neutral hydrogen surviving reionization (Ciardi & Madau 2003; Furlanetto, Sokasian & Hernquist 2004; Zaldarriaga, Furlanetto & Hernquist 2004; Furlanetto, Zaldarriaga & Hernquist 2004b; He et al. 2004; Mellema et al. 2006b; Santos et al. 2007), and by minihalos with virial temperatures below 10^4 K (Iliev et

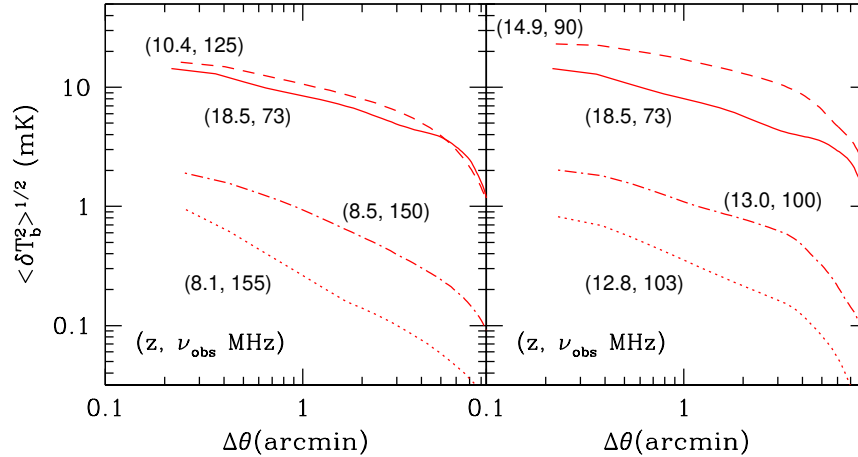


Figure 35. Expected rms brightness temperature fluctuations as a function of beam size for a model with reionization at $z \approx 7.5$ (left panel) and at $z \approx 12.5$ (right panel). A fixed bandwidth $\Delta\nu = 1$ MHz has been assumed. Each curve corresponds to a different emission redshift or, equivalently, observed frequency (see Ciardi & Madau 2003).

al. 2002, 2003; Furlanetto & Oh 2006; Shapiro et al. 2006); (ii) a global feature (“reionization step”) in the continuum spectrum of the radio sky that may mark the abrupt overlapping phase of individual intergalactic H II regions (Shaver et al. 1999); (iii) and the 21 cm narrow lines generated in absorption against very high-redshift radio sources by the neutral IGM (Carilli, Gnedin, & Owen 2002; Furlanetto 2006) and by intervening minihalos and protogalactic disks (Furlanetto & Loeb 2002; Furlanetto 2006). While an absorption signal would be preferable, being of a higher intensity, it relies on the existence of powerful radio sources at high redshift, which have not yet been found. A possibility would be the radio afterglow of GRBs or hypernovae (which could in principle be visible up to $z \approx 20 - 30$), but the estimated absorption lines are very difficult to detect also with the next generation of radio telescopes (Ioka & Meszaros 2004). On the other hand, a signal in emission, although weaker than the one in absorption, would always be present, as long as the IGM is not completely ionized and its temperature is above the one of the CMB.

Ciardi & Madau (2003) were the first to use large scale numerical simulations of hydrogen reionization by stellar sources to investigate the 21 cm signal expected from the diffuse, neutral IGM. They found that the predicted brightness temperature fluctuations on arcmin scales have typical values in the range 5 – 20 mK on scales below 5 arcmin,

with the maximum corresponding to the epoch when roughly 50% of the IGM is ionized, in agreement with subsequent studies (see Fig. 35). Ilev et al. (2002, 2003) find that the signal expected from minihalos is comparable to the signal from the IGM if feedback effects are assumed to be negligible. Shapiro et al. (2006) use numerical simulations to calculate the relative importance of IGM and minihalos, finding that the latter dominate the emission at $z \lesssim 18$, while they are negligible at higher redshifts. In their analysis though they neglect the effect of Ly α pumping and feedback, which can be crucial once the first sources of radiation start to shine. The inclusion of such mechanisms shows that the contribution from minihalos is almost always lower than that from the diffuse IGM (Furlanetto & Oh 2006).

More specific applications of the 21 cm signal allow to track the physical properties of individual H II regions as they form and grow around reionization sources, in particular Pop III stars and QSOs (e.g. Wyithe, Loeb & Barnes 2005; Zaroubi & Silk 2005; Chen & Miralda-Escudé 2006; Cen 2006; Rhook & Haehnelt 2006; Liu et al. 2007; Thomas & Zaroubi 2008). As the expected angular resolution is sensitive to scales that correspond to the transition between ionized and neutral regions for hard ionizing photons sources, additional information on their nature could come from observations of single ionized regions (Zaroubi & Silk 2005), also in the form of spectral dips in frequency space along single lines of sight (Kohler et al. 2005). This technique though would be compromised once ionized regions start to overlap. In addition, the 21 cm radiation emitted from the partially neutral IGM outside H II regions, if detected, could provide a novel way to probe the growth of BHs (Rhook & Haehnelt 2006).

A key physical mechanism to ensure a detectable 21 cm signal is the decoupling of the CMB temperature from the spin temperature, as the latter regulates the 21 cm line absorption/emission. It has been shown (Chuzhoy & Shapiro 2006) that the exact value of the spin temperature depends on physical processes that usually are not included in the calculations, the most important being the backreaction of resonant scattering on the pumping radiation and the scattering by resonant photons other than Ly α . In addition, it is usually assumed that the spin temperature is decoupled from the CMB temperature due to scattering with Ly α photons (the Wouthuysen-Field effect; Wouthuysen 1952; Field 1959) but its strength can be overestimated if a proper treatment of the Lyman series cascades is not included (Hirata 2006; Pritchard & Furlanetto 2006). Moreover, before a Ly α background is established, the bias in the galaxy distribution can induce fluctuations in the Ly α , and thus 21 cm, flux (Chen & Miralda-Escudé 2006). These fluctuations could be used to probe the distribution of the very first

galaxies (Barkana & Loeb 2005b; Wyithe & Loeb 2007). Additional fluctuations arise if the natural broadening of the line is considered. In this case in fact the optical depth in the wings causes scattering to happen nearer to the source, with a distribution function that depends on the optical depth and the frequency of the photon (Chuzhoy & Zheng 2007). These fluctuations though should affect the 21 cm signal only during a narrow range of redshift near the beginning of reionization, as a later times there are so many UV photons that these corrections are minor.

Kuhlen, Madau & Montgomery (2006) use hydrodynamic simulations of structure formation to study the effect of X-rays on 21 cm line. In a simulation without sources they find that, while in regions with $\delta \lesssim 1$ decoupling is not effective, for higher density contrasts H-H collisions are efficient at decoupling and most of the gas is shock heated, producing a signal in emission. When the effect of mini-quasars is included, the X-ray radiation preheats the IGM to a few thousand kelvins and the increased electron fraction boosts both the H-H and the H-e collisions (see also Nusser 2005a for the efficiency of H-e collisions in the decoupling during the very early stages of reionization). Thus also low density regions in the IGM can be seen in emission. It should be noted though that, although X-ray are usually considered to uniformly penetrate the IGM, this is not true at all times and might affect the 21 cm line signature (Pritchard & Furlanetto 2007).

Also the mechanism that can heat the gas above the CMB temperature is crucial for the observation of the line in emission. In addition to $\text{Ly}\alpha$ and X-ray photons (e.g. Madau, Meiksin & Rees 1997; Chen & Miralda-Escudè 2004; Pelupessy, Di Matteo & Ciardi 2007; Ciardi & Salvaterra 2007; Ripamonti, Mapelli & Zaroubi 2008), also UHE-CRs and decaying dark matter particles can heat the gas (Shchekinov & Vasiliev 2007). But it's been shown that $\text{Ly}\alpha$ scattering is not an efficient mechanism to heat the IGM (Chen & Miralda-Escudè 2004; Chuzhoy & Shapiro 2006; Furlanetto & Pritchard 2006), while X-rays are better, although they can uniformly heat the IGM only sometime after the first structure formation (Pritchard & Furlanetto 2007; Zaroubi et al. 2007).

Another signal detectable in the 21 cm radiation is its polarization. Although intrinsically unpolarized, in the presence of a magnetic field, the 21 cm line would show a left- and right-handed polarized component due to the Zeeman effect (Cooray & Furlanetto 2005). In addition, scattering between electrons produced during reionization and the 21 cm quadrupole would induce polarization (Babich & Loeb 2005). Such observations would probe the magnetic field on scale of H II regions around bright quasars or the intergalactic magnetic fields. An alter-

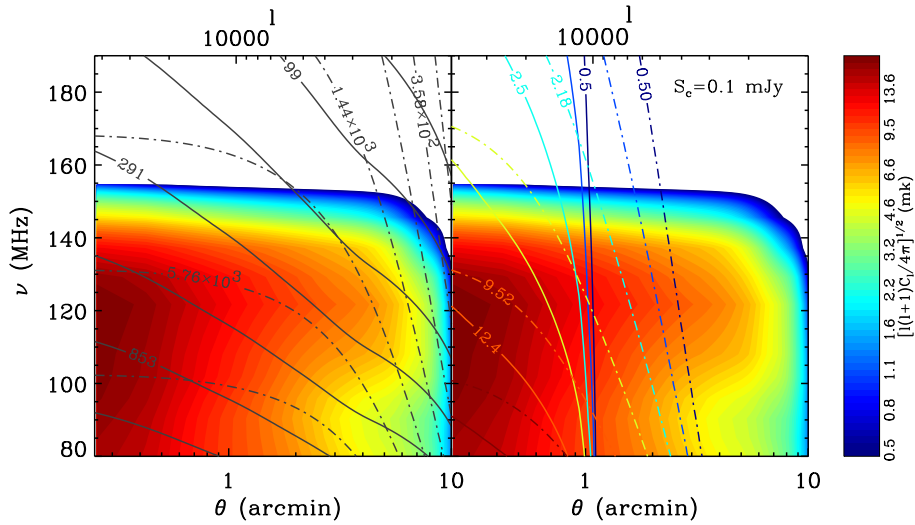


Figure 36. Contours of the angular power spectrum (in mK) of the the 21 cm fluctuations (shaded area) and the angular power spectra due to intensity fluctuations of radio galaxies (solid contours) and radio halos (dot-dashed contours) as a function of angle (l) and frequency. The lines in the right panel show the contours for the total foreground signals. In the left panel, foreground sources above a flux limit $S_c \approx 0.1$ mJy have been removed (see Ciardi & Madau 2003; Di Matteo, Ciardi & Miniati 2004).

native method to probe such magnetic fields would be through the imprint they leave on the brightness temperature fluctuations (Tashiro & Sugiyama 2006b).

The signatures in the brightness temperature discussed above can possibly be detected by the planned facilities SKA, LOFAR, 21cmA/PAST and MWA (see e.g. Valdes et al. 2006; Mellema et al. 2006b for the observability of its fluctuations). The same telescopes should also be able to distinguish between different reionization models and discriminate, e.g., a history with discrete H II regions from one with partial uniform ionization or from a double reionization (Furlanetto, Zaldarriaga & Hernquist 2004b). In principle, if peculiar velocities are associated with H I, they could induce non linear distortions in the redshift space and reduce the power spectrum of the brightness temperature. Wang & Hu (2006) though find that the next generation of radio telescopes are unlikely to be affected by such distortions.

However, these experiments are extremely challenging due to foreground contamination from unresolved extragalactic radio sources (e.g. Di Matteo et al. 2002), free-free emission from the same reionizing halos

(e.g. Oh & Mack 2003), synchrotron emission from cluster radio halos and relics (Di Matteo, Ciardi & Miniati 2004) and the Galactic free-free and synchrotron emission (Shaver et al. 1999). As the foregrounds are slowly varying as a function of frequency, it appears that the best strategy for measuring the 21 cm signal would be to search for frequency rather than angular fluctuations (Di Matteo et al. 2002; Gnedin & Shaver 2004; Zaldarriaga, Furlanetto & Hernquist 2004; Santos, Cooray & Knox 2005; Wang et al. 2006; Gleser, Nusser & Benson 2008). Di Matteo, Ciardi & Miniati (2004) have used cosmological simulations to predict the impact of extragalactic foreground produced by both extended (e.g. cluster radio halos and relics) and point-like (e.g. radio galaxies and free-free emission from ISM) sources in a self-consistent way. They find that the contribution to the angular fluctuations at scales $\theta \gtrsim 1$ arcmin is dominated by the spatial clustering of bright sources. Hence, efficient removal of such sources may be sufficient to allow the detection of angular fluctuations in the 21 cm emission free of extragalactic foregrounds (see Fig. 36).

5.5.5. *CMB Footprints*

In addition to the temperature anisotropies discussed in Sec. 2, reionization introduces also a polarization signal in the CMB spectrum. It is well known that the primordial polarization is generated at the recombination epoch through Thomson scattering of the quadrupole of the temperature anisotropy. The same mechanism operates during the reionization epoch and again distorts the shape of the polarization power spectrum. The *WMAP* telescope during the first year of operation detected a correlation between CMB temperature and polarization on large angular scales (Kogut et al. 2003; Spergel et al. 2003), whose amplitude is related to the total optical depth of CMB photons to Thomson scattering, giving $\tau_e \approx 0.16 \pm 0.04$ (the uncertainty quoted for this number depends on the analysis technique employed). This high value strongly favored an early reionization; e.g. $0.12 < \tau_e < 0.20$ translates into a reionization redshift of $13 < z < 19$ for a model of instantaneous reionization. The limits shift at lower redshift for a more realistic reionization, their precise value depending on the adopted history. In the light of the first three years of the *WMAP* experiment, the above results have been revised to $\tau_e = 0.09 \pm 0.03$ (see Fig. 37; Page et al. 2006; Spergel et al. 2006). Such value has been only marginally updated by the five years *WMAP* results, having now converged to $\tau_e = 0.087 \pm 0.017$ (Dunkley et al. 2008); note, however, the considerably smaller errorbar. The updated Thomson scattering optical depth can be better interpreted by a reionization redshift $z \approx 10$ (Spergel et al. 2006; Dunkley et al. 2008), substantially lower than the first year value.

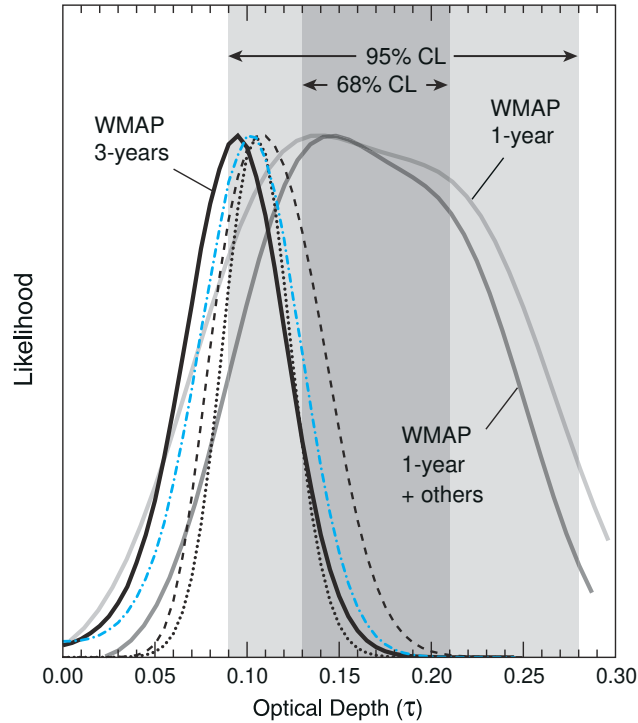


Figure 37. Comparison between the likelihood curves for τ in the WMAP-1yr and WMAP-3yr data. Different curves refer to different analysis (see Page et al. 2006 for details).

An interesting analysis by Hansen et al. (2004) shows that the estimate of τ_e varies substantially when inferred from power spectra computed separately on the northern and the southern hemispheres, and that the full sky estimate by the WMAP team could in large part originate in structures associated with the southern hemispheres. In addition, the interpretation of the Thomson scattering optical depth could change if magnetic fields were present during the epoch of reionization. In this case, the observed anisotropies at large scales could be partially explained with the existence of magnetic fields (Gopal & Sethi 2005).

Another valuable tool to study the reionization process is to detect the imprint it should leave on the CMB on small angular scales. When the IGM gets reionized, Thomson scattering off the newly formed electrons would, on one hand, blend photons initially coming from different directions thus damping the primary anisotropies, and on the other hand, create small-scale secondary anisotropies. Several groups have studied the CMB temperature anisotropies produced by an inhomogeneous reionization (Knox, Scoccimarro & Dodelson 1998; Bruscoli et

al. 2000; Benson et al. 2001; Gnedin & Jaffe 2001; Santos et al. 2003; McQuinn et al. 2006; Salvaterra et al. 2005; Zahn et al. 2005; Iliev et al. 2006c). In particular, calculations of anisotropies from simulations of patchy reionization give peak values of the power spectrum between $\approx 10^{-14}$ (e.g. Gnedin & Jaffe 2000) and \approx few 10^{-13} (e.g. Salvaterra et al. 2005; Iliev et al. 2006c), which might be probed by future interferometers like ALMA, ACT³² or CQ³³. The detection of such anisotropies would be an invaluable tool to discriminate between different sources of ionizing photons (e.g. McQuinn et al. 2006), especially in combination with measurements of 21 cm line emission (Salvaterra et al. 2005; Alvarez et al. 2006a; Holder, Iliev & Mellema 2007; Adshead & Furlanetto 2007; Tashiro et al. 2008; but see also Cooray 2004), taking advantage of the correlation between the two signals.

Future missions, like PLANCK³⁴, should also be able to distinguish between different reionization models (e.g. single, double reionization) based on the temperature-polarization power spectrum (e.g. Holder et al. 2003; Hu & Holder 2003; Kaplinghat et al. 2003; Naselsky & Chiang 2004; Zhang, Pen & Trac 2004; Colombo et al. 2005). The overall differences in the temperature (polarization) angular power spectra between prompt and extended reionization models with equal optical depths are less than 1% (10%) (Bruscoli, Ferrara & Scannapieco 2002). The same observations should also allow to discriminate a contribution to reionization from decaying particles (e.g. Naselsky & Chiang 2004).

Analogously to free electrons, heavy elements leave an imprint on the CMB due to scattering in their fine-structure lines, partially erasing original temperature anisotropies and generating new fluctuations. The main difference with the Thomson scattering is that the latter gives equal contribution over the whole CMB spectrum, while the line scattering gives different contributions to different spectral regions. Since every line affects only a given range of redshift, having observations at different wavelengths can provide an upper limit to abundances of different species at various epochs (Basu, Hernández-Monteagudo & Sunyaev 2004; Hernández-Monteagudo, Verde & Jimenez 2006; Hernández-Monteagudo et al. 2007, 2008).

It should be noted that the time and duration of recombination directly influence the characteristics of CMB anisotropies. Several authors (e.g. Leung et al. 2004; Dubrovich & Grachev 2005; Chluba & Sunyaev 2006) have found that the detailed treatment of processes such as the physics of the H⁺ and He⁺ populations, the softening of the matter equation of state due to the transition from ionized

³² <http://www.hep.upenn.edu/angelica/act/act.html>

³³ <http://brown.nord.nw.ru/CG/CG.htm>.

³⁴ <http://astro.estec.esa.nl/SA-general/Projects/Planck>

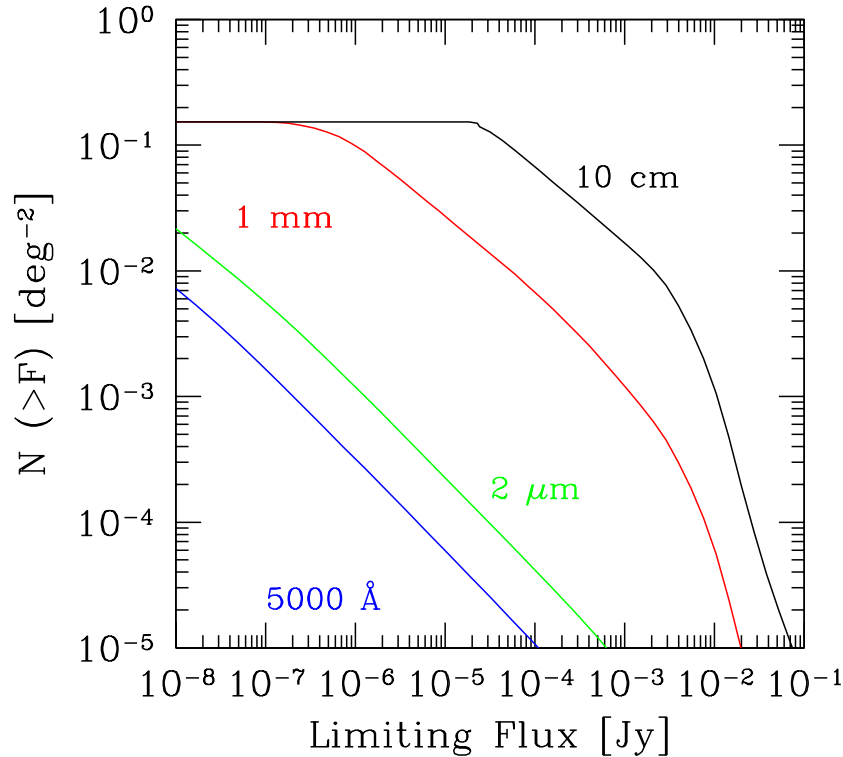


Figure 38. Predicted number of GRBs with observed flux greater than a limiting flux F , at different observed wavelengths (see Ciardi & Loeb 2000 for more details).

to neutral matter, the induced emission of the softer photons which change the two-photon decay rate of the 2s level of H, affect the value of the anisotropies at large multipoles at a percent level. Thus, in this epoch of precision cosmology, also those processes that can affect the anisotropies at a percentage level, should be included in the analysis.

5.5.6. Gamma Ray Bursts as Cosmic Lighthouses

The observation of the high- z universe, beyond the epoch of reionization, could be feasible directly if bright enough sources are present. If indeed GRBs are related to the SFR of the host galaxy and occur at high redshift (the highest GRB has been detected by SWIFT at $z = 6.29$, Watson et al. 2006), their afterglow emission can be used to probe the ionization history of the IGM (Totani et al. 2006). In contrast to other sources, such as galaxies or quasars, the observed

infrared flux from a GRB afterglow at a fixed observed age is only a weak function of its redshift (e.g. Ciardi & Loeb 2000). Thus, the afterglow of these sources could be detected by the next generation of telescopes, e.g. JWST, and used to probe the SF and ionization history of the universe (see Fig. 38; e.g. Ciardi & Loeb 2000; Blain & Natarajan 2000; Lamb & Reichart 2000; Porciani & Madau 2001; Bromm & Loeb 2002; Choudhury & Srianand 2002; Gallerani et al. 2008; McQuinn et al. 2008), as well as the characteristics of the circumburst medium (e.g. Frail et al. 2006). A proof that very high-redshift GRBs could be observed is GRB 080319B, that would have been easily detected in K band with meter-class telescopes up to $z \approx 17$ (Bloom et al. 2008). In particular, it has been noted (Inoue, Yamazaki & Nakamura 2004) that as the detection of a GRB afterglow through a NIR filter i beyond the Ly α drop-out redshift, $z_{\text{Ly}\alpha, \text{out}}^i$, probes the ionization state of the IGM around $z_{\text{Ly}\alpha, \text{out}}^i$, the I , J , H and K filters would be suitable to probe the ionization state at $z \approx 5 - 8$, $8 - 11$, $11 - 15$ and $15 - 20$, respectively. Thus, the null detection of the GRB afterglows at $z \approx 11$ in J -band would imply a high neutral fraction at $z \approx 8 - 11$. The Subaru³⁵ telescope has sufficient resolution to do the photometry. To better constrain the redshift, spectroscopy is required and it will be only feasible with SWIFT or future missions as ASTRO-F or JWST.

Free electrons along the light path cause distortions in the spectrum and light curve of an early radio afterglow. This distortion can be quantified through the Dispersion Measure (DM). At $z > 6$ the DM due to the ionized IGM probably dominates the contribution from the Galactic plasma and the plasma in the host galaxy. Thus, DM of GRBs at various redshifts and directions would help in determining the reionization history and possibly the topology of the H II regions. Both SKA and LOFAR should be able to detect bright afterglows and measure the DM towards high redshift GRBs (Ioka 2003; Inoue 2004).

5.5.7. Helium Reionization

The Gunn-Peterson trough technique to infer the abundance of neutral hydrogen in the IGM can be extended to the determination of He II abundance. The first evidence of such a trough has been found in the spectrum of the quasar Q0302-003 ($z = 3.286$, Jakobsen et al. 1994), followed by more determinations in the range $2.4 < z < 3.5$ (e.g. Davidsen, Kriss & Zheng 1996; Hogan, Anderson & Rugers 1997; Anderson et al. 1999; Smette et al. 2002; Jakobsen et al. 2003; Zheng et al. 2004). In particular, high resolution spectra of the quasar HE 2347-4342 at $z = 2.885$ (and more recently of QSO 1157+3143, Reimers et

³⁵ <http://subarutelescope.org/>

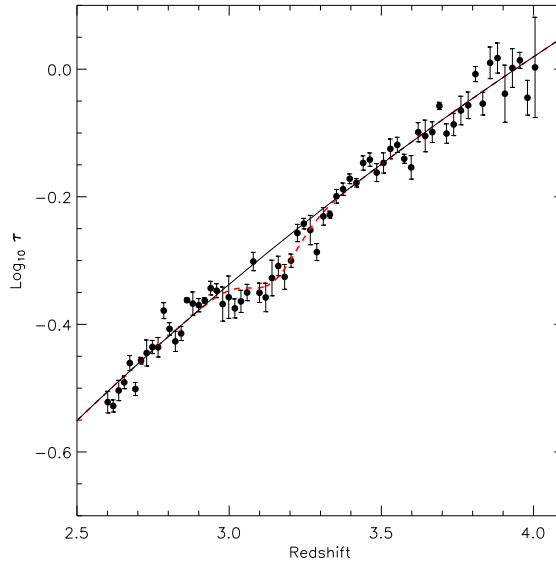


Figure 39. Effective optical depth as a function of redshift as measured from a sample of 1061 QSO spectra from the SDSS database (Bernardi et al. 2003).

al. 2005a) have shown a largely fluctuating η , in the range 0.1 – 1000, with an average of 80 (e.g. Reimers et al. 1997; Kriss et al. 2001; Smette et al. 2002; Shull et al. 2004). This implies that the metagalactic radiation field exhibits inhomogeneities at the scale of ~ 1 Mpc and has been interpreted as evidence for a patchy He II ionization in the IGM. However, it is unclear if the fluctuations could be caused by fluctuations of the IGM density or of the ionizing background flux (Miralda-Escudé, Haehnelt & Rees 2000; Kriss et al. 2001; Bolton et al. 2006), a wide range in the QSO spectral indexes (Telfer et al. 2002), finite QSO lifetimes (Reimers et al. 2005b) or the filtering of QSO radiation by radiative transfer effects (Shull et al. 2004; Maselli & Ferrara 2005). In fact, also QSOs that are believed to be in the post-reionization phase (e.g. HS 1700+6416, that, together with HE 2347-4342, is the only line of sight with He II absorption resolved in the Ly α forest structure) show a large variation in η (Fechner et al. 2006). Particular care should be taken when estimating the η value. In fact, if the same line width is assumed for He II and H I absorption features without including thermal broadening, as done in most analysis, this leads to a spurious correlation of the inferred η value with H I column density (Fechner & Reimers 2007).

An He II reionization at $z \approx 3$ was initially favored by a claim of an abrupt change at that redshift in the Si IV / C IV ratio in a sample of 13 QSO spectra, indicating that, while at $z \lesssim 3$ the ionization balance is

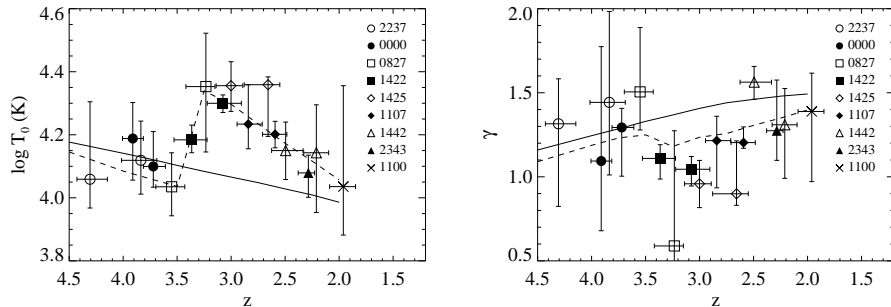


Figure 40. Temperature at the mean density (left panel) and slope of the effective equation of state (right panel) as a function of redshift. The dashed lines are from a simulation designed to fit the data. For more details see Schaye et al. (2000b).

consistent with a pure power-law ionizing spectrum, at higher redshift the spectrum must be softer. An analogous result is obtained by Heap et al. (2000), who analyzed the Gunn-Peterson He II absorption trough at $z = 3.05$, finding that the spectrum is much softer than the one deduced at $z = 2.87$. However, a more recent VLT/UVES study (Kim, Cristiani & D’Odorico 2002) using 7 QSOs finds no strong discontinuity for the quantity Si IV / C IV around $z \approx 3$ and suggests that it might not be a good indicator of He II reionization. Also the analysis of 19 high-quality quasar absorption spectra by Aguirre et al. (2004) seems to indicate no evolution in the Si IV / C IV ratio. Finally, Boksenberg, Sargent & Rauch (2003) find no jump at $z \approx 3$ in the median column density ratio Si IV / C IV, and also other ionic ratios vary continuously with redshift. On the other hand, the presence of a significant amount of O VI at $z \gtrsim 3$ suggests either a considerable volume of He III bubbles embedded in the more general region in which the ionizing flux is heavily broken, or the addition of collisional ionization to the simple photoionization models (Songaila 1998).

As usually $\eta = N(\text{He II}) / N(\text{H I}) \gg 1$ and $\tau_{\text{HeII}} = (\eta/4)\tau_{\text{HI}}$, He II can be tracked into much lower density regions than H I, making the He II absorption a good probe of low-density regions or hot, collisionally ionized regions in the IGM. Shull et al. (2004) find that η is systematically larger in voids ($\tau_{\text{HI}} < 0.05$), compared to filaments, possibly implying a softer ionizing radiation field.

There have also been suggestions (Ricotti, Gnedin & Shull 2000; Schaye et al. 2000b; Theuns, Schaye & Haehnelt 2000) for a relatively sudden increase in the line widths between $z = 3.5$ and 3.0, which could be associated with entropy injection resulting from the reionization of He II. In particular, Theuns et al. (2002b) use hydrodynamical

simulations to show that the observed temperature increase leads to a relatively sudden decrease in the hydrogen Ly α effective optical depth. Bernardi et al. (2003) find clear evidence for such a feature in the evolution of the effective optical depth determined from a sample of about 1100 quasars obtained from the SDSS (Fig. 39). However, the existence of the peak in the IGM temperature evolution is still quite uncertain, as the data are also consistent with no feature at $z = 3$. From Fig. 40 it is clear that the temperature peaks at $z \approx 3$ and that the gas becomes close to isothermal (adiabatic index $\gamma \approx 1$), but the present constraints are not sufficient to distinguish between a sharp rise (as indicated by the dashed line) and a more gradual increase. In addition, several different reionization histories and radiative transfer effects can fit the observed temperature data equally well, as is discussed in detail by Miniati et al. (2004).

The IGM temperature might be affected also by the energy deposited by dark matter particles if these are either decaying or annihilating (the most interesting candidates being sterile neutrinos with masses of a few keV, light dark matter with mass ≈ 100 MeV and neutralinos). If so, the IGM temperature might deviate from adiabatic evolution before the heat input from luminous sources comes into play (Mapelli, Ferrara & Pierpaoli 2006; Ripamonti, Mapelli & Ferrara 2007a; 2007b; Valdes et al. 2007).

5.5.8. *Metal Enrichment*

Observationally, our best view of the IGM is still provided by the Ly α forest in the spectra of distant QSOs and the detection of metals in the forest ranks as one of the most significant discoveries initially made possible by the Keck telescopes (Cowie et al. 1995; Burles & Tytler 1996) and now also exploiting the power of VLT/UVES. From an analysis of these data, Hellsten et al. (1997) and Rauch, Haehnelt, & Steinmetz (1997) concluded that the measured column density ratios $N(\text{C IV})/N(\text{H I})$ imply a typical $[\text{C}/\text{H}] \simeq -2.5$ at $z \simeq 3$, with a one order of magnitude dispersion in the metallicity of different clouds about this mean value. These measurements, however, still refer to overdense regions of the universe, traced by Ly α clouds with column densities in excess of $\log N(\text{H I}) = 14.5$.

The situation is far less clear-cut when we turn to regions with $\log N(\text{H I}) < 14.5$ and density increasingly closer to the mean (a good fitting formula is given by $\rho_b/\bar{\rho}_b \simeq 0.8 [N_{\text{H I}}/10^{13}\text{cm}^{-2}]^{0.7}$), where the observations are very challenging even with a 10-m telescope. Two early studies addressed this problem, with conflicting results. Lu et al. (1998) applied a stacking technique to nearly 300 C IV regions in QSO spectra, but still found no composite signal. They interpreted

this non-detection as evidence for a highly non-uniform degree of metal enrichment at $z \simeq 3$, with the voids having $[C/H] \lesssim -3.5$. On the other hand, Cowie & Songaila (1998) used a pixel-to-pixel optical depth technique to conclude that the average C IV /H I ratio remains essentially constant over the full range of neutral hydrogen column densities tested, down to $\log N(\text{H I}) \simeq 13.5$. If this is indeed the case, the ejection and transport of metals away from galaxies must have been much more efficient than envisaged. Ellison et al. (1999, 2000) re-examined the problem and found that both approaches suffer from limitations which had not been properly taken into account in previous analysis.

To date, the number of direct metal line detections associated with $\log N(\text{H I}) < 14.5$ lines is small. For this reason, searches of warm photoionized O VI have been used. Schaye et al. (2000a) reported the first (statistical) detection of O VI in the low-density IGM at high redshift ($2 < z < 4.5$). By performing a pixel-by-pixel search for O VI absorption in eight quasar spectra, they detected O VI in the form of a positive correlation between the H I Ly α optical depth and the optical depth in the corresponding O VI pixel, down to $\tau_{\text{H I}} \approx 0.1$. However, the interpretation of the O VI data is not straightforward because the ionization mechanism is often ambiguous. Simcoe et al. (2002) found evidence that the O VI corresponding to strong H I absorbers ($\log N(\text{H I}) > 15$) closely resemble hot, collisionally ionized gas found near regions of significant overdensity ($\delta > 300$) with a tiny filling factor of about 10^{-4} ; furthermore, they seem to be clustered on velocity scales of $100 - 300 \text{ km s}^{-1}$ and show weaker clustering out to 750 km s^{-1} . The O VI corresponding to low H I absorbers ($\log N(\text{H I}) < 15$) on the other hand, is more consistent with warm, photo-ionized gas (Carswell et al. 2002; Bergeron et al. 2002; Simcoe et al. 2004). The presence of O VI has been detected down to $\tau_{\text{H I}} \approx 0.2$ also by Aracil et al. (2004), but associated only with gas located within $\approx 400 \text{ km s}^{-1}$ from strong H I lines, i.e. possibly associated with galactic winds. As a caveat on these studies one should keep in mind that such difficult experiments could be affected by a number of errors. For example, the apparent O VI absorptions could be due to spurious coincidences with H I absorptions at other redshifts and thus the O VI optical depth would be independent on that of the H I (Pieri & Haehnelt 2004).

Considerable progress has been made concerning the distribution of predominantly photoionized species, as C IV and Si IV. Schaye et al. (2003) have measured the distribution of carbon in the IGM as a function of redshift z and overdensity δ , obtaining the following fit to its median abundance:

$$[C/H] = -3.47_{-0.06}^{+0.07} + 0.08_{-0.10}^{+0.09}(z - 3) + 0.65_{-0.14}^{+0.10}(\log \delta - 0.5), \quad (20)$$

which is valid in the range $1.8 < z < 4.1$ and $-0.5 < \log \delta < 1.8$ (the quoted errors are statistical; systematic errors due to the uncertainty in the spectral shape of the UV background radiation can be substantially greater, see Schaye et al. 2003). Two points are worth noticing about this formula. The first is that even in underdense regions ($\delta = -0.5$) carbon is detected with an abundance $[\text{C}/\text{H}] \approx -4$. Secondly, it appears that very little evolution has occurred in such a long cosmic time span (2.16 Gyr). The slow evolution with column density and redshift is observed up to $z = 5.7$ (Ryan-Weber, Pettini & Madau 2006).

The former evidence implies that metal transport must have occurred efficiently and at early times to simultaneously account for the cool temperatures and widespread distribution of elements like C and Si. Thus, observations of metals can possibly allow testing of the mechanisms that distributed them or establish when/where they were produced. For example, if metals are carried by galactic winds, they should be seen in absorption against bright background sources, such as quasars or GRBs, in narrow lines, with characteristic equivalent widths $0.5 \text{ \AA} \lesssim W \lesssim 5 \text{ \AA}$ (Furlanetto & Loeb 2003).

The “no evolution” trend seems to extend to even higher redshifts, as already pointed out by Songaila (2001) (and further supported by Pettini et al. 2003), who concluded as well that the C IV column density distribution function is consistent with being invariant throughout the redshift range $z = 1.5 - 5.5$. This range has been extended to $z \approx 6$ by Simcoe (2006). This is quite a puzzling result as, even if the observed elements were produced by a high- z pre-enrichment episode, large variations of the ionizing radiation field would be expected anyway during such extended time intervals. Alternatively, the C IV systems may be associated with outflows from massive star-forming galaxies at later times, while the truly intergalactic metals may reside in regions of the Ly α forest of density lower than those probed up to now. Songaila (2006) finds that, in the redshift range $z = 2 - 3.5$, of a total sample of 53 absorbers, only half of those with $\text{NC IV} > 2 \times 10^{13} \text{ cm}^{-2}$ could be associated with galactic outflows, while all the rest lie in the IGM.

Only recently, since a larger number of observations has been available, long-duration GRBs (which are thought to be associated with the death of massive metal-poor stars) have been used to probe the metallicity of the host galaxies. The available sample is still too small to draw conclusive results, but it looks like they can probe more metal-rich galaxies compared to QSOs absorption lines. Although these studies are still in their infancy, they look extremely promising in probing metal-enrichment (Savaglio 2006).

6. Conclusions

The investigation of the first cosmic structures has started to attract a huge collective effort, as the distant universe is progressively disclosed by the most advanced observing facilities. Compared to just a few years ago, the progresses made in the understanding of several of the fundamental aspects in the field are indeed impressive. It is then not inappropriate to claim that a qualitatively clear scenario of these early epochs, whose current status is broadly summarized in this review, is becoming rapidly established. However, as for any new frontier, we do not yet fully know its extent and the territories beyond it. The uncertainties in the basic cosmological constants are pinned down to the point that “precision cosmology” has become a fashionable way to present the data. Nevertheless, the shape of the primordial fluctuation spectrum is still uncertain and needs to be constrained, along with the degree of non-gaussianity of the density field. The nature of dark matter is likely to remain an extremely challenging problem, which may have intimate connections with the highly debated halo density profiles. Both problems affect the way in which galaxies build up and their observable properties; hence their importance extends beyond the realm of purely theoretical speculations.

Aside from these general issues, the formation of the first structures exhibits its complexity in the large number of different aspects, ranging from galaxy formation to stellar evolution. In principle, the advantage of having to deal with the simplest native environment of the first stars (no heavy elements, dust, dynamically significant magnetic fields, UV radiation background) is rapidly dissolved within the lack of similar counterparts in the local universe that can be used as working laboratories. Although the formation of small mass stars in a primordial environment is possible, we tend to believe that the first stars were very massive, but as yet, no ultimate study has shown the formation of such stars starting from realistic conditions, including all the relevant physics (turbulence, radiative transfer, rotation) in detail. For this reason, we have essentially no clue regarding what the mass distribution, i.e. the IMF, of such stars could be; even indirect observations are of limited help due to the poor number statistics. Other constraints have been proposed, but they remain very weak. Also the evolution of massive stars is under work: for example, the combined effects of metallicity, rotation, and mass loss still need to be thoroughly studied and understood.

These uncertainties must be added to the one related to the physical mechanism driving the characteristic stellar mass to lower (and more common) values with time. Metallicity increase is probably the most ac-

cepted explanation, but one can suspect that other agents may drive the transition: turbulence in the protostellar clumps, strengthening of the UV radiation field, or heating due to cosmic rays. A sudden change in the properties of the first stars would noticeably affect the evolution of reionization history, as the ionizing power would drop dramatically with increasing (decreasing) stellar metallicity (mass). An equally uncertain quantity is the fraction of emitted ionizing photons able to escape from galaxies. Theoretical approaches to this problem have not yet clarified the dependence of such crucial parameter on redshift, galactic mass, and internal structure, and it is likely that the next major advance will come from a dedicated observational campaign.

Despite the wealth of literature on the formation and evolution of low mass galaxies and on the variety of feedback effects which may hinder their formation, these remain controversial topics in the study of the first structures. Also, no general consensus has been reached on their contribution to the global star formation rate, IGM metal enrichment and reionization. For this reason, a stronger effort will be required in the future to clarify these issues.

The widespread interest stimulated by reionization has produced, as a side effect, a rapid growth of numerical radiative transfer techniques. At the same time additional physical ingredients, like the plethora of feedback effects which are equally important as radiative transfer in shaping the reionization history, should be properly included in simulations. On the observational side, a major cornerstone to map reionization history will be provided by 21 cm HI line measurements, which hold the promise to open a paved road toward the distant “gray ages”.

Similar arguments should also apply to the study of the intermediate-low redshift IGM, i.e. the Ly α forest. Despite its simplicity, which allowed early successes in matching the observed properties in the framework of hierarchical cosmological models, few issues remain unsolved. A long standing puzzle involves the observed temperature distribution, which seems to indicate an IGM warmer than predicted by numerical simulations. Also, an alleged temperature jump at $z \approx 3$ has not yet been either fully interpreted theoretically or confirmed experimentally. For this reason, it is crucial to devote more attention to the study of He II reionization. In addition, the IGM temperature deserves further investigation as it is often used to set a maximum redshift for hydrogen reionization.

Finally, the importance of winds from galaxies, both at intermediate and high redshifts, has only recently started to be appreciated, both theoretically and observationally. Do all galaxies go through a wind phase? What fraction of their mass did they lose in such events? What

fraction of the IGM has been inside galaxies, and possibly polluted by nucleosynthetic products of massive stars, as a function of redshift? What is the cosmic filling factor of metals and do we understand its evolution? The answers we currently possess on these and many other questions concerning the cosmic chemical evolution are very partial. The hope is that the pace we have kept so far will bring us close to the final answers during our life time.

Acknowledgements

We thank D.R. Flower, F. Haardt, J. Le Bourlot, C. Larmour, F. Primas, M. Ricotti and R. Schneider for comments, materials, discussions and reading of the original version (in 2005) of the manuscript.

References

- Abel T., Anninos P., Zhang Y., Norman M. L., 1997, *NewA*, 2, 181
 Abel T., Anninos P., Norman M. L., Zhang Y., 1998, *ApJ*, 508, 518
 Abel T., Bryan G. L., Norman M. L., 2000, *ApJ*, 540, 39
 Abel T., Haehnelt M., 1999, *ApJ*, 520, 13
 Abel T., Norman M. L., Madau P., 1999, *ApJ*, 523, 66
 Abel T., Wise J. H., Bryan G. L., 2007, *ApJ*, 659, L87
 Adshead P. J., Furlanetto S. R., 2007, *astro-ph/0706.3220*
 Aguirre A., Hernquist L., Katz N., Gardner J., Weinberg, D. H., 2001a, *ApJ*, 556, L11
 Aguirre A., Hernquist L., Schaye J., Weinberg D. H., Katz N., Gardner J., 2001b, *ApJ*, 560, 599
 Aguirre A., Hernquist L., Schaye J., Katz N., Weinberg D. H., Gardner J., 2001c, *ApJ*, 561, 521
 Aguirre A., Schaye J., Kim T.-S., Theuns T., Rauch M., Sargent, W. L. W., 2004, *ApJ*, 602, 38
 Aharonian F. et al., 2006, *Nature*, 2006, 440, 1018
 Ahn K., Shapiro P. R., 2007, *MNRAS*, 375, 881
 Ali S. S., Bharadwaj S., Panday B., 2005, *MNRAS*, 363, 251
 Allen S. W., Schmidt R. W., Fabian A. C., 2002, *MNRAS*, 334, L11
 Altay G., Croft R. A. C., Pelupessy I., 2008, *astro-ph/0802.3698*
 Alvarez M. A., Abel T., 2007, *MNRAS*, 380, L30
 Alvarez M. A., Bromm V., Shapiro P. R., 2006, *ApJ*, 639, 621
 Alvarez M. A., Komatsu E., Doré O., Shapiro P. R., 2006a, *ApJ*, 647, 840
 Alvarez M. A., Shapiro P. R., Ahn K., Iliev I. T., 2006b, *ApJ*, 644, L101
 Anderson S. F., Hogan C. J., Williams B. F., Carswell R. F., 1999, *ApJ*, 117, 56
 Anninos P., Norman M. L., 1996, *ApJ*, 460, 556
 Aracil B., Petitjean P., Pichon C., Bergeron J., 2004, *A&A*, 419, 811
 Arefiev V. A., Priedhorsky W. C., Borozdin K. N., 2003, *ApJ*, 586, 1238
 Asplund, M., Lambert, D. L., Nissen, P. E., Primas, F., Smith, V. V. 2006, *ApJ*, 644, 229

- Avelino P. P., Barbosa D., 2004, *Phys. Rev. D*, 63, 067302
- Avila-Reese V., Firmani C., Klypin A., Kravtsov A. V., 1999, *MNRAS*, 310, 527
- Babich D., Loeb A., 2005, *ApJ*, 635, 1
- Bahcall N. A., Fan X., 1998, *ApJ*, 504, 1
- Balbi A., et al. 2000, *ApJ*, 545, L1
- Balbi A., et al. 2001, *ApJ*, 558, L145
- Ballero S. K., Matteucci F., Chiappini C., 2006, *NewA*, 11, 306
- Banerjee R. & Jedamzik K. 2005, *Phys. Review D*, 70, 123003
- Baraffe I., Heger A., Woosley S. E., 2001, *ApJ*, 550, 890
- Bardeen J. M., Bond J. R., Kaiser N., Szalay A., 1986, *ApJ*, 304, 15
- Barkana R., 2002, *NewA*, 7, 85
- Barkana R., Loeb A., 1999, *ApJ*, 523, 54
- Barkana R., Loeb A., 2001, *Phys. Rep.*, 349, 125
- Barkana R., Loeb A., 2002, *ApJ*, 578, 1
- Barkana R., Loeb A., 2004, *ApJ*, 609, 474
- Barkana R., Loeb A., 2005a, *MNRAS*, 363, L36
- Barkana R., Loeb A., 2005b, *MNRAS*, 626, 1
- Bartelmann M., 1996, *A&A*, 313, 697
- Bartelmann M., King L. J., Schneider P., 2001, *A&A*, 378, 361
- Basu K., Hernández-Monteagudo C., Sunyaev R., 2004, *A&A*, 416, 447
- Becker R. H., et al. 2001, *AJ*, 122, 2850
- Becker R. H., Rauch M., Sargent W. L. W., 2007, *ApJ*, 662, 72
- Beers T. C., Rossi S., Norris J. E., Ryan S. G., Molaro P., Rebolo R., 1998, *Space Sci. Rev.*, 84, 139
- Belczynski K., Bulik T., Rudak B., 2004, *ApJ*, 608, 45
- Belczynski K., Bulik T., Heger A., Fryer C., 2007, *ApJ*, 664, 986
- Bennett C. L., et al. 2003, *ApJS*, 148, 1
- Benson A. J., Nusser A., Sugiyama N., Lacey C. G., 2001, *MNRAS*, 320, 153
- Benson A. J., Sugiyama N., Nusser A., Lacey C. G., 2006, *MNRAS*, 369, 1055
- Bergeron J., Aracil B., Petitjean P., Pichon C., 2002, *A&A*, 396, 11
- Bernardi M., et al., 2003, *ApJ*, 125, 32
- Bertone S., White S. D. M., 2006, *MNRAS*, 367, 247
- Bessel M. S., Norris J., 1984, *ApJ*, 285, 622
- Bessel M. S., Christlieb N., Gustafsson B., 2004, *ApJ*, 612, 61
- Bharadwaj S., Ali S. S., 2005, *MNRAS*, 356, 1519
- Bi H. G., Davidsen A., 1997, *ApJ*, 479, 523
- Bianchi S., Cristiani S., Kim T.-S., 2001, *A&A*, 376, 1
- Bianchi S., Ferrara A., 2005, *MNRAS*, 358, 379
- Biermann P. L., Kusenko A., 2006, *Phys. Rev. Lett.*, 96, 091301
- Blain A. W., Natarajan P., 2000, *MNRAS*, 312, 35
- Blake C., Collister A., Bridle S., Lahav O., 2007, *MNRAS*, 374, 1527
- Bland-Hawthorn J., Maloney P. R., 1999, *ApJ*, 510, 33
- Bland-Hawthorn J., Maloney P. R., 2001, *ApJ*, 550, 231.
- Bloom J. S., et al., 2008, *astro-ph/0803.3215*
- Boksenberg A., Sargent W. L. W., Rauch M., 2003, *astro-ph/0307557*
- Bolton J. S., Haehnelt M. G., Viel M., Carswell R. F., 2006, *MNRAS*, 366, 1378
- Bolton J. S., Haehnelt M. G., 2007a, *MNRAS*, 374, 493
- Bolton J. S., Haehnelt M. G., 2007b, *MNRAS*, 381, L35
- Bolton J. S., Viel, M., Kim, T.-S., Haehnelt M. G., Carswell, R. F. 2008, *astro-ph/07011.2064*
- Bolton J. S., Meiksin A., White M., 2004, *MNRAS*, 348, L43

- Bond J. R., Arnett W. D., Carr B. J., 1984, *ApJ*, 280, 825
 Bond J. R., Cole S., Efstathiou G., Kaiser N., 1991, *ApJ*, 379, 440
 Borgani S., et al. 2001, *ApJ*, 561, 13
 Borriello A., Salucci P., 2001, *MNRAS*, 323, 285
 Bouwens R. J., et al., 2004, *ApJ*, 616, L79
 Bouwens R. J., Illingworth G. D., Thompson R. I., Franx M., 2005, *ApJ*, 624, L5
 Bowman J. D., Morales M. F., Hewitt J. N., 2007, *ApJ*, 661, 1
 Brocato E., Castellani V., Poli F. M., Raimondo G., 2000, *A&AS*, 164, 91
 Bromm V., Coppi P. S., Larson R. B., 1999, *ApJ*, 527, L5
 Bromm V., Coppi P. S., Larson R. B. 2002, *ApJ*, 564, 23
 Bromm V., Ferrara A., Coppi P. S., Larson R. B., 2001, *MNRAS*, 328, 969
 Bromm V., Kudritzki R. P., Loeb A., 2001, *ApJ*, 552, 464
 Bromm V., Loeb A., 2002, *ApJ*, 575, 111
 Bromm V., Loeb A., 2003, *Nature*, 425, 812
 Bromm V., Loeb A., 2004, *NewA*, 9, 353
 Bromm V., Loeb A., 2006, *ApJ*, 642, 382
 Bromm V., Yoshida N., Hernquist L., 2003, *ApJ*, 596, L153
 Bruscoli M., Ferrara A., Fabbri R., Ciardi B., 2000, *MNRAS*, 318, 1068
 Bruscoli M., Ferrara A., Scannapieco E., 2002, *MNRAS*, 330, L43
 Bryan G. L., Machacek M. E., 2000, *ApJ*, 534, 57
 Bryan G. L., Norman M., 1998, *ApJ*, 495, 80
 Bullock J. S., Kolatt T. S., Sigad Y., Somerville R. S., Kravtsov A. V., Klypin A. A., Primack J. R., Dekel A., 2001, *MNRAS*, 321, 559
 Buonanno A., Sigl G., Raffelt G. G., Janka H.-T., Müller E., 2005, *Phys. Rev. D*, 72, 084001
 Burkert A., Silk J., 1997, *ApJ*, 488, L55
 Burles S., Tytler D., 1996, *ApJ*, 460, 584
 Carilli C. L., Gnedin N. Y., Owen F., 2002, *ApJ*, 577, 22
 Carretta E., Gratton R., Cohen J. G., Beers T. C. Christlieb N., 2002, *AJ*, 124, 481
 Carswell B., Schaye J., Kim T.-S., 2002, *ApJ*, 578, 43
 Cassisi S., Castellani V., Tornambè A., 1996, *A&A*, 317, 108
 Cen R., 2002, *ApJS*, 141, 211
 Cen R., 2003a, *ApJ*, 591, 12
 Cen R., 2003b, *ApJ*, 591, L5
 Cen R., 2003c, *ApJ*, 597, L13
 Cen R., 2005, *ApJ*, 624, 485
 Cen R., 2006, *ApJ*, 648, 47
 Cen R., Dong F., Bode P., Ostriker J. P., 2004, *astro-ph/0403352*
 Cen R., Haiman Z., 2000, *ApJ*, 542, L75
 Cen R., Ostriker J. P., 1999, *ApJ*, 519, 109
 Chen X., Cooray A., Yoshida N., Sugiyama N., 2003, *MNRAS*, 364, L31
 Chen X., Kamionkowski M., 2004, *Phys. Rev. D*, 70, 043502
 Chen X., Miralda-Escudé J., 2004, *ApJ*, 602, 1
 Chen X., Miralda-Escudé J., 2006, *astro-ph/0605439*
 Chiosi C., 2000, *The First Stars*, eds. A. Weiss, T. Abel & V. Hill (Berlin: Springer), p. 95
 Chiang L.-Y., Naselsky P. D., Verkhodanov O. V., Way M. J., 2003, *ApJ*, 590, L65
 Chiu W. A., Gnedin N. Y., Ostriker J. P., 2001, *ApJ*, 563, 21
 Chiu W. A., Ostriker J. P., 2000, *ApJ*, 534, 507
 Chluba J., Sunyaev R. A., 2006, *A&A*, 446, 39
 Choudhury T. R., Ferrara A., 2006, *MNRAS*, 371, L55

- Choudhury T. R., Srianand R., 2002, MNRAS, 336, L27
- Christlieb N., Bessell M. S., Beers T. C., Gustafsson B., Korn A., Barklem P. S., Karlsson T., Mizuno-Wiedner M., Rossi S., 2002, Nature, 419, 904
- Christlieb N., Gustafsson B., Korn A., Barklem P. S., Beers T. C., Bessell M. S., Karlsson T., Mizuno-Wiedner M., 2004, ApJ, 603, 708
- Chuzhoy L., Shapiro P. R., 2006, ApJ, 651, 1
- Chuzhoy L., Zheng Z., 2007, ApJ, 670, 912
- Ciardi B., Bianchi S., Ferrara A., 2002, MNRAS, 331, 463
- Ciardi B., Ferrara A., Abel T., 2000, ApJ, 533, 594
- Ciardi B., Ferrara A., Governato F., Jenkins A., 2000, MNRAS, 314, 611
- Ciardi B., Ferrara A., Marri S., Raimondo G., 2001, MNRAS, 324, 381
- Ciardi B., Ferrara A., 2001, MNRAS, 324, 648
- Ciardi B., Ferrara A., White S. D. M., 2003, MNRAS, 344, L7
- Ciardi B., Loeb A., 2000, ApJ, 540, 687
- Ciardi B., Madau P., 2003, ApJ, 596, 1
- Ciardi B. et al., 2006, MNRAS, 366, 689
- Ciardi B., Salvaterra R., 2007, MNRAS, 381, 1137
- Ciardi B., Stoehr F., White S. D. M., 2003, MNRAS, 343, 1101
- Clark P. C., Glover S. C. O., Klessen R. S., 2008, ApJ, 672, 757
- Clarke C. J., Oey S., 2002, MNRAS, 337, 1299
- Coc A., Vangioni-Flam E., Descouvemont P., Adahchour A., Angulo C., 2004, ApJ, 600, 544
- Cohn J. D., Chang T.-C., 2007, MNRAS, 374, 72
- Cojazzi P., Bressan P., Lucchin F., Pantano O., Chavez M., 2000, MNRAS, 315, 51
- Cooray A., 2004, Phys. Rev. D., 70, 063509
- Cooray A., Bock J. J., Keating B., Lange A. E., Matsumoto T., 2004, ApJ, 606, 611
- Cooray A., Furlanetto S. R., 2005, MNRAS, 359, L47
- Cooray A., et al., 2007, ApJ, 659, L91
- Cooray A., Li C., Melchiorri A., 2008, astro-ph/0801.3463
- Cooray A., Yoshida N., 2004, MNRAS, 351, 71
- Colombo L. P. L. et al., 2005, A&A, 435, 413
- Cowie L. L., Songaila A., 1998, Nature, 394, 44
- Cowie L. L., Songaila A., Kim T.-S., Hu E. M., 1995, AJ, 109, 1522
- Crighton N. H. M., Webb J. K., Ortiz-Gill A., Fernàndez-Soto A., 2004, MNRAS, 355, 1042
- Croft R. A. C., Altay G., 2008, astro-ph/0709.2362
- Croft R. A. C., et al., 2002, ApJ, 581, 20
- Croft R. A. C., Weinberg D. H., Katz N., Hernquist L., 1998, ApJ, 495, 44
- Croft R. A. C., Weinberg D. H., Pettini M., Hernquist L., Katz N., 1999, ApJ, 520, 1
- Daigne F., Olive K. A., Vangioni-Flam E., Silk J., Audouze J., 2004, ApJ, 617, 693
- Davidson A. F., Kriss G. A., Zheng W., 1996, Nature, 380, 47
- de Blok W. L. G., Bosma A., McGaugh S. S., 2003, MNRAS, 340, 657
- de Blok W. L. G., McGaugh S. S., Bosma A., Rubin V. C., 2001, ApJ, 552, 23
- Dekel A., Devor J., Hetzroni G., 2003, MNRAS, 341, 326
- Del Popolo A., Gambera M., Recami E., Spedicato E., 2000, A&A, 353, 427
- Dijkstra M., Haiman Z., Rees M. J., Weinberg D. H., 2004, ApJ, 601, 666
- Dijkstra M., Wyithe J. S. B., Haiman Z., 2007, MNRAS, 379, 253
- Di Matteo T., Ciardi B., Miniati F., 2004, MNRAS, 355, 1053
- Di Matteo T., Perna R., Abel T., Rees M. J., 2002, ApJ, 564, 576
- Djorgovski S. G., Castro S., Stern D., Mahabal A. A., 2001, ApJ, 560, L5

- Dove J. B., Shull J. M., 1994, *ApJ*, 430, 222
Dove J. B., Shull J. M., Ferrara A., 2000, *ApJ*, 531, 846
Dubrovich V. K., Grachev S.I., 2005, *Astron. Lett.*, 31, 359
Dunkley et al. 2008, [astro-ph/0803.0586](#)
Dwek E., Arendt R. G., Krennrich F., 2005, *ApJ*, 635, 784
Dwek E., Krennrich F., Arendt R. G., 2005, *ApJ*, 635, 784
Efstathiou G., Bond J. R., White S. D. M., 1992, *MNRAS*, 258, 1
Eisenstein D. J., Loeb A., 1995, *ApJ*, 439, 520
Eke V. R., Cole S., Frenk C. S., Henry J. P., 1998, *MNRAS*, 298, 1145
Ekström S., Meynet G., Maeder A., 2006, *ASPC*, 353, 141
Ellison S. L., Geraint F., Pettini M., Chaffee F. H., Irwin M. J., 1999, *ApJ*, 520, 456
Ellison S. L., Songaila A., Schaye J., Pettini M., 2000, *AJ*, 120, 1175
El-Zant A., Shlosman I., Hoffman Y., 2001, *ApJ*, 560, 636
Eriksen E. K., Banday A. J., Górski K. M., Hansen F. K., Lilje P. B., 2007, *ApJ*, L81
Erni P., Richter P., Ledoux C., Petitjean P., 2006, *A&A*, 451, 19
Fan X., et al. 2000, *AJ*, 120, 1167
Fan X., et al. 2001, *AJ*, 122, 2833
Fan X., et al. 2003, *AJ*, 125, 1649
Fan X., et al. 2004, *AJ*, 128, 515
Fan X., et al. 2006, *AJ*, 132, 117
Fang T., Cen R., 2004, *ApJL*, 616, 87
Fardal M. A., Katz N., Gardner J. P., Hernquist L., Weinberg D. H., Davé R., 2001, *ApJ*, 562, 605
Fazio G. G., et al., 2004, *ApJS*, 154, 39
Fechner C., et al., 2006, *A&A*, 455, 91
Fechner C., Reimers D., 2007, *A&A*, 461, 847
Feng L.-L., Bi H.-G., Liu J.-R., Fang L.-Z., 2008, [astro-ph/0710.5476](#)
Fernández-Soto A., Lanzetta K. M., Chen H.-W., 2003, *MNRAS*, 342, 1215
Ferrara A., 1998, *ApJ*, 499, 17L
Ferrara A., Ferrini F., Barsella B., Franco J., 1991, *ApJ*, 381, 137
Ferrara A., Scannapieco E., Bergeron J., 2005, *ApJ*, 634, L37
Ferrara A., Tolstoy E., 2000, *MNRAS*, 313, 291
Field G. B., 1958, *Proc. IRE*, 46, 240
Field G. B., 1959, *ApJ*, 129, 551
Figer D. F., 2005, *Nature*, 34, 192
Figer D. F., Najarro F., Morris M., McLean L. S., Geballe T. R., Ghez A. M., Langer N., 1998, *ApJ*, 506, 384
Flower D. R., 2000, *MNRAS*, 318, 875
Flower D. R., Le Bourlot J., Pineau des Forêts G., Roueff E., 2000, *MNRAS*, 314, 753
Flower D. R., Pineau des Forêts G., 2001, *MNRAS*, 323, 672
Frail D. A., et al., 2006, *ApJ*, 646, 99
Frebel A., et al. 2005, *Nature*, 434, 871
Freedman W. L., et al. 2001, *ApJ*, 553, 47
Fryer C. L., 1999, *ApJ*, 522, 413
Fryer C. L., Holz D. E., Hughes S. A., 2002, *ApJ*, 565, 430
Fryer C. L., Woosley S. E., Heger A., 2001, *ApJ*, 550, 372
Fujita A., Martin C., Mac Low M.-M., Abel T., 2003, *ApJ*, 599, 50
Fukugita M., Kawasaki M., 1994, *MNRAS*, 269, 563
Fukushige T., Kawai A., Makino J., 2004, *ApJ*, 606, 625

- Fuller T. M., Couchman H. M. P., 2000, *ApJ*, 544, 6
 Fuller G. M., Woosley S. E., Weaver T. A., 1986, *ApJ*, 307, 675
 Furlanetto S. R., 2006, *MNRAS*, 370, 1867
 Furlanetto S. R., Hernquist L. & Zaldarriaga M., 2004, *MNRAS*, 354, 695
 Furlanetto S. R., Loeb A., 2002, *ApJ*, 579, 1
 Furlanetto S. R., Loeb A., 2003, *ApJ*, 588, 18
 Furlanetto S. R., Oh S. P., 2005, *MNRAS*, 363, 1031
 Furlanetto S. R., Oh S. P., 2006, *ApJ*, 652, 849
 Furlanetto S. R., Oh S. P., 2008, *astro-ph/0711.0751*
 Furlanetto S. R., Pritchard J. R., 2006, *MNRAS*, 372, 1093
 Furlanetto S. R., Sokasian A., Hernquist L., 2004, *MNRAS*, 347, 187
 Furlanetto S. R., Zaldarriaga M., Hernquist L., 2004a, *ApJ*, 613, 1
 Furlanetto S. R., Zaldarriaga M., Hernquist L., 2004b, *ApJ*, 613, 16
 Gallerani S., Choudhury T. R., Ferrara A., 2006, *MNRAS*, 370, 1401
 Gallerani S., Ferrara A., Fan X., Choudhury T. R., 2007, *astro-ph/0706.1053*
 Gallerani S., Salvaterra R., Ferrara A., Choudhury T. R., 2008, *astro-ph/0710.1303*
 Galli D., Palla F., 1998, *A&A*, 335, 403
 Galli D., Palla F., 2002, *Plan. Space Science*, 50, 1197
 Gao L. et al., 2007, *MNRAS*, 378, 449
 Gibson B. K., Stetson P. B., 2001, *ApJ*, 547, L103
 Ghigna S., Moore B., Governato F., Lake G., Quinn T., Stadel J., 2000, *ApJ*, 544, 616
 Gleser L. et al., 2005, *MNRAS*, 361, 1399
 Gleser L., Nusser A., Benson A. J., 2008, *astro-ph/0712.0497*
 Gleser L., Nusser A., Ciardi B., Desjacques V., 2006, *MNRAS*, 370, 1329
 Glover S. C. O., Brand, P. W. J. L., 2001, *MNRAS*, 321, 385
 Glover S. C. O., Brand P. W. J. L., 2003, *MNRAS*, 340, 210
 Glover S. C. O., Savin D. W., Jappsen A.-K., 2006, *ApJ*, 640, 553
 Gnedin N. Y., 1998, *MNRAS*, 294, 407
 Gnedin N. Y., 2000a, *ApJ*, 535, 530
 Gnedin N. Y., 2000b, *ApJ*, 542, 535
 Gnedin N. Y., Abel T., 2001, *NewA*, 6, 437
 Gnedin N. Y., Ferrara A., Zweibel E. G., 2000, *ApJ*, 539, 505
 Gnedin N. Y., Jaffe A. H., 2001, *ApJ*, 551, 3
 Gnedin N. Y., Kravtsov A. V., Chen H.-W., 2008, *ApJ*, 672, 765
 Gnedin N. Y., Ostriker J. P., 1997, *ApJ*, 486, 581
 Gnedin N. Y., Prada F., 2004, *ApJ*, 608, 77
 Gnedin N. Y., Shaver P. A., 2004, *ApJ*, 608, 611
 Gopal R., Sethi S. K., 2005, *Phys. Rev. D.*, 72, 103003
 Goto T., 2006, *MNRAS*, 371, 769
 Greif T. H., Bromm V., 2006, *MNRAS*, 373, 128
 Greif T. H., Johnson J. L., Bromm V., Klessen R. S., 2007, *ApJ*, 670, 1
 Gunn J. E., Peterson B. A., 1965, *ApJ*, 142, 1633
 Haehnelt M. G., Madau P., Kudritzki R., Haardt F., 2001, *ApJ*, 549, L151
 Haiman Z., 2002, *ApJ*, 576, L1
 Haiman Z., Abel T., Madau P., 2001, *ApJ*, 551, 599
 Haiman Z., Abel T., Rees M. J., 2000, *ApJ*, 534, 11
 Haiman Z., Bryan G. L., 2006, *ApJ*, 650, 7
 Haiman Z., Holder G. P., 2003, *ApJ*, 595, 1
 Haiman Z., Loeb A., 1997, *ApJ*, 483, 21
 Haiman Z., Loeb A., 1999, *ApJ*, 519, 479

- Haiman Z., Rees M. J., Loeb A., 1997, *ApJ*, 476, 458
Haiman Z., Spaans M., 1999, *ApJ*, 518, 138
Haiman Z., Spaans M., Quataert E., 2000, *ApJ*, 537, L5
Haiman Z., Thoul A. A., Loeb A., 1996, *ApJ*, 464, 523
Hansen F. K., Balbi A., Banday A.J. & Gorski K. M., 2004, *MNRAS*, 354, 905
Hansen S. H., Haiman Z., 2004, *ApJ*, 600, 26
He P., Liu J., Feng L.-L., Bi H.-G., Fang L.-Z., 2004, *ApJ*, 614, 6
Heap R. S., Williger G. M., Smette A., Hubeny I., Meena S. S., Jenkins E. B., Winkler T. M. T., 2000, *ApJ*, 534, 69
Heckman T. M., Sembach K. R., Meurer G. R., Leitherer C., Calzetti D., Martin C. L., 2001, *ApJ*, 558, 56
Heger A., Woosley S. E., 2002, *ApJ*, 567, 532
Heger A., Woosley S. E., 2008, *astro-ph/0803.3161*
Heise J., in/t Zand J., Kippen R. M., Woods P. M., 2001, *Gamma-Ray Bursts in the Afterglow Era*, eds. E. Costa, F. Frontera & J. Hjorth (Berlin: Springer), p. 16
Hellsten U., Davè R., Hernquist L., Weinberg D. H., Katz N., 1997, *ApJ*, 487, 482
Hernandez X., Ferrara A., 2001, *MNRAS*, 324, 484
Hernández-Monteagudo C., Haiman Z., Jimenez R., Verde L., 2007, *ApJ*, 660, L85
Hernández-Monteagudo C., Haiman Z., Verde L., Jimenez R., 2008, *astro-ph/0709.3313*
Hernández-Monteagudo C., Verde L., Jimenez R., 2006, *astro-ph/0604324*
Hilbert S., Metcalf R. B., White S. D. M., 2007, *MNRAS*, 382, 1494
Hinshaw, G. et al. 2008, *astro-ph/0803.0732*
Hirata C. M., 2006, *MNRAS*, 367, 259
Hirata C. M., Padmanabhan N., 2006, *MNRAS*, 372, 1175
Hirata C. M., Sigurdson K., 2007, *MNRAS*, 375, 1241
Hoekstra H., et al. 2001, *ApJ*, 548, L5
Hoekstra H., Yee H. K. C., Gladders M. D., 2002, *ApJ*, 577, 595
Hogan C. J., Anderson S. F., Rugers M., 1997, *AJ*, 113, 1495
Holder G. P., Haiman Z., Kaplinghat M., Knox L., 2003, *ApJ*, 595, 13
Holder G. P., Iliev I. T., Mellema G., 2007, *ApJ*, L1
Hollenbach D., McKee C. F., 1989, *ApJ*, 342, 306
Hopkins A. M., 2004, *ApJ*, 615, 209
Hu E. M., Cowie L. L., Capak P., McMahon R. G., Hayashino T., Komiyama Y., 2004, *ApJ*, 127, 563
Hu E. M., Cowie L. L., McMahon R. G., Capak P., Iwamuro F., Kneib J.-P., Maihara T., Motohara K., 2002, *ApJ*, 568, L75
Hu W., Fukugita M., Zaldarriaga M., Tegmark M., 2001, *ApJ*, 549, 669
Hu W., Holder G. P., 2003, *Phys. Rev. D*, 68, 3001
Hui L., Gnedin N., Zang Y., 1997, *ApJ*, 486, 599
Hui L., Haiman Z., 2003, *ApJ*, 596, 9
Hunter D. A., Light R. M., Holtzman J. A., Lynds R., O'Neil E. J., Grillmair C. J., 1997, *ApJ*, 478, 124
Hurwitz M., Jelinsky P., Dixon W. V., 1997, *ApJ*, 481, L31
Iliev I. T. et al., 2006a, *MNRAS*, 369, 1625
Iliev I. T. et al., 2006b, *MNRAS*, 371, 1057
Iliev I. T., Mellema G., Shapiro P. R., Pen U.-L., 2007a, *MNRAS*, 376, 534
Iliev I. T., Pen U.-L., Bond J. R., Mellema G., Shapiro P. R., 2006c, *New AR.*, 50, 909
Iliev I. T., Scannapieco E., Martel H., Shapiro P. R., 2003, *MNRAS*, 341, 81

- Iliev I. T., Shapiro P. R., Ferrara A., Martel H., 2002, *ApJ*, 572, L123
- Iocco F., Murase K., Nagataki S., Serpico P. D., 2007, *astro-ph/0707.0515*
- Ioka K., 2003, *ApJ*, 598, L79
- Ioka K., Meszaros P., 2004, *ApJ*, 613, 17
- Inoue S., 2004, *MNRAS*, 348, 999
- Inoue A. K., Iwata I., Deharveng J.-M., 2006, *MNRAS*, 371, L126
- Inoue A. K., Yamazaki, R. Nakamura, T. 2004, *ApJ*, 601, 644
- Islam R. R., Taylor J. E., Silk J., 2003, *MNRAS*, 340, 647
- Iye M. et al., 2006, *Nature*, 443, 186
- Iwamoto N., Umeda H., Tominaga N., Nomoto K., Maeda K., 2005, *Science*, 309, 451
- Jakobsen P., et al., 1994, *Nature*, 370, 35
- Jakobsen P., Jansen R. A., Wagner S., Reimers D., 2003, *A&A*, 397, 891
- Jasche J., Ciardi B., Enßlin T. A., 2007, *MNRAS*, 380, 417
- Jeans J. H., 1928, *Astronomy and Cosmogony*, Cambridge, U.K., Cambridge University Press
- Jha S., et al. 1999, *ApJS*, 125, 73
- Jimenez R., Verde L., Oh S. P., 2003, *MNRAS*, 339, 243
- Jimenez R., Haiman Z., 2006, *Nature*, 441, 120
- Jing Y. P., 2000, *ApJ*, 535, 30
- Jing Y. P., Suto Y., 2000, *ApJ*, 529, L69
- Johnson J. L., Bromm V., 2006, 366, 247
- Johnson J. L., Greif T. H., Bromm V., 2007, *ApJ*, 665, 85
- Johnson J. L., Greif T. H., Bromm V., 2008, *astro-ph/0711.4622*
- Juvela M., 2005, *A&A*, 440, 531
- Kamaya H., Silk J., 2002, *MNRAS*, 332, 251
- Kamaya H., Silk J., 2003, *MNRAS*, 339, 1256
- Kaplinghat M., Chu M., Haiman Z., Holder G., Knox L. Skordis C., 2003, *ApJ*, 583, 24
- Kashikawa N., et al., 2006, *ApJ*, 648, 7
- Kashlinsky A., 2005, *ApJ*, 633, 5
- Kashlinsky A., Arendt R., Gardner J. P., Mather J., Moseley S. H., 2004, *ApJ*, 608, 1
- Kashlinsky A., Arendt R., Mather J., Moseley S. H., 2005, *Nature*, 438, 54
- Kashlinsky A., Arendt R., Mather J., Moseley S. H., 2007a, *ApJ*, 657, L131
- Kashlinsky A., Arendt R., Mather J., Moseley S. H., 2007b, *ApJ*, 654, L1
- Kasuya S., Kawasaki M., 2004, *Phys. Rev. D*, 70, 103519
- Kauffmann G., Colberg J. M., Diaferio A., White S. D. M., 1999, *MNRAS*, 303, 188
- Kim T.-S., Cristiani S., D'Odorico S., 2002, *A&A*, 383, 747
- Kim T.-S., Viel M., Haehnelt M. G., Carswell R. F., Cristiani S., 2004, *MNRAS*, 347, 355
- Kitayama T., Susa H., Umemura M., Ikeuchi S., 2001, *MNRAS*, 326, 1353
- Kitayama T., Tajiri T., Umemura M., Susa H. Ikeuchi S., 2000, *MNRAS*, 315, L1
- Kitayama T., Yoshida N., 2005, *ApJ*, 630, 675
- Kitayama T., Yoshida N., Susa H., Umemura M., 2004, *ApJ*, 613, 631
- Kitsionas S., Whitworth A. P., 2002, *MNRAS*, 330, 129
- Kleyna J. T., Wilkinson M. L., Gilmore G., Evans N. W., 2003, *ApJ*, 588, L21
- Kneib J.-P., Ellis R. S., Santos M. R., Richard J., 2004, *ApJ*, 607, 697
- Knop R. A., et al. 2003, *ApJ*, 598, 102
- Knox L., Scoccamarro R., Dodelson S., 1998, *Phys. Rev. Lett.*, 81, 2004
- Kodaira K., et al. 2003, *Publ. Astron. Observ. Japan*, 55, L17

- Kogut A., et al. 2003, ApJS, 148, 161
 Kohler K., Gnedin N. Y., Miralda-Escudé J., Shaver P. A., 2005, ApJ, 633, 552
 Kohler K., Gnedin N. Y., Hamilton A. J. S., 2007, ApJ, 657, 15
 Kramer R. H., Haiman Z., Oh S. P., 2006, ApJ, 649, 570
 Kravtsov A. V., Klypin A. A., Bullock J. S., Primack J. R. 1998, ApJ, 502, 48
 Kriss G. A., et al. 2001, Science, 293, 1112
 Kroupa P., 2001, MNRAS, 322, 231
 Krtička J., Kubát J., 2006, A&A, 446, 1039
 Kudritzki R., 2000, The First Stars, eds. A. Weiss, T.G. Abel & V. Hill (Berlin: Springer), p. 127
 Kudritzki R., 2002, ApJ, 577, 389
 Kuhlen M., Madau P., 2005, MNRAS, 363, 1069
 Kuhlen M., Madau P., Montgomery R., 2006, ApJ, 637, L1
 Kurk J. D. et al., 2004, A&A, 422, L13
 Lacey C., Cole S., 1994, MNRAS, 271, 676
 Lahav O., et al. 2002, MNRAS, 333, 961
 Lamb D. Q., Reichart D. E., 2000, ApJ, 536, 1
 Langer M., Puget J.-L., Aghanim N., 2003, Phys. Rev. D, 67, 043505
 Langer M., Aghanim N., Puget J.-L., 2005, A&A, 443, 367
 Larson R. B., 1998, MNRAS, 301, 569
 Le Bourlot J., Pineau des Forêts G., Flower D. R., 1999, MNRAS, 305, 802
 Leitherer C., Ferguson H. C., Heckman T. M., Lowenthal J. D., 1995, ApJ, 454, L19
 Lepp S., Shull J. L., 1984, ApJ, 280, 465
 Leung P. K., Chan C. W., Chu M.-C., 2004, MNRAS, 349, 632
 Levshakov S. A., Dessauges-Zavadsky M., D'Odorico S., Molaro P., 2002, ApJ, 565, 696
 Lewis A., Challinor A., Phys Rev D, 76, 083005
 Lidz A., McQuinn M., Zaldarriaga M., Hernquist L., Dutta S., 2007, ApJ, 670, 39
 Limongi M., Chieffi A., Bonifacio P., 2003, ApJ, 594, L123
 Linke F., Font J. A., Janka H.-T., Miller E., Papadopoulos P., 2001, A&A, 376, 568
 Lipovka A., Núñez-Lopez R., Avila-Reese V., 2005, 361, 850
 Liu J., Bi H., Fang L.-Z., 2008, astro-ph/0711.0773
 Liu J., Bi H., Feng L.-L., Fang L.-Z., 2006, ApJ, 645, L1
 Liu J., Fang L.-Z., Feng L.-L., Bi H.-G., 2004, ApJ, 601, 54
 Liu J., et al., 2007, ApJ, 663, 1
 Liu M. C., Graham J. R., 2001, ApJ, 557, L31
 Loeb A., Rybicki G. B., 1999, ApJ, 524, 527
 Loeb A., Zaldarriaga M., 2004, Phys. Rev. Lett., 92, 211301
 Lu T., Pen U.-L., 2008, astro-ph/0710.1108
 Lu L., Sargent W. L. W., Barlow T. A., Rauch M., 1998, astro-ph/9802189
 Lucatello S., Gratton R. G., Beers T. C., Carretta E., 2005, ApJ, 625, 833
 Macciò A. V., et al., 2007, MNRAS, 378, 55
 Machacek M. M., Bryan G. L., Abel T., 2001, ApJ, 548, 509
 Machida M. N., Omukai K., Matsumoto T., Inutsuka S., 2006, ApJ, 647, L1
 Machida M. N., Omukai K., Matsumoto T., Inutsuka S., 2007, astro-ph/0711.0069
 Mackey J., Bromm V., Hernquist L., 2003, ApJ, 586, 1
 Mac Low M.-M., Ferrara A., 1999, ApJ, 513, 142
 Madau P., Ferrara A., Rees, M. J., 2001, ApJ, 555, 92
 Madau P., Haardt F., Rees M. J., 1999, ApJ, 514, 648
 Madau P., Meiksin A., Rees M. J., 1997, ApJ, 475, 429
 Madau P., Rees M. J., 2000, ApJ, 542, L69

- Madau P., Rees M. J., Volonteri M., Haardt F., Oh S. P., 2004, *ApJ*, 604, 484
- Madau P., Silk J., 2005, *MNRAS*, 359, L37
- Maeder A., Meynet G., 2000, *A&A*, 61, 159
- Magliocchetti M., Salvaterra R., Ferrara A., 2003, *MNRAS*, 342, L25
- Maio U., Dolag K., Ciardi B., Tornatore L., 2007, *MNRAS*, 379, 963
- Malhotra S. et al., 2005, *ApJ*, 626, 666
- Malhotra S., Rhoads J. E., 2006, *ApJ*, 647, 95
- Mao Y., et al., 2008, *astro-ph/0802.1710*
- Mapelli M., Ferrara A., 2005, *MNRAS*, 364, 2
- Mapelli M., Ferrara A., Pierpaoli E., 2006, *MNRAS*, 369, 1719
- Marigo P., Chiosi C., Girardi L., Kudritzki R.-P., 2003, *A Massive Star Odyssey: From Main Sequence to Supernova*, ed. K. van der Hucht, A. Herrero & E. Cesar (San Francisco: Astronomical Society of the Pacific), p. 334
- Marigo P., Chiosi C., Kudritzki R.-P., 2003, *A&A*, 399, 617
- Martel H., Evans II N. J., Shapiro P. R., 2006, *ApJS*, 163, 122
- Martin P. G., Schwarz D. H., Mandy M. E., 1996, *ApJ*, 461, 265
- Mashchenko S., Couchman H. M. P., Wadsley J., 2006, *Nature*, 442, 539
- Maselli A., Ferrara A., 2005, *MNRAS*, 364, 1429
- Maselli A., Ferrara A., Ciardi B., 2003, *MNRAS*, 345, 379
- Maselli A., Gallerani S., Ferrara A., Choudhury T. R., 2007, *MNRAS*, 376, L34
- Mashchenko S., Couchman H. M. P., Sills A., 2006, *ApJ*, 639, 633
- Massey P., 1998, *The Stellar Initial Mass Function*, eds. G. Gilmore & D. Howell. ASP Conf. Series, Vol. 142, p. 17
- Mather J. C., et al. 1994, *ApJ*, 420, 439
- Matsumoto T. et al., 2005, *ApJ*, 626, 31
- Matteucci F., Calura F., 2005, *MNRAS*, 360, 447
- McCray R., Kafatos M., 1987, *ApJ*, 317, 190
- McDonald P., Miralda-Escudé J., 2001, *ApJ*, 549, L11
- McDonald P., Miralda-Escudé J., Rauch M., Sargent W. L. W., Barlow T. A., Cen R., 2001, *ApJ*, 562, 52
- McDonald P. et al., 2005, *ApJ*, 635, 761
- McEwen J. D., Hobson M. P., Lasenby A. N., Mortlock D. J., 2008, *astro-ph/0803.2157*
- McKee C. F., Tan J. C., 2008, *astro-ph/0711.1377*
- McQuinn M., Furlanetto S. R., Hernquist L., Zahn O., Zaldarriaga M., 2005, *ApJ*, 630, 643
- McQuinn M., Lidz A., Zaldarriaga M., Hernquist L., Dutta S., 2008, *astro-ph/0710.1018*
- McQuinn M. et al., 2007, *astro-ph/0610094*
- McQuinn M., Zahn O., Zaldarriaga M., Hernquist L., Furlanetto S. R., 2006, *ApJ*, 653, 815
- McWilliam A., Preston G. W., Sneden C., Searle L., 1995, *AJ*, 109, 2757
- Meiksin A., Bryan G., Machacek M., 2001, *MNRAS*, 327, 296
- Mellema G., Iliev I. T., Alvarez M. A., Shapiro P. R., 2006a, *NewA*, 11, 374
- Mellema G., Iliev I. T., Pen U.-L., Shapiro P. R., 2006b, *MNRAS*, 372, 679
- Merritt D., Fridman T., 1996, *ApJ*, 460, 136
- Mesinger A., Bryan G. L., Haiman Z., 2006, *ApJ*, 648, 835
- Mesinger A., Haiman Z., 2004, *ApJ*, 611, 69
- Mesinger A., Haiman Z., 2007, *ApJ*, 660, 923
- Mesinger A., Haiman Z., Cen R., 2004, *ApJ*, 613, 23
- esinger A., Furlanetto S. R., 2007, *ApJ*, 669, 663

- Mészáros P., Waxman E., 2001, *Phys. Rev. Lett.*, 87, 171102
- Metcalfe R. B., White S. D. M., 2007, *astro-ph/0611862*
- Metcalfe R. B., White S. D. M., 2008, *astro-ph/0801.2571*
- Meynet G., Ekström S., Maeder A., 2006, *A&A*, 447, 623
- Miniati F., Ferrara A., White S. D. M., Bianchi S., 2004, *MNRAS*, 348, 964
- Miralda-Escudé J., 1998, *ApJ*, 501, 15
- Miralda-Escudé J., Haehnelt M., Rees M. R., 2000, *ApJ*, 530, 1
- Miralda-Escudé J., Rees M. R., 1994, *MNRAS*, 266, 343
- Mizusawa H., Nishi R., Omukai K., 2004, *PASJ*, 56, 487
- Mizusawa H., Omukai K., Nishi R., 2005, *PASJ*, 57, 951
- Mo H. J., White S. D. M., 2002, *MNRAS*, 336, 112
- Mobasher B. et al., 2005, *ApJ*, 635, 832
- Moore B., Quinn T., Governato F., Stadel J., Lake G., 1999, *MNRAS*, 310, 1147
- Mori M., Ferrara A., Madau P., 2002, *ApJ*, 571, 40
- Mould J. R., et al. 2000, *ApJ*, 529, 786
- Nagakura T., Omukai K., 2005, *MNRAS*, 364, 1378
- Nagao T. et al., 2004, *AJ*, 128, 2066
- Nagao T. et al., 2008, *astro-ph/0802.4123*
- Nagashima M., Gouda N., Sugiura N., 1999, *MNRAS*, 305, 449
- Nakamura F., Umemura M., 2001, *ApJ*, 548, 19
- Nakano T., 1998, *A&A*, 494, 587
- Naselsky P., Chiang L.-Y., 2004, *MNRAS*, 347, 795
- Navarro J. F., Frenk C. S., White S. D. M., 1996, *ApJ*, 462, 563
- Navarro J. F., Frenk C. S., White S. D. M., 1997, *ApJ*, 490, 493
- Navarro J. F. et al., 2004, *MNRAS*, 349, 1039
- Nishi R., Susa H., 1999, *ApJ*, 523, L103
- Nishi R., Tashiro M., 2000, *ApJ*, 537, 50
- Nolta, M. R. et al. 2008, *astro-ph/0803.0593*
- Norris J. E., Peterson R. C., Beers T. C., 1993, *ApJ*, 415, 797
- Norris J. E., Ryan S. G., Beers T. C., 2001, *ApJ*, 561, 1034
- Nozawa T., Kozasa T., Umeda H., Maeda K., Nomoto K., 2003, *ApJ*, 598, 785
- Nugis T., Lamers H. J. G. L. M., 2000, *A&A*, 360, 227
- Nusser A., 2005a, *MNRAS*, 359, 183
- Nusser A., 2005b, *MNRAS*, 364, 743
- Nusser A., Sheth R. K., 1999, *MNRAS*, 303, 685
- Oey M. S., Clarke C. J., 2005, *ApJ*, 620, L43
- Oguri M., Taruya A., Suto Y., 2001, *ApJ*, 559, 572
- Oh S. P., 2001, *ApJ*, 553, 499
- Oh S. P., 2002, *MNRAS*, 336, 1021
- Oh S. P., Furlanetto S. R., 2005, *ApJ*, 620, L9
- Oh S. P., Haiman Z., 2002, *ApJ*, 569, 558
- Oh S. P., Haiman Z., 2003, *MNRAS*, 346, 456
- Oh S. P., Haiman Z., Rees M. J., 2001, *ApJ*, 553, 73
- Oh S. P., Mack K. J., 2003, *MNRAS*, 346, 871
- Ohkubo T. et al., 2006, *ApJ*, 645, 1352
- Olum K. D., Vilenkin A., 2006, *Phys. Rev. D.*, 74, 063516
- O’Meara J. M., Tytler D., Kirkman D., Suzuki N., Prochaska J. X., Lubin D., Wolfe A. M., 2001, *ApJ*, 552, 718
- Omukai K., 2000, *ApJ*, 534, 809
- Omukai K., 2001, *ApJ*, 546, 635
- Omukai K., Kitayama T., 2003, *ApJ*, 599, 738

- Omukai K., Nishi R., 1998, *ApJ*, 508, 141
 Omukai K., Nishi R., 1999, *ApJ*, 518, 64
 Omukai K., Palla F., 2001, *ApJ*, 561, L55
 Omukai K., Palla F., 2003, *ApJ*, 589, 677
 Omukai K., Tsuribe T., Schneider R., Ferrara A., 2005, *ApJ*, 626, 627
 Omukai K., Yoshii Y., 2003, *ApJ*, 599, 746
 Onken C. A., Miralda-Escudé J., 2004, *ApJ*, 610, 1
 Oppenheimer B. D., Davé R., 2006, *MNRAS*, 373, 1265
 O'Shea B., Abel T., Whalen D., Norman M. L., 2005, *ApJ*, 628, L5
 O'Shea B., Norman M. L., 2007, *ApJ*, 654, 66
 O'Shea B., Norman M. L., 2008, *ApJ*, 673, 14
 O'Shea B., Heger, A. & Abel T., 2008, *First Stars III*, AIP Conference 990
 Ota K., et al., 2007, *astro-ph/0707.1561*
 Page L. et al., 2007, *ApJS*, 170, 335
 Palla F., Galli D., Silk J., 1995, *ApJ*, 451, 44
 Paschos P., Norman M. L., Bordner J. O., Harkness R., 2008, *astro-ph/0711.1904*
 Pawlik A. H., Schaye J., 2008, *astro-ph/0802.1715*
 Peebles P. J. L., 1993, *Principles of Physical Cosmology*, Princeton University Press, New Jersey
 Pelló R., Richard J., Le Borgne J.-F. Schaerer D., 2004b, *astro-ph/0407194*
 Pelló R., Schaerer D., Richard J., Le Borgne J.-F., Kneib J.-P., 2004a, *A&A*, 416, L35
 Pelupessy F. I., Di Matteo T., Ciardi B., 2007, *ApJ*, 665, 107
 Pen U.-L., 1998, *ApJ*, 498, 60
 Pen U.-L., Wu X.-P., Peterson J., 2004, *astro-ph/0404083*
 Pentericci L., et al. 2002, *ApJ*, 123, 2151
 Perlmutter S., et al. 1999, *ApJ*, 517, 565
 Persic M., Salucci P., Stel F., 1996, *MNRAS*, 281, 27
 Peterson J.-B., Pen U.-L., Wu X.-P., 2005, *ASPC*, 345, 441
 Pettini M., 2006, in “The Fabulous Destiny of Galaxies: Bridging Past and Present”, proceedings of the Vth Marseille International Cosmology conference, June 20-24, 2005, Marseille, France. Edited by V. LeBrun, A. Mazure, S. Arnouts and D. Burgarella. Paris: Frontier Group, 2006, p.319
 Pettini M., Bowen D. V., 2001, *ApJ*, 560, 41
 Pettini M., Madau P., Bolte M., Prochaska J. X., Ellison S. L., Fan X., 2003, *ApJ*, 594, 695
 Piau L. et al., 2006, *ApJ*, 653, 300
 Pieri M. M., Haehnelt M. G., 2004, *MNRAS*, 347, 985
 Pieri M. M., Martel H., Grenon C., 2007, *ApJ*, 658, 36
 Pillepich A., Porciani C., Matarrese S., 2007, *ApJ*, 662, 1
 Porciani C., Madau P., 2001, *ApJ*, 548, 522
 Porciani C., Matarrese S., Lucchin F., Catelan P., 1998, *MNRAS*, 298, 1097
 Portinari L., Chiosi C., Bressan A., 1998, *A&A*, 334, 505
 Power C., Navarro J. F., Jenkins A., Frenk C. S., White S. D. M., Springel V., Stadel J., Quinn T., 2003, *MNRAS*, 338, 14
 Press W. H., Schechter P., 1974, *ApJ*, 187, 425
 Primas F., Molaro P., Castelli F., 1994, *A&A*, 290, 885
 Pritchard J. R., Furlanetto S. R., 2006, *MNRAS*, 367, 1057
 Pritchard J. R., Furlanetto S. R., 2007, *astro-ph/0507234*
 Pryke C., Halverson N. W., Leitch E. M., Kovac J., Carlstrom J. E., Holzzapfel W. L., Dragovan M., 2002, *ApJ*, 568, 46

- Qian Y.-Z., Wasserburg G. J., 2005, *ApJ*, 623, 17
- Qiu J.-M., Shu C.-W., Feng L.-L., Fang L.-Z., 2006, *New A.*, 12, 1
- Räth C., Schuecker P., Banday A. J., 2007, *MNRAS*, 380, 466
- Rauch M., Haehnelt M. G., Steinmetz M., 1997, *ApJ*, 481, 601
- Razoumov A. O., Norman M. L., Abel T., Scott D., 2002, *ApJ*, 572, 695
- Razoumov A. O., Scott D., 1999, *MNRAS*, 309, 287
- Razoumov A. O., Sommer-Larsen J., 2006, *ApJ*, 651, 89L
- Reed D. S., Governato F., Verde L., Gardner J., Quinn T., Stadel J., Merritt D., Lake G., 2005a, *MNRAS*, 357, 82
- Reed D. S., et al., 2005b, *MNRAS*, 363, 393
- Rees M. J., Ostriker J. P., 1977, *MNRAS*, 179, 541
- Reimers D., et al. 1997, *A&A*, 326, 489
- Reimers D., et al. 2005a, *A&A*, 442, 63
- Reimers D., et al. 2005b, *A&A*, 436, 465
- Reynoso E. M., Mangum J. G., 2001, *AJ*, 121, 347
- Rhoads J. E., Dey A., Malhotra S., Stern D., Spinrad H., Jannuzi B. T., Dawson S., Brown M. J. I., Landes E., 2003, *AJ*, 125, 1006
- Rhook K. J., Haehnelt M. G., 2007, *MNRAS*, 373, 623
- Ricotti M., 2002, *MNRAS*, 336, 33
- Ricotti M., 2003, *MNRAS*, 344, 1237
- Ricotti M., Gnedin N. Y., Shull J. M., 2000, *ApJ*, 534, 41
- Ricotti M., Gnedin N. Y., Shull J. M., 2001, *ApJ*, 560, 580
- Ricotti M., Gnedin N. Y., Shull J. M., 2002, *ApJ*, 575, 49
- Ricotti M., Ostriker J. P., 2004a, *MNRAS*, 350, 539
- Ricotti M., Ostriker J. P., 2004b, *MNRAS*, 352, 547
- Ricotti M., Pontzen A., Viel M., 2007, *ApJ*, 663, L53
- Ricotti M., Shull J. M., 2000, *ApJ*, 542, 548
- Rijkhorst E.-J., Plewa T., Dubey A., Mellema G., 2006, *A&A*, 452, 907
- Ripamonti E., Haardt F., Ferrara A., Colpi M., 2002, *MNRAS*, 334, 401
- Ripamonti E., Mapelli M., Ferrara A., 2007a, *MNRAS*, 374, 1067
- Ripamonti E., Mapelli M., Ferrara A., 2007b, *MNRAS*, 375, 1399
- Ripamonti E., Mapelli M., Zaroubi S., 2008, *astro-ph/0802.1857*
- Rollinde E., Vangioni E., Olive K. A., 2006, *ApJ*, 651, 658
- Rowan-Robinson M., 2002, *MNRAS*, 332, 352
- Rozas J. M., Miralda-Escudé J., Salvador-Solé E., 2006, *astro-ph/0511489*
- Ryan-Weber E., Pettini M., Madau P., 2006, *MNRAS*, 371, L78
- Rybicki G. B., Loeb A., 1999, *ApJ*, 520, L79
- Salpeter E. E., 1955, *ApJ*, 121, 161
- Salucci, P. Lapi, A., Tonini, C., Gentile, G., Yegorova, I. & Klein, U., 2007, *MNRAS*, 378, 41
- Salvaterra R., Ciardi B., Ferrara A. & Baccigalupi C., 2005, *MNRAS*, 360, 1063
- Salvaterra R., Ferrara A., 2003a, *MNRAS*, 339, 973
- Salvaterra R., Ferrara A., 2003b, *MNRAS*, 340, 17
- Salvaterra R., Ferrara A., 2006, *MNRAS*, 367, L11
- Salvaterra R., Ferrara A., Schneider R., 2003, *NewA*, 10, 113
- Salvaterra R., Haardt F., Ferrara A., 2005, *MNRAS*, 362, 50
- Salvaterra R., Haardt F., Volonteri M., 2007, *MNRAS*, 374, 761
- Salvaterra R., Magliocchetti M., Ferrara A., Schneider R., 2006, *MNRAS*, 368, L6
- Sandick P., Olive K. A., Daigne F., Vangioni E., 2006, *Phys. Rev. D.*, 73, 104024
- Santoro F., Shull J. M., 2006, *ApJ*, 643, 26

- Santos M. G., Amblard A., Pritchard J., Trac H., Cen R., Cooray A., 2007, *astro-ph/0708.2424*
- Santos M. G., Cooray A., Haiman Z., Knox L., Ma C.-P., 2003, *ApJ*, 598, 756
- Santos M. G., Cooray A., Knox L., 2005, *ApJ*, 625, 575
- Santos M. R., 2004, *MNRAS*, 349, 1137
- Santos M. R., Bromm V., Kamionkowski M., 2002, *MNRAS*, 336, 1082
- Savaglio S., 2006, *NJPh*, 8, 195
- Scalo J. M., 1986, *Fundam. Cosmic Phys.*, 11, 1
- Scalo J. M., 1998, *The Stellar Initial Mass Function*, eds. G. Gilmore & D. Howell. ASP Conference Series, Vol. 142, p. 201
- Scannapieco E., 2005, *ApJ*, 624, L1
- Scannapieco E. et al., 2006, *MNRAS*, 366, 1118
- Scannapieco E., Barkana R., 2002, *ApJ*, 571, 585
- Scannapieco E., Ferrara A., Broadhurst T., 2000, *ApJ*, 536, L11
- Scannapieco E., Ferrara A., Madau P., 2002, *ApJ*, 574, 590
- Scannapieco E., Madau P., Woosley S., Heger A., Ferrara A., 2005, *ApJ*, 633, 1031
- Scannapieco E., Schneider R., Ferrara A., 2003, *ApJ*, 589, 35
- Schaerer D., 2002, *A&A*, 382, 28
- Schaerer D., 2003, *A&A*, 397, 527
- Schaerer D., Pelló R., 2005, *MNRAS*, 362, 1054
- Schaye J., Aguirre A., Kim T.-S., Theuns T., Rauch M., Sargent W. L. W., 2003, *ApJ*, 596, 768
- Schaye J., Rauch M., Sargent W. L. W., Kim T.-S., 2000a, *ApJ*, 541, L1
- Schaye J., Theuns T., Rauch M., Efstathiou G., Sargent W. L. W., 2000b, *ASPC*, 215, 7
- Schmidt B. P., et al. 1998, *ApJ*, 507, 46
- Schneider R., Ferrara A., Ciardi B., Ferrari V., Matarrese S., 2000, *MNRAS*, 317, 385
- Schneider R., Ferrara A., Natarajan P., Omukai K., 2002, *ApJ*, 571, 30
- Schneider R., Ferrara A., Salvaterra R., Omukai K., Bromm V., 2003, *Nature*, 422, 869
- Schneider R., Guetta D., Ferrara A., 2002, *MNRAS*, 334, 173
- Schneider R., Ferrara A., Salvaterra R., 2004, *MNRAS*, 351, 1379
- Schneider R., Omukai K., Inoue A. K., Ferrara A., 2006b, *MNRAS*, 369, 1437
- Schneider R., Salvaterra R., Ferrara A., Ciardi B., 2006a, *MNRAS*, 369, 825
- Schuecker P., Böhringer H., Collins C. A., Guzzo L., 2003, *A&A*, 398, 867
- Schwarzschild M., Spitzer L., 1953, *The Observatory*, 73, 77
- Sciama D. W., 1990, *ApJ*, 364, 549
- Scott D., Rees M. J., Sciama D. W., 1991, *A&A*, 250, 295
- Seljak U. et al., 2005, *Phys. Rev. D*, 71, 103515
- Seljak U., Slosar A., McDonald P., 2006, *JCAP*, 10, 014
- Sesana A., Haardt F., Madau P., Volonteri M., 2004, *ApJ*, 611, 623
- Sethi S. K., Subramanian K., 2005, *MNRAS*, 356, 778
- Shapiro P. R. et al., 2006, *ApJ*, 646, 681
- Shapiro P. R., Giroux M. L., 1987, *ApJ*, 321, L107
- Shapiro P. R., Iliev I. T., Raga A. C., 1999, *MNRAS*, 307, 203
- Shapiro P. R., Iliev I. T., Raga A. C., 2004, *MNRAS*, 348, 753
- Shaver P., Windhorst R., Madau P., de Bruyn G., 1999, *A&A*, 345, 380
- Shchekinov Y. A., Vasiliev E. O., 2004, *A&A*, 419, 19
- Shchekinov Y. A., Vasiliev E. O., 2006, *MNRAS*, 368, 454
- Shchekinov Y. A., Vasiliev E. O., 2007, *MNRAS*, 379, 1003

- Sheth R. K., Mo H. J., Tormen G., 2001, MNRAS, 323, 1
 Sheth R. K., Tormen G., 2002, MNRAS, 329, 61
 Shull J. M., Tumlinson J., Giroux M. L., Kriss G. A., Reimers D., 2004, ApJ, 600, 570
 Sievers J. L., et al. 2003, ApJ, 591, 599
 Sigward F., Ferrara A., Scannapieco E., 2005, MNRAS, 358
 Silk J., 2003, MNRAS, 343, 249
 Simcoe R. A., 2006, ApJ, 653, 977
 Simcoe R. A., Sargent W. L. W., Rauch M., 2002, ApJ, 578, 737
 Simcoe R. A., Sargent W. L. W., Rauch M., 2004, ApJ, 606, 92
 Smette A., Heap S. R., Williger G. M., Tripp T. M., Jenkins E. B., Songaila A., 2002, ApJ, 564, 542
 Smith N., et al., 2007, ApJ, 666, 1116
 Smith N., Owocki S., 2006, ApJ, 645, 45
 Smith B. D., Sigurdsson S., 2007, ApJ, 661, L5
 Smoot G. F., et al. 1992, ApJ, 142, 419
 Sneden C., Lambert D. L., Whitaker R. W., 1979, ApJ, 234, 964
 Sneden C., Preston G. W., McWilliams A., Searle L., 1994, ApJ, 431, L27
 Sokasian A., Abel T., Hernquist L. E., 2001, NewA, 6, 359
 Sokasian A., Abel T., Hernquist L. E., Springel V., 2003, MNRAS, 344, 607
 Sokasian A., Yoshida N., Abel T., Hernquist L. E., Springel V., 2004, MNRAS, 350, 47
 Somerville R. S., Bullock J. S., Livio M., 2003, ApJ, 593, 616
 Songaila A., 1998, AJ, 115, 2184
 Songaila A., 2001, ApJ, 561, L153
 Songaila A., 2006, ApJ, 131, 24
 Spergel D. N., et al. 2003, ApJS, 148, 175
 Spergel D. N., et al. 2007, ApJS, 170, 377
 Spitzer L. Jr., 1978, *Physical Processes in the Interstellar Medium*, (Wiley-Interscience: New York)
 Springel V., Hernquist L., 2003, MNRAS, 339, 289
 Stacy A., Bromm V., 2007, MNRAS, 382, 229
 Stamatellos D., Whitworth A. P., 2005, AAP, 439, 153
 Stahler S. W., Shu F. H., Taam R. E., 1980, ApJ, 241, 637
 Stark D. P., Bunker A. J., Ellis R. S., Eyles L. P., Lacy M., 2007a, ApJ, 659, 84
 Stark D. P., et al., 2007b, ApJ, 663, 10
 Steidel C. C., et al. 2000, ApJ, 532, 170
 Steidel C. C., Pettini M., Adelberger K. L., 2001, ApJ, 546, 665
 Steigman G., 2005, astro-ph/0501591
 Stern D., et al., 2005, ApJ, 619, 12
 Stoehr F., 2006, MNRAS, 365, 147
 Subramanian K., Cen R., Ostriker J. P., 2000, ApJ, 538, 528
 Sugiyama N., Zaroubi S., Silk J., 2004, MNRAS, 354, 543
 Susa H., 2006, PASJ, 58, 445
 Susa H., Kitayama T., 2000, MNRAS, 317, 175
 Susa H., Umemura M., 2004a, ApJ, 600, 1
 Susa H., Umemura M., 2004b, ApJ, 610, L5
 Susa H., Umemura M., 2006, ApJ, 645, 93
 Suwa Y., Takiwaki T., Kotake K., Sato K., 2007a, PASJ, 59, 771
 Suwa Y., Takiwaki T., Kotake K., Sato K., 2007b, ApJ, 665, L43
 Swaters R. A., Madore B. F., Trewella M., 2000, ApJ, 531, L107

- Talbot R. J., Arnett W. D., 1971, *Nature*, 229, 150
- Tan J. C., McKee C., 2004, *ApJ*, 603, 383
- Tashiro H., Aghanim N., Langer M., Douspis M., Zaroubi S., 2008, *astro-ph/0802.3893*
- Tashiro H., Sugiyama N., 2006a, *MNRAS*, 368, 965
- Tashiro H., Sugiyama N., 2006b, *MNRAS*, 372, 1060
- Tegmark M., et al. 2004, *Phys. Rev. D*, 69, 103501
- Tegmark M., Silk J., Blanchard A., 1994, *ApJ*, 434, 395
- Tegmark M., Silk J., Rees M. J., Blanchard A., Abel T., Palla F., 1997, *ApJ*, 474, 1
- Telfer R. C., Zheng W., Kriss G. A., Davidsen A. F., 2002, *ApJ*, 565, 773
- Thacker R. J., Scannapieco E., Davis M., 2002, *ApJ*, 581, 836
- Theuns T., Schaye J., Haehnelt M. G., 2000, *MNRAS*, 315, 600
- Theuns T., Schaye J., Zaroubi S., Kim T.-S., Tzanavaris P., Carswell B., 2002a, *ApJ*, 567, L103
- Theuns T., Bernardi M., Frieman J., Hewett P., Schaye J., Sheth, R. K., Subbarao M., 2002b, *ApJ*, 574, L111
- Theureau G., Hanski M., Ekholm T., Bottinelli L., Gouguenheim L., Paturel G., Teerikorpi P., 1997, *A&A*, 322, 730
- Thomas R. M., Zaroubi S., 2008, *astro-ph/0709.1657*
- Thoul A. A., Weinberg B. H., 1996, *ApJ*, 465, 608
- Tonry J. L., Blakeslee J. P., Ajhar E. A., Dressler A., 1997, *ApJ*, 475, 399
- Tornatore L., Ferrara A., Schneider R., 2007, *MNRAS*, 382, 945
- Totani T., et al., 2006, *PASJ*, 58, 485
- Tozzi P., Madau P., Meiksin A., Rees M. J., 2000, *ApJ*, 528, 597
- Trac H., Cen R., 2007, *astro-ph/0612406*
- Truran J. E., 1980, *Nucleonica*, 25, 1472
- Tsujimoto T., Shigeyama T., Yoshii Y., 1999, *ApJ*, 519, 63L
- Tsuribe T., Omukai K., 2006, *ApJ*, 642, L61
- Tsuribe T., Omukai K., 2008, *ApJ*, 676, L45
- Tumlinson J., Giroux M. L., Shull J. M., 2001, *ApJ*, 550, L1
- Tumlinson J., Giroux M. L., Shull J. M., Stocke J. T., 1999, *AJ*, 118, 2148
- Tumlinson J., Shull J. M., 2000, *ApJ*, 528, 65
- Tumlinson J., Shull J. M., Venkatesan A., 2003, *ApJ*, 584, 608
- Tumlinson J., Venkatesan A., Shull J. M., 2004, *ApJ*, 612, 602
- Tutui Y., Sofue Y., Honma M., Ichikawa T., Wakamatsu K., 2001, *Publ. Astron. Soc. Japan*, 53, 701
- Tyson J. A., Kochanski G. P., Dell'Antonio I. P., 1998, *ApJ*, 498, L107
- Tytler D., O'Meara J., Suzuki N., Lubin D., 2000, *Phys. Rep.*, 333, 409
- Uehara H., Inutsuka S., 2000, *ApJ*, 531, L91
- Umeda H., Nomoto K., 2005, *ApJ*, 619, 427
- Umemura M., Nakamoto T., Susa H., 1999, *Numerical Astrophysics*, eds. Miyama et al. (Kluwer: Dordrecht), p.43
- Valageas P., Silk J., 1999, *A&A*, 347, 1
- Valdes M., Ciardi B., Ferrara A., Johnston-Hollitt M., Rottgering H., 2006, *MNRAS*, 369, 66
- Valdes M., Ferrara A., Mapelli M., Ripamonti E., 2007, *MNRAS*, 377, 245
- van den Bergh S., 1962, *AJ*, 67, 486
- van den Bosch F. C., Robertson B. E., Dalcanton J. J., de Blok W. J. G., 2000, *AJ*, 119, 1579
- van den Bosch F. C., Swaters R. A., 2001, *MNRAS*, 325, 1017
- Vasiliev E. O., Shchekinov Y. A., 2005, *Ap*, 48, 491

- Vasiliev E. O., Shchekinov Y. A., 2007, astro-ph/0604403
- Venkatesan A., Giroux M. L., Shull J. M., 2001, ApJ, 563, 1
- Venkatesan A., Tumlinson J., Shull J. M., 2003, ApJ, 584, 621
- Verde L., et al. 2002, MNRAS, 335, 432
- Viana P. T. P., Liddle A. R., 1999, MNRAS, 303, 535
- Viel M., Haehnelt M. G. & Springel V., 2004, MNRAS, 354, 684
- Viel M., Haehnelt M. G. & Lewis A., 2006, MNRAS, 370, 51
- Vishniac E. T., 1983, ApJ, 274, 152
- Volonteri M., Haardt F., Madau P., 2003, ApJ, 552, 559
- von Hippel T., Gilmore G., Tanvir N., Robinson D., Jones D. H. P., 1996, AJ, 112, 192
- Wada K., Venkatesan A., 2003, ApJ, 591, 38
- Wang J. X., Malhotra S., Rhoads J. E., 2005, ApJ, 622, 77
- Wang X., Hu W., 2006, ApJ, 643, 585
- Wang X., Tegmark M., Santos M. G., Knox L., 2006, ApJ, 650, 529
- Watson D. et al., 2006, ApJ, 637, 69
- Weatherley S. J., Warren S. J., Babbedge T. S. R., 2004, A&A, 428, 29
- Wechsler R. H., Bullock J. S., Primack J. R., Kravtsov A. V., Dekel A., 2002, ApJ, 568, 52
- Weinmann S. M., Lilly S. J., 2005, ApJ, 624, 526
- Weiss A., Schlattl H., Salaris M., Cassisi S., 2004, A&A, 422, 217
- Whalen D., Abel T., Norman M. L., 2004, ApJ, 610, 14
- Whalen D., Norman M. L., 2006, ApJS, 162, 281
- Whalen D., Norman M. L., 2007, astro-ph/0708.2444
- Whalen D., O'Shea B. W., Smidt J., Norman M. L., 2007, astro-ph/0708.1603
- Whalen D., van Veelen B., O'Shea B. W., Norman M. L., 2008, astro-ph/0801.3698
- White R. L., Becker R. H., Fan X., Strauss M. A., 2003, AJ, 126, 1
- White S. D. M., Rees M. J., 1978, MNRAS, 183, 341
- Whitehouse S. C., Bate M. R., Monaghan J. J., 2005, MNRAS, 364, 1367
- Willick J. A., Batra P., 2001, ApJ, 584, 564
- Willis J. P., Courbin F., 2005, MNRAS, 357, 1348
- Wise J. H. & Abel T., 2005, ApJ, 629, 615
- Wise J. H. & Abel T., 2008, astro-ph/0710.3160
- Wood K., Loeb A., 2000, ApJ, 545, 86
- Woodsley S. E., Weaver T. A., 1995, ApJS, 101, 181
- Wouthuysen S. A., 1952, AJ, 57, 31
- Wright E. L., et al. 1992, ApJ, 396, L13
- Wyithe J. S. B., Cen R., 2007, ApJ, 659, 890
- Wyithe J. S. B., Loeb A., 2003a, ApJ, 586, 693
- Wyithe J. S. B., Loeb A., 2003b, ApJ, 588, L69
- Wyithe J. S. B., Loeb A., 2003c, ApJ, 590, 691
- Wyithe J. S. B., Loeb A., 2004, Nature, 427, 815
- Wyithe J. S. B., Loeb A., 2005, ApJ, 625, 1
- Wyithe J. S. B., Loeb A., 2007, MNRAS, 375, 1034
- Wyithe J. S. B., Loeb A., Barnes D. G., 2005, ApJ, 634, 715
- Wyithe J. S. B., Loeb A., Carilli C., 2005, ApJ, 628, 575
- Yoshii Y., Sabano Y., 1980, PASJ, 32, 229
- Yoshida N., Abel T., Hernquist L., Sugiyama N., 2003a, ApJ, 592, 645
- Yoshida N., Omukai K., Hernquist L., Abel T., 2006, ApJ, 652, 6
- Yoshida N., Omukai K., Hernquist L., 2007, ApJ, 667, L117
- Yoshida N., Sokasian A., Hernquist L., Springel V., 2003b, ApJ, 591, L1

- Yoshida N., Sokasian A., Hernquist L., Springel V., 2003c, *ApJ*, 598, 73
Yu Q., Lu Y., 2005, *ApJ*, 620, 31
Zahn O., Zaldarriaga M., 2006, *ApJ*, 653, 922
Zahn O., Zaldarriaga M., Hernquist L., McQuinn M., 2005, *ApJ*, 630, 657
Zaldarriaga M., Furlanetto S. R., Hernquist L., 2004, *ApJ*, 608, 622
Zaldarriaga M., Hui L., Tegmark M., 2001, *ApJ*, 557, 519
Zaroubi S., Silk J., 2005, *MNRAS*, 360, 64
Zaroubi S., Thomas R. M., Sugiyama N., Silk J., 2007, *MNRAS*, 375, 1269
Zeldovich Y. B., 1970, *A&A*, 5, 84
Zhang P., Pen U.-L., Trac H., 2004, *MNRAS*, 347, 1224
Zhang J., Hui L., Haiman Z., 2007, *MNRAS*, 375, 324
Zhao D., Mo H., Jing Y., Boerner G., 2003, *ApJ*, 339, 12
Zheng W., Chiu K., Anderson S. F., Schneider D. P., Hogan C. J., York D. G.,
Burles S., Brinkmann J. V., 2004, *AJ*, 127, 656